STRUCTURAL MODIFICATION OF POLY(*N*-ISOPROPYLACRYLAMIDE) FOR DRUG DELIVERY APPLICATIONS

A Thesis
Presented to
The Academic Faculty

by

Kai Chang

In Partial Fulfillment
of the Requirements for the Degree
Doctor of Philosophy in the
School of Chemical & Biomolecular Engineering

Georgia Institute of Technology
August 2013

STRUCTURAL MODIFICATION OF POLY(*N*-ISOPROPYLACRYLAMIDE) FOR DRUG DELIVERY APPLICATIONS

Approved by:

Professor Lakeshia J. Taite, Advisor
School of Chemical & Biomolecular Engineering
Georgia Institute of Technology

Professor Andreas Bommarius
School of Chemical & Biomolecular Engineering
Georgia Institute of Technology

Professor Julie Champion
School of Chemical & Biomolecular Engineering
Georgia Institute of Technology

Professor Valeria Milam
School of Materials Science and Engineering
Georgia Institute of Technology

Professor Mark Prausnitz
School of Chemical & Biomolecular Engineering
Georgia Institute of Technology

Date Approved: 3 May 2013

To my wife,

Sarah Chang,

for being my constant companion and encouragement.

ACKNOWLEDGEMENTS

This PhD dissertation would not be possible without a lot of support from many people.

First, I thank my advisor, Dr. Taite, who gave me guidance and encouragement. Thank you for your patience with me and trying to give me perspective when I got bogged down by the details of individual experiments. I also thank Dr. Joe Schork for involving me in the modeling collaborations and Drs. André Gobin and Guandong Zhang for providing me with nanoparticles. I also thank my committee for giving me valuable feedback and suggestions in this work. Your questions helped me greatly focus the writing of my work.

I also thank the Taite lab. I especially Dr. Dhaval Patel and Dr. Shahana Safdar who helped me through many technical discussions and made the Taite lab such a fun place to work. I also thank the undergraduate assistants who helped me with a lot of the lab work, especially Nathan Rubright, Zach Dicke, and Ben Laccetti. Ben in particular collected most of the data for Chapter 3 and it would not have been possible without his help. I thank Dr. Michelle Gaines for continuing this project. I have great hopes! I also thank the current graduate students: Mykel Green, Michael Tanes, Candice Hovell, and Betsy Campbell for taking over the lab responsibilities and keeping me company in the office and the lab.

Finally I thank my family, especially my wife Sarah and my parents for their constant support. I could not have done it without you.

TABLE OF CONTENTS

LIST OF TABLES

LIST OF FIGURES

List of Schemes

LIST OF SYMBOLS OR ABBREVIATIONS

3Me3PenOH	3-methyl-3-pentanol
AAc	acrylic acid
AAm	acrylamide
AIBN	azobisisobutyronitrile
ATRP	atom transfer radical polymerization
AuNP	gold nanoparticle
CRP	controlled radical polymerization
CTA	chain transfer agent
DLS	dynamic light scattering
DMA	dimethyl acrylamide
DMSO	dimethyl sulfoxide
DOX	doxorubicin hydrochloride
ELS	evaporative light scattering
GPC	gel permeation chromatography
HB	highly branched
IPN	interpenetrating network
LCST	lower critical solution temperature
MALDI	matrix-assisted laser desorption/ionization
nIR	near-infrared
NIPAAm	*n*-isopropylacrylamide
NMP	nitroxide mediated radical polymerization
NMR	nuclear magnetic resonance

NP	nanoparticle
PBS	phosphate buffered saline
PDI	polydispersity index
pNIPAAm	poly(*n*-isopropylacrylamide)
RAFT	reversible addition fragmentation chain transfer
RI	refractive index
T_{cp}	cloud point temperature
UV-Vis	ultraviolet-visible

SUMMARY

Polymeric biomaterials have become ubiquitous in modern medical devices. 'Smart' materials, materials that respond to external stimuli, have been of particular interest for biomedical applications such as drug delivery. Poly(*n*-isopropylacrylamide) (pNIPAAm) is the best studied thermally responsive, biocompatible, 'smart' polymer and has been integrated into many potential drug delivery devices; however, the architectural design of the polymer in these devices is often overlooked. In this thesis, pNIPAAm architecture is explored for biological applications and two biomaterials are synthesized as a result.

Architectural modification of linear pNIPAAm was used to synthesize a well-defined homopolymer pNIPAAm with a sharp transition slightly above normal body temperature under isotonic conditions. This polymer required a combination of polymerization and control techniques including controlled radical polymerization, hydrogen bond induced tacticity, and end-group manipulation. The synthesis of this polymer opened up a variety of biomedical possibilities, one of which is the use of these polymers in a novel hydrogel system. Through the use of the controlled linear pNIPAAm synthesized through chain architectural modification, hydrogels with physiological transition temperatures were also synthesized. These hydrogels showed greater shrinking properties than traditional hydrogels synthesized in the same manner and showed physiological mechanical properties.

Highly branched pNIPAAm was also optimized for biological applications. In this case, the branching reduced the efficacy of end-groups in transition temperature modification but increased the efficacy of certain copolymers. The resulting biomaterial was incorporated into a nanoparticle drug delivery system. By combining highly

branched pNIPAAm, which was synthesized to entrap small molecule drugs, with gold nanoparticles, a hybrid system was synthesized where heating of the nanoparticle through surface plasmon resonance can trigger drug release from the pNIPAAm. This system proved to be easy to synthesize, effective in loading, and controlled in release.

As shown from the applications described herein, architectural control of pNIPAAm can open up new possibilities with this polymer for biomedical applications. Small structural changes can lead to significant changes in the bulk properties of the polymer and should be considered in future pNIPAAm based medical devices.

CHAPTER I

INTRODUCTION

1.1 Summary

The use of responsive, 'smart', polymers in biological applications is a burgeoning field in modern science. Many prominent journals in polymer chemistry, biomaterials, and drug delivery have been dominated by papers on this subject in recent years. These polymers have been applied to medical diagnostics, implantable materials, drug delivery systems, and combinations thereof with a degree of success. While these polymers, such as the thermally responsive poly(*N*-isopropylacrylamide) (pNIPAAm), are increasingly relied upon for more and more complex systems, the effects of many of the modifications on the macroscopic properties of these polymers are often overlooked and assumed to be consistent with those of linear chains polymerized under standard protocols. These assumptions often result in sub-optimal designs and, subsequently, sub-optimal results.

In order to address this issue, the behavior of these polymers need to be well-characterized in the common architectural iterations. Points of control where architecture affects macroscopic properties also need to be identified. With the control points and their effects identified, optimal architectural designs can be formulated and higher-performing results can be achieved. It is to this end that this thesis describes the points of control for pNIPAAm and demonstrates the efficacy of this control in two biomedical applications: tuning the temperature response of pNIPAAm hydrogels and developing a pNIPAAm-nanoparticle drug delivery system.

1.2 Polymeric Biomaterials

Biomaterials, materials used to repair or augment a person's ability to function, have been used since ancient times [120, 210, 211]. In recent decades, advances in biology, chemistry, and materials have rapidly advanced the variety, type, and functionality of biomaterials [210, 211]. Polymeric biomaterials are an important class of biomaterials due to the plethora of properties that can be manipulated through the chemistry and structural architecture of the polymer.

1.2.1 History and Uses

Modern uses of polymeric biomaterials date to the 1940s upon the advent of synthetic plastics [211, 7, 122, 123, 124]. The use of nylon sutures, for example, was first published in 1941 [7, 211]. By the 1960s the concept of biocompatability was formalized [210] and successful implants were developed. First generation joint replacement prostheses[38, 37], vascular grafts [19, 270, 66], and heart valves[242] were all developed between the 1950s and the 1960s, with polymers playing key roles in each. Polymeric biomaterials provided properties as diverse as low-friction surfaces [38], optical clarity [210, 211], and mechanical compliance [19, 66], even in these early biomaterials.

Since that time, several classes of polymeric biomaterials have emerged as broad-based solutions to different types of biomedical problems. These include polyurethanes [204], poly(ethylene glycol) (PEG) based polymers [68], and poly(lactic-glycolic acid) (PLGA) based polymers [235] among others [211]. These materials have been designed to solve particular problems such as resisting protein adsorption (PEG) or controlling biodegradation (PLGA) and have become standard tools in modern polymeric biomaterial design [68, 235, 211]. As the fields of polymer science and biology continue to advance, more recent polymeric biomaterials such as 'smart', responsive materials are also becoming standard tools in biomaterial design.

1.2.2 'Smart' Materials

'Smart' materials, materials that respond to external stimuli, have become increasingly important in recent years [302]. These materials include polymers that are thermally responsive [79, 165], pH responsive [165], ionically responsive [54], and biochemically responsive [264], among others [211]. The ability to respond to the external environment produces more dynamic biomaterials with diverse applications. Prominent examples include the pH responsive hydrogels used to encapsulate islets for diabetes treatment [213] and thermally responsive injectable hydrogels for drug delivery applications [82].

1.3 pNIPAAm

pNIPAAm is one of the most commonly used 'smart' polymers and is considered a model system for thermally responsive biocompatible polymers. As such, the architectures applied to this polymer have been varied and extensive. Nevertheless, despite over 7000 research articles on the topic and over 35 years of research, there are few commercial products using this polymer.

pNIPAAm was characterized in the late 1970s [69, 47] and popularized in the late 1980s and early 1990s by Fujishige and others for its sharp phase transition and related large difference between swollen and shrunken states [78, 79, 145, 225]. The original fascination with the sharp phase transition phenomena quickly became a race towards new materials based on the polymer [303, 240, 284]. Within a short period of time, pNIPAAm became a standard polymer as it is today, where it is used as a model of responsive polymers in a similar vein as poly(styrene) or PEG [207, 8]. Because of this, any new polymer architecture, control method [81, 166], or other modification technique developed was quickly replicated using pNIPAAm when possible.

1.3.1 pNIPAAm Properties

pNIPAAm's most intriguing property is the hydrophilic to hydrophobic transition that occurs near 32 °C [21, 86]. Thermal activation of pNIPAAm through the heating of the polymer above its lower critical solution temperature (LCST) causes a linear hydrodynamic radius change of almost an order of magnitude with gels showing an even greater difference [282, 108, 86, 79]. This chain collapse can take place over the course of a temperature change as small as 0.5 °C [79, 35], and has been used in a variety of applications, ranging from cell sheet detachment [195] to microfluidic gates [85]. This effect is due to the location and size of the amphiphilic pendant groups. Studies have shown that the water surrounding and solvating the polymer is highly structured, with 11 water molecules solvating each pendant group as shown in Scheme 1.1 [190, 191]. Complete dehydration is then achieved through raising the temperature above the LCST [190].

This understanding provides insight into the mechanism of the transition and ways in which it can be modified. For example, any method that would stabilize the structured water will raise the LCST. This includes polymerizing with hydrophilic comonomers and imposing syndiotactic polymerization. Conversely, any method that disrupts the structured water will lower the LCST, including the use of chaotropes and hydrophobic comonomers. With this understanding, modification of the LCST can be achieved in a variety of ways.

1.3.1.1 pNIPAAm Copolymers

By far the most common method of manipulating the LCST of pNIPAAm is to synthesize pNIPAAm copolymers. Early in the exploration of pNIPAAm, the understanding was that the LCST was a thermodynamic issue between hydrophilic and hydrophobic sections of the polymer. Manipulation therefore required the introduction of more hydrophilic sections to raise the LCST or more hydrophobic sections to reduce the

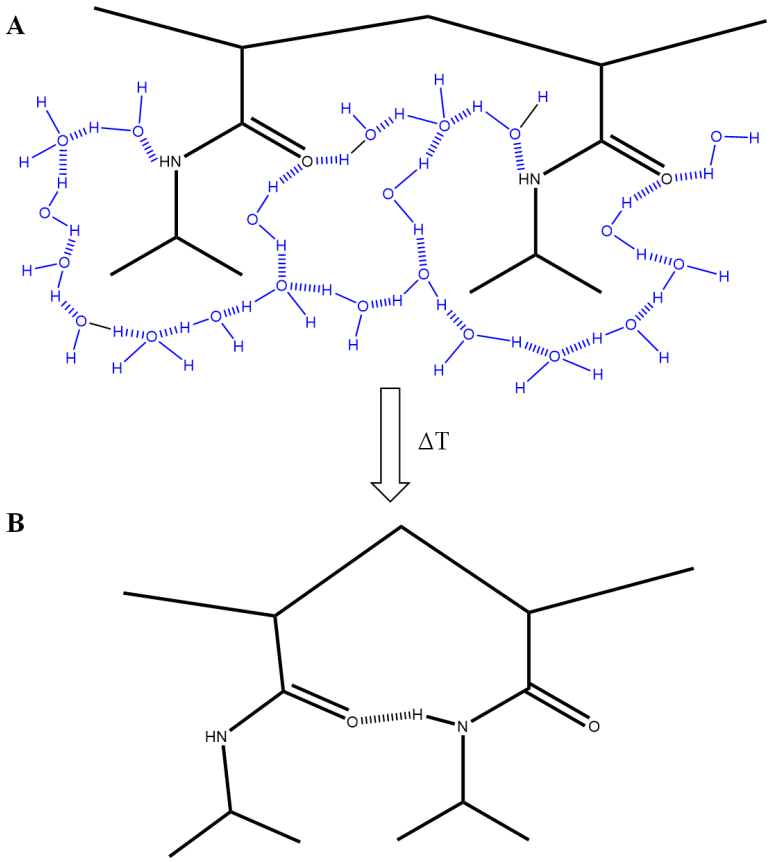

Scheme 1.1: Hydrogen bonding of water to pNIPAAm. A) At temperatures below the LCST, pNIPAAm is dissolved in water with water forming structured cages around the pendant groups. B) At temperatures above the LCST, pNIPAAm is completely dehydrated and is no longer soluble in water.

LCST. While this method works very well, it does not take into consideration the specific effects of the co-monomers. For example, using a common copolymer of pNIPAAm and acrylic acid (AAc) can significantly increase the LCST with relatively little co-monomer content; however, the greater the co-monomer content, the less sharp the transition.

Copolymerization with AAc has the effect of widening the LCST from a transition that occurs over $< 0.5\,^{\circ}\mathrm{C}$ to a transition that takes place over a range of 5-10 °C, or even larger depending on the desired LCST [21, 197, 4]. This increase in transition range is due to the charge on AAc at neutral pH [143], and is less than ideal for any application requiring a sharply defined response [127]. Similarly, copolymerization with dimethylacrylamide (DMA), another hydrophilic co-monomer, yields a higher LCST but with a much sharper transition than AAc copolymers [232]. Nevertheless, DMA is far less effective than AAc at raising the LCST, requiring a much greater percentage DMA to affect the same rise in LCST, despite both co-monomers being hydrophilic [232, 197]. This difference is related to the interaction energies between the copolymers and the solvent [232].

If the differences were only in the transition temperature and range, the effect of the co-monomer could be compensated for. However, thermodynamic theory of the chain collapse indicates that the transition is a bulk dehydration [233, 190]. It is highly unfavorable for most hydrophilic co-monomers such as the charged AAc to not be solvated in aqueous solution. Therefore, the chain collapse is likely to be less dramatic than pure pNIPAAm, yielding a smaller hydrodynamic change similar to the deswelling data from comparable hydrogels [143]. This reduces the overall efficacy of pNIPAAm as a 'smart' polymer and likely contributes to the limited commercial success of the polymer. Nevertheless, copolymerizing as a method of raising LCST is widely used and the focus of much prior research has been to optimize copolymer content in order to change the LCST under various conditions [65, 300].

1.3.2 pNIPAAm Architecture

Since the LCST is dictated by the stability of the structured water surrounding the pendant groups, changing the architecture of pNIPAAm has major effects on the LCST. Furthermore, architectural changes provide flexibility to add functionalities or characteristics to the polymer. As with any polymer, pNIPAAm architecture can be broken down into two sections: chain architecture, and bulk architecture.

Chain architecture in a polymer includes copolymers of various forms such as AB, ABA, or ABC block copolymers as well as random copolymers. Additionally, chain architecture can be manipulated by modifying polymer stereochemistry. Subsequently, even polymers with one repeat unit such as pNIPAAm have modifiable chain architecture. Polymer bulk architecture is what is traditionally meant by "polymer architecture". It is the branching of the polymer chains into various forms such as stars, combs, and dumbbells. Changes in chain or bulk architecture can change pNIPAAm properties and be used or misused in the design of pNIPAAm-based devices.

1.3.2.1 Polymer Chain Architecture - Tacticity

Polymer chain architecture consists of the type and location of copolymers throughout the backbone as well as the orientation of the pendant groups along the backbone. The previous discussion on the effects of copolymers is relevant for that aspect of chain architecture; however, recent developments in tacticity control have opened up the possibility of chain architectural control to homopolymers.

Tacticity describes the orientation of the pendant groups along the backbone of the polymer, as shown in Scheme 1.2. Specifically, it refers to the pendant groups' orientation. Isotactic polymers are composed of meso diads which correspond to pendant groups oriented in the same direction. Syndiotactic polymers are composed of racemo diads which alternate in orientation. Atactic polymers have roughly equivalent amounts of meso and racemo diads, showing no preference in orientation.

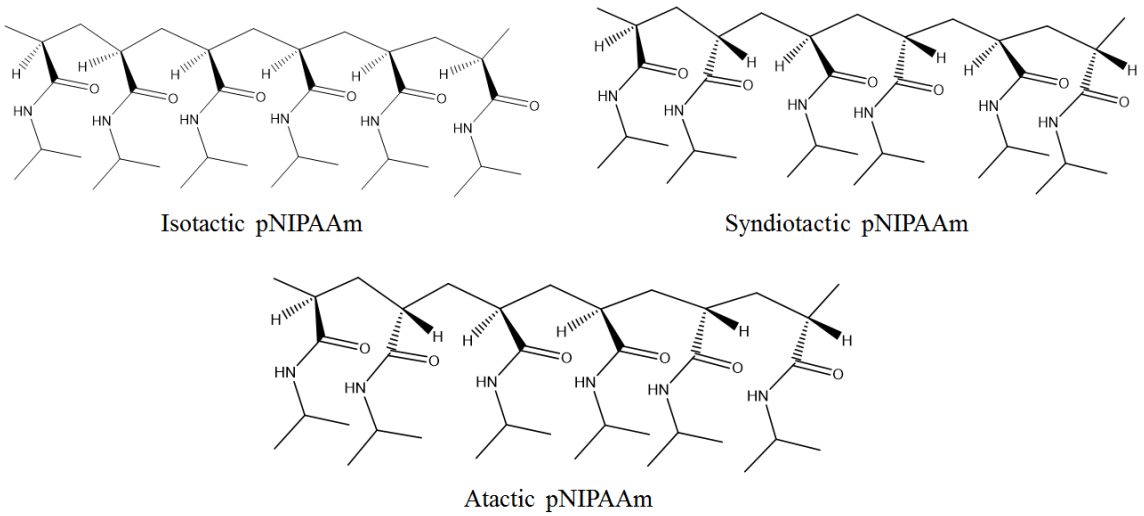

Scheme 1.2: pNIPAAm in syndiotactic, isotactic, and atactic forms.

For the purposes of raising the LCST, selectively polymerizing in the racemo conformation can be a useful method because it modifies the rotational energy required to orient the polymer such that it undergoes the cooperative dehydration that is observed macroscopically as the LCST [190, 100, 107]. pNIPAAm with a majority of meso diads exhibits a lower LCST while pNIPAAm with a majority racemo diads exhibits a higher LCST [217, 107, 134]. The difference in LCST seen using this method is usually on the order of 3-5 °C, a significant enhancement [107]. Additionally, racemo diads not only increase the LCST but also sharpen the transition [107, 102].

1.3.2.2 Polymer Bulk Architecture

Bulk polymer architecture deals with the branching of the polymer. In the past few decades, polymers of various shapes have been synthesized. These include star polymers, comb polymers, brush polymers, dumbbell polymers, dendrimers, and hyperbranched polymers among others (see Scheme 1.3). These shapes lend themselves to various applications and, for example in nanomedicine, have been designed into a multiplicity of constructs.

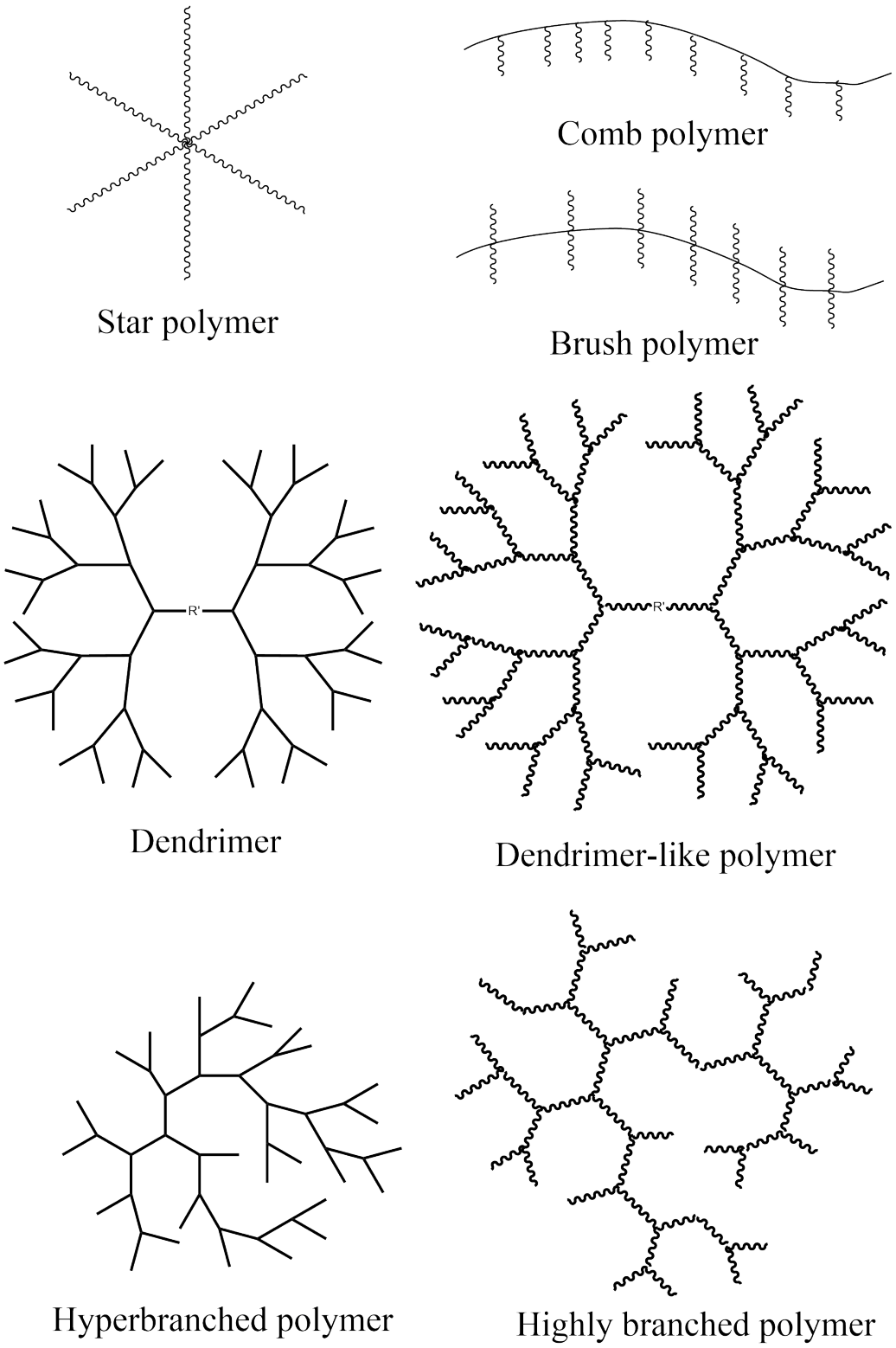

Scheme 1.3: Common bulk polymer architectures.

The advantages to these architectures are legion, including facilitating multiresponsive systems, encapsulating and delivering drugs, and forming or stabilizing larger constructs such as micelles or liposomes. These architectures also affect the macroscopic properties of the polymers such as the glass transition temperature. Branching has also been shown to lower the LCST of pNIPAAm [30, 268]. Properly understanding the interplay between chain and bulk architecture is therefore key in the design of pNIPAAm for biomedical applications.

1.3.2.3 Dendrimers

Out of the various branched architectures, dendrimers have a particular place in biological applications. Dendrimers are perfectly defined macromolecules that have distinct branching structures (Scheme 1.3) [182, 20, 297]. Since their inception in the 1980s, they have been studied extensively for biological applications [253, 20, 163, 147, 297, 45]. Their tree-like architecture provides a dense surface full of functional end groups while also providing a relatively sparse interior. These end groups can be extended with copolymers to synthesize unimolecular micelles [297]. They can also be crosslinked into hydrogels [112] or conjugated with targeting peptides or antibodies, making them effective targeted drug delivery vehicles [147]. The large number of end groups in this type of material also gives them a better defined three dimensional structure when compared with most other architectures.

The key weakness in the use of dendrimers is the difficulty in synthesis. Dendrimers are characterized by their generation number, which is determined by the number of branching layers. Each layer is added in series to ensure low defects. Dendrimer synthesis is accomplished either using the divergent route, in which dendrimers are grown outward from a central core [56, 55], or the convergent route [76], in which dendrimers are grown inward from the branches. Divergent synthesis was pioneered in the 1980s and was the first dendrimer synthesis method [183, 262]. This

method starts at the dendrimer core and expands outward in a branching fashion. As a result, this type of synthesis requires many protection/deprotection steps and many reactions with each generation is built by a separate synthesis step.

Convergent dendrimer synthesis was pioneered by Hawker and Fréchet in 1990 [97] and involves using a monomer that has symmetric reactive groups and a protected group. An initiating group with the desired final surface functionality is reacted with the reacting groups on the monomer. The dendrons are then deprotected and reacted with more monomers which are then deprotected and reacted with yet more monomers. This continues until the desired number of generations is reached.

Regardless of method, the synthesis of dendrimers is a tedious process, and modifications in the constitutive elements of dendrimers are even more so. The requirements of each branching element requires orthoganol chemistry and efficient reactions. Additionally, separation and purification methods must be re-optimized to account for the changes.

Since a pNIPAAm dendrimer consisting of single monomers between branching units would not have the chain collapse properties desired from using pNIPAAm, the analogue would be a dendrimer-like polymer. Dendrimer-like polymers are formed using the same concepts as dendrimers; however, they are even more difficult to synthesize than dendrimers due to the decrease in availability of end-groups to react as the polymer chain gets longer. Defects are therefore a much larger problem in long-chain dendrimer-like polymers and it can be argued that they are not superior to the much easier to synthesize highly branched polymer.

1.3.2.4 Highly Branched (HB) Polymers

Highly branched polymers are akin to hyperbranched polymers in the way that dendrimer-like polymers are to dendrimers [71]. They are long-chain polymers that can be synthesized by a process, similar to convergent dendrimer synthesis, which

utilizes a branching agent to converge towards a central moiety [97, 99]. Such architecture provides a dense surface and a relatively sparse interior with ample space to encapsulate drugs, while bypassing many of the challenges posed by traditional dendrimer synthesis. The basic scheme for highly branched polymer synthesis is a one-pot condensation or polymerization in which branching moieties are present, as shown in Scheme 1.4 [95, 30, 32, 99]. By condensing the branching units, a three-dimensional globular structure, not unlike that of a dendrimer, can be achieved.

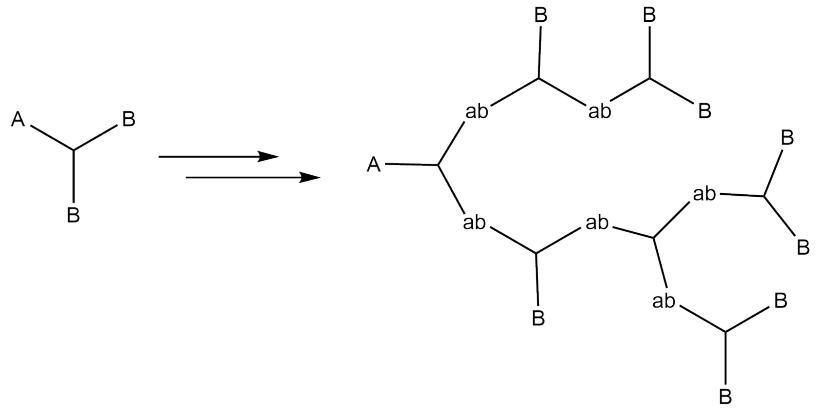

Scheme 1.4: Typical hyperbranched polymer synthesis scheme using AB_2 monomers. A reacts efficiently with B to form ab. Lack of control yields branch segments of different lengths.

The advantages to HB polymers are obvious. The simplicity of synthesis allows for easier experimentation, concurrent polymerization yields long-chain polymers, and semi-controlled branching produces globular structures. The main disadvantages are the lack of segment molecular weight control and less branching control than dendrimer synthesis. When applied to pNIPAAm systems, HB polymers form long enough segment chains to allow for chain collapse; however, the LCST is significantly reduced due to the disruption in the structured water from branching and tightly packed segments.

1.3.2.5 Hydrogels

Highly crosslinked systems such as hydrogels consist of a broad range of architectures and are of significant interest in biological applications. Their biomimetic properties make them good scaffolds for cell and tissue engineering applications [200, 239] as well as drug delivery vehicles [199, 201, 198, 132, 229].

Hydrogels can be made using a wide variety of methods and consist of both physically crosslinked gels and chemically crosslinked gels. Physically crosslinked gels such as interpenetrating networks (IPNs) are synthesized by entangling polymers on a polymer chain scale in such a way that they cannot be separated [159, 87, 94]. Chemically crosslinked hydrogels are synthesized by chemically reacting the polymer chains so that they form a network. Generally this is done with a crosslinking agent which has multiple reactive groups, similar to a branching unit. Chemically crosslinked hydrogels can be synthesized concurrently with polymerization or crosslinked afterwards and can be initiated using a variety of methods [93, 256].

The main structural difference between a crosslinked gel and a highly branched or even dendrimer-like polymer is the degree of control over the branching. Crosslinked gels can form linkages to other chains at a number of locations, yielding a mesh polymer network. Highly branched and dendrimer-like polymers can only link, or branch, at certain locations and therefore form discreet polymers. There have been studies converting HB polymers into crosslinked gels through the use of reversible bonds, but it is thermodynamically unfavorable to convert a less ordered gel into a more ordered HB polymer [294].

When pNIPAAm is synthesized into a hydrogel, it continues to exhibit a thermal transition, in this case expelling a significant portion of the water from the network above the transition temperature. This transition however, takes place over a range of temperatures and is not as sharp as the transition observed in free-floating polymer. As such, architectural modification of the polymer chains have the potential to change

the gel properties.

1.4 pNIPAAm in Drug Delivery Applications

The polymer architectures and features described above can be used in the design of a variety of medically interesting constructs [179]. Drug delivery, with its broad possibilities and preconditions, in arenas ranging from nanoparticle drug delivery, to implantables, to more traditional drug delivery mechanisms provides a great field to explore the points of macroscopic and systems control afforded pNIPAAm through architectural modification.

1.4.1 Hydrogel Drug Delivery

Hydrogels are a major class of biomaterial and have been used in a variety of drug delivery constructs [199, 201, 198, 132, 229]. These constructs include many 'smart' release systems such as glucose sensors [239] and controlled transdermal drug release systems [306]. 'Smart' hydrogels, including pH responsive [43, 119], ionically responsive [119], chemically responsive [264, 229], ultrasound responsive [229], magnetically responsive [67], electrically responsive [229], and thermally responsive hydrogels [42], have played critical roles in these applications.

pNIPAAm hydrogels are the best studied thermally responsive hydrogels and despite the difficulty in using an LCST in the relatively isothermal physiological conditions, several examples of pNIPAAm hydrogel drug delivery devices have been studied [59, 255]. The porosity of the hydrogels however, are only able to modulate the diffusion rate of small molecule drugs and generally do not stop it completely [59, 54].

1.4.2 pNIPAAm-Nanoparticle Constructs

Interest in metallic nanoparticles for biomedical applications has recently increased greatly. Silver [154, 214], gold [154], and iron nanoparticles [287] in particular have

been used for a variety of applications ranging from antimicrobials to imaging. Polymer coatings and tetherings have played a major role in expanding the applications of this technology. pNIPAAm has been associated with all three major classes of metal nanoparticles in a variety of configurations; however, nanogold has a particular synergy with pNIPAAm.

1.4.2.1 Gold Nanoparticle Properties

Nanoparticles (NPs) have received a lot of academic and media attention recently [24, 243]. Metal nanoparticles display a variety of properties not seen in macroparticles of the same material [154, 126]. One of the most interesting of these properties is the resonance of surface plasmons [154]. The localized surface plasmon resonance(LSPR) effect is due to the collective motion of free electrons oscillating with the excitation from resonant frequencies of electromagnetic waves [154]. This effect, which is dampened in bulk and non-existent in single atoms, can generate a significant amount of heat [154].

Gold nanoparticles (AuNPs), in particular, are biocompatible and have the ability to absorb certain wavelengths of light to such a degree as to significantly heat up their surrounding area [128]. Their light scattering and absorbing properties also allow for imaging [161, 162, 129]. Currently, their applications in cancer treatment are being pursued by multiple research groups [109, 243]. Gold nanoshells and nanorods in particular have received much attention due to their ability to be easily tuned for absorption at different wavelengths. While nanorods are easily synthesized and controlled, they suffer from photothermal instability and undergo remodeling after activation [305, 154, 147, 115]. This makes them less ideal for drug release applications that require lengthy or cyclic activation. Gold nanoshells provide a better way to incorporate heating into a drug delivery system.

Gold nanoshells and nanocages are typically synthesized by chemically depositing

a thin layer of gold over a core made of another material such as silica or gold sulfide [313, 209, 238, 41, 40]. The symmetric nature of gold nanoshells prevents the photothermal remodeling as seen in the nanorods. The thin layer of gold exhibits the LSPR effect, yet has the length scale of a much larger particle, thereby allowing for the shifting of the absorption wavelength into the near-IR region.

The absorbance wavelengths of nanoshells can be tuned by the core to shell thickness ratio [128, 314]. This wavelength can be adjusted to be within the realm of near-IR light, which can penetrate over to a centimeter of human tissue with no ill effects [109]. Temperatures up to $60.6 \pm 2.4\,^{\circ}\mathrm{C}$ have been reported in the surrounding tissue [88]. This increase in temperature is more than enough to cause thermal ablation of the surrounding cells [109, 188, 88]. Combined with the enhanced permeation and retention (EPR) effect where leaky tumor vasculature allows nano-sized structures to collect in tumors, nanoshells have the ability to revolutionize cancer treatment.

1.4.2.2 pNIPAAm Coated Gold Nanoparticles

To take advantage of the heating effects of AuNPs, several groups have combined them with pNIPAAm. In theory the combination can provide physicians with precision control over the release of drugs. In practice, nano and microgel coatings of pNIPAAm onto AuNPs have shown mixed drug delivery results [135]. This can be ameliorated through design solutions such as coated nanocages that rely upon the cages to encapsulate drugs [299]; nevertheless, linear pNIPAAm coatings do a poor job containing small molecule drugs until release. As such, applying pNIPAAm architectural design to this application is a great demonstration of the power of various types of pNIPAAm control.

1.5 Engineering strict structural control of pNIPAAm

Increasing structural control over pNIPAAm without significantly increasing synthesis complexity is not a trivial task. The desire for simultaneous control over molecular weight, copolymer composition, tacticity, end-groups, and branching requires a combination of strategies. Fortunately, in the past 15 years, several polymer chemistries have been developed to facilitate this.

1.5.1 Chemistries of Control

Molecular weight control has greatly advanced with the invention of 'living' controlled radical polymerization (CRP). CRP controls the molecular weight primarily by reducing the number of active free radicals polymerizing in solution at any given period without permanently removing the radicals from the system. These schemes, including atom transfer radical polymerization (ATRP) [272, 170], nitroxide mediated polymerization (NMP) [96, 227], and reversible addition-fragmentation chain transfer (RAFT) polymerization [48, 80], are therefore able to reduce bimolecular termination reactions that is the leading cause of high polydispersities. ATRP and RAFT are particularly useful for pNIPAAm polymerization because of their efficiency and ease of use [139, 166, 288, 215, 81].

1.5.1.1 ATRP

ATRP controls polymerization by using a transition metal-ligand complex (usually with copper) to reversibly react with the ATRP initiator (usually a halide such as bromine) as shown in Scheme 1.5. The transition metal is reversibly oxidized by the initiator, leaving a free radical for free radical polymerization. At any point, this free radical can react again with the halide, regenerating the metal. The chemical equilibrium is driven to favor capped radicals, which in turn reduces the number of actively polymerizing chains and grants excellent control over the molecular weight with very low polydispersity indexes [170, 169].

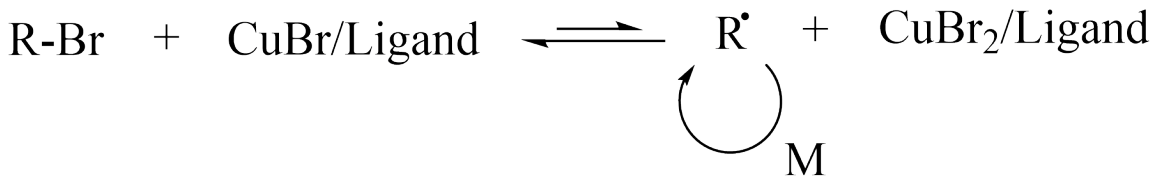

Scheme 1.5: ATRP polymerization. The rate of the reverse reaction is greater than the forward reaction leading to fewer polymerizing radicals at any given point and much better polymer molecular weight control.

Beyond the molecular weight control, ATRP offers the key advantage of being able to grow linear chains off of any prepared ATRP initiator. With the proper initiator, star, comb, and brush polymers with well-defined molecular weights can easily be synthesized [139]. Additionally, ATRP can be used with great efficacy on solid substrates despite diffusion being a major challenge with these types of polymerizations.

1.5.1.2 RAFT

The RAFT scheme controls polymerization by introducing a chain transfer agent (CTA). The chain transfer agent, usually a di- or tri-thiocarbonate, reacts with polymerizing chains to form an intermediate during free radical polymerization, as shown in Scheme 1.6. This reaction kicks off the other end of the CTA (the R group in Scheme 1.6), forming another free radical to continue polymerization. This series of reactions, which are reversible, forms a dynamic equilibrium between active and dormant chains of polymers. Because of the rapid association and dissociation with the CTA, fewer polymer chains are actively polymerizing at one time. This causes a significant decrease in the polydispersity index (PDI) of the final polymers due to fewer termination reactions occurring during polymerization.

In addition to controlling polymerization, using a CTA provides opportunities for further functionalization of polymer ends. The CTA can be formulated to have reactive end groups, upon which other chemical conjugations may take place after

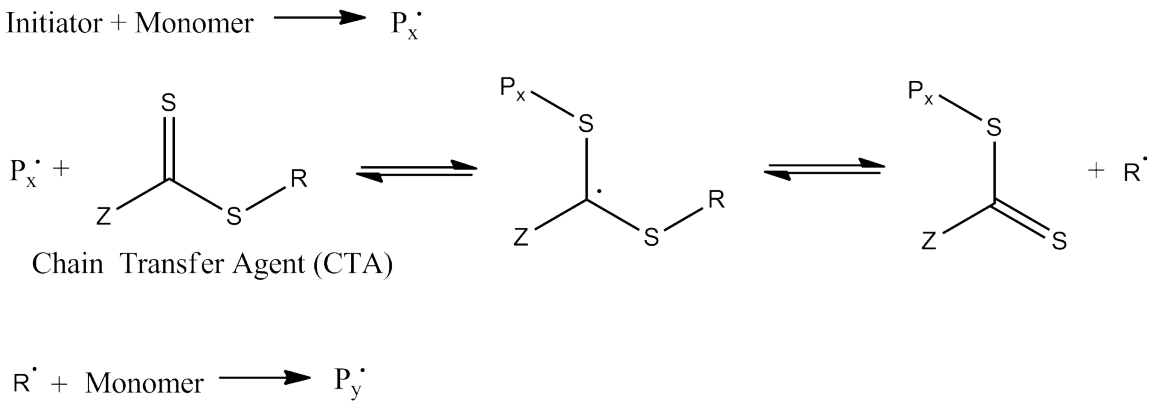

Scheme 1.6: RAFT polymerization. The CTA reversibly reacts with the polymerizing chain, forming a radical and another polymer chain. Excess CTAs cause rapid chain transfer and reduce the number of termination reactions.

polymerization. This has been exploited by many groups to form various polymer functionalities [151, 208, 50].

1.5.2 Improving pNIPAAm design for drug delivery applications

Current drug delivery designs using pNIPAAm tend to focus on complex branching, targeting, responsive copolymer schemes to add ever more functionality to drug delivery vehicles [152, 119]. Multi-responsive, 'smart' drug delivery systems are the current frontier in polymeric drug delivery constructs [9, 136, 60, 263]. Concurrently, recent advances in the understanding and manipulation of pNIPAAm has introduced new design possibilities. The bridges between these new possibilities and their applications, however, are still rather sparse.

Different groups have discovered the importance of end-groups [286], molecular weight [286], tacticity [217], and branching [30] on pNIPAAm LCST but they have not been optimized for biological applications. More importantly, the interactions between these new methods of control have not been explored. To this end, I have combined the most promising structural modifications of pNIPAAm and optimized them for biological applications. The interactions between these structural modifications are analyzed and the implications for drug delivery are noted. Additionally, two

drug delivery constructs, a hydrogel and a nanoparticle, are synthesized using structurally modified pNIPAAm and preliminary characteristics are compared. Results from these studies illuminate several new considerations when designing pNIPAAm based drug delivery devices and demonstrate that well-controlled pNIPAAm architecture can have a dramatic effect on the final drug delivery construct.

CHAPTER II

ARCHITECTURAL CONTROL OF LINEAR PNIPAAM FOR LCST MODIFICATION

2.1 Summary

The pNIPAAm temperature transition, with its potential for biomedical applications, is at its core based upon a thermodynamic phenomenon. This phenomenon occurs due to the hydrophilic/hydrophobic interactions between the side chains of the polymer and water. This study focuses on the modification of the LCST of linear pNIPAAm through architectural control. We combined the use of RAFT polymerization with tacticity control to synthesize well-defined pNIPAAm that demonstrates sharp transitions under physiological conditions. By selecting a RAFT agent with appropriate end groups, controlling molecular weight, and increasing the racemo diad content, we were able to increase the thermal transition temperature of pure pNIPAAm to a sharp transition at 37.6 °C under isotonic conditions. These properties open the door for the use of pNIPAAm homopolymers in biological applications, thereby reducing the complexity of the system and the potential for adverse effects caused by copolymer content.

2.2 Introduction

As expounded in Chapter 1, new developments in biomedical diagnostics, theranostics, and sensing applications increasingly rely upon smart materials, materials which have properties that can be triggered to change upon exposure to an external stimulus. pNIPAAm, one of the most promising of this class of materials, is not only biocompatible, but also thermally responsive within the biological temperature range. pNIPAAm

has been extensively studied by many groups for use in applications in biotechnology, ranging from protein purification [31] to drug delivery [18, 98] to biosensing [244]. One of the many requirements for successful application in biological systems is an LCST at physiological or higher temperatures [31, 18, 250, 4]. This is especially true for drug delivery applications since these systems are designed for use *in vivo*. Since these applications must operate within very narrow temperature ranges, the ability to manipulate the LCST to higher temperatures without sacrificing the sharpness of the transition is essential. Though the current trend in research on pNIPAAm-based thermo-responsive polymers lies in the preparation of amphiphilic random, block, graft, or star-shaped copolymers for biomedical applications, through a combination of simple LCST modification techniques we have synthesized a pure pNIPAAm that can be manipulated to transition at physiological temperature under isotonic conditions. These polymers, and the ease with which the transition temperature can be modified using the synthesis techniques we describe, present a novel strategy for the formation of polymer systems with highly homogeneous properties that can be used in applications in biotechnology.

The LCST of pNIPAAm is influenced by a variety of factors, and there are several methods used to modify it, as described extensively in Chapter 1. The most common is to copolymerize with a small amount of hydrophilic co-monomer. While several copolymer blends exist to raise the LCST with sharp transitions [223, 232], some of the most popular blends for biological applications such as acrylic acid (AAc) have a broadening effect on the LCST [21, 4]. This concept has recently been extended into attaching specific end-groups to the polymer, which can significantly affect lower molecular weight pNIPAAm although its utility is inversely proportional to the molecular weight [153]. In addition, the tacticity of the polymer can be modified to affect the LCST. Specifically, using a bulky alcohol cosolvent can induce racémo diad formation, and has previously been shown to raise the LCST of radical polymerized

pNIPAAm by 3-5 °C [107].

While the intrinsic properties of the polymer play a large role in the LCST, solvent properties cannot be discounted in this discussion. Certain co-solvents such as methanol can significantly reduce the LCST [280], while pH can have a mild effect [197] and salts can have a large effect on the LCST [312]. This is especially important in biological applications because biological systems require certain osmolarity and salt concentrations, without which cells will undergo apoptosis. The cumulative result of these LCST-depressing effects renders the polymer all but useless for biological applications in its native form.

2.2.1 Controlled Radical Polymerization

Secondary to the issue of LCST manipulation is the need for well-defined polymers, a problem that is easily rectified using a living radical polymerization scheme. As discussed in Chapter 1, the most common methods of CRP for pNIPAAm as of this writing are atom transfer radical polymerization (ATRP) [166, 170] and reversible addition-fragmentation chain transfer (RAFT) polymerization [216, 80]. ATRP is a versatile method that works well with acrylamides including pNIPAAm; however, it requires a metal catalyst, which can sometimes be difficult to remove and can by cytotoxic [288]. This leaves RAFT as the best solution for molecular weight control for pNIPAAm synthesis for biomedical applications.

As described in Chapter 1, the RAFT scheme controls polymerization by introducing a chain transfer agent (CTA). The CTA chosen for this study is the well-documented, symmetric chain transfer agent, S, S' bis(α,α'-dimethyl-α"-acetic acid)trithiocarbonate (**1**) [146, 260, 52, 180, 186, 218], which has been previously shown to be very versatile and produce good results with pNIPAAm [52, 180, 186]. By utilizing RAFT polymerization along with the LCST manipulation principles outlined above, we have successfully synthesized well-defined pNIPAAm with a sharp

LCST of 37.6 °C in phosphate buffered saline (PBS) without the use of copolymerization, thereby introducing another method to optimize pNIPAAm synthesis for biological applications. Furthermore, the incorporation of this living process allows for additional chain extension polymerization which can be used in the synthesis of hydrogels or for the addition of functionalities through subsequent polymerizations and conjugations.

2.3 Materials and Methods

N-isopropylacrylamide was purchased from TCI America and recrystallized in a 9:1 ratio of hexanes:benzene. Carbon disulfide, tetrabutylammonium hydrogen sulfate, mineral spirits, 1, 4 dioxane, Aliquat 336 and 3-methyl-3-pentanol (3Me3PenOH) were purchased from Sigma Aldrich and used without further purification. Chloroform and acetone were purchased from BDH Chemicals and used without further purification.

2.3.1 S, S' bis(α,α'-dimethyl-α"-acetic acid)trithiocarbonate (1) Synthesis

Synthesis of **1** was done similarly to the procedure set forth by Lai et al. [146] 6.62 mL (0.1 mol) acetone was reacted with 7.26 mL (0.1 mol) chloroform, 2.16 mL (0.04 mol) carbon disulfide, and 0.241 g (0.7 mmol) tetrabutylammonium hydrogen sulfate in 12 mL of mineral spirits. The reaction mixture was purged with nitrogen for five minutes and run in a water bath at room temperature. 10 mL of 50% NaOH was added drop-wise over 90 minutes and the reaction was left to run overnight. 90 mL of water was then added, followed by 42 mL of 6N HCl. The reaction mixture was then purged under nitrogen for half an hour and filtered. The resulting product was recrystallized in acetone to yield 4 grams of product. Synthesis of **1** was confirmed by electrospray mass spectrometry (see Figure B.1 in Appendix B).

2.3.2 Polymerization

Polymerization of NIPAAm was carried out under six different conditions. High transition temperature pNIPAAm was synthesized using a temperature shock treatment in which the reaction was thermally initiated at 65 °C for one hour and immediately placed into a room temperature bath to react at room temperature for the rest of the polymerization time, typically 95 hrs. The purpose of this method was to slow the reaction kinetics to allow for better tacticity control, a hydrogen bond induced process. It also served as a method to control molecular weight through polymerization time. Typically, a 3.2 g mixture of 100:1:0.5 ratio of NIPAAm:**1**:AIBN was placed in a sealed 25 mL round-bottom flask equipped with a magnetic stir bar. The mixture was purged with nitrogen for 10 minutes and 20 mL of nitrogen-purged 1, 4 dioxane was added. The solution was reacted at 65 °C for 1 hour and at room temperature for 95 hours.

To test the effects of majority racemo diads, 3Me3PenOH was added to the reaction mixture. Accordingly, a 3.2 g mixture of 100:**1**:0.5 ratio of NIPAAm:**1**:AIBN was placed in a sealed 50 mL round-bottom flask equipped with a magnetic stir bar. 6.7 mL of 3Me3PenOH was added to the reaction mixture. The mixture was purged with nitrogen for 10 minutes and 20 mL of nitrogen-purged 1, 4 dioxane was added. The solution was reacted at 65 °C for 1 or 1.5 hours to initiate polymerization and at room temperature for up to 95 hours thereafter.

Control polymers were synthesized using typical RAFT polymerization techniques with **1**. Briefly, a 3.2 g mixture of 100:1:0.5 ratio of NIPAAm:**1**:AIBN was placed in a sealed 25 mL round-bottom flask equipped with a magnetic stir bar. 6.7 mL of 3Me3PenOH was added to the reaction mixture for a control polymer with majority racemo diads while this step was omitted for the atactic polymer control. The mixture was purged with nitrogen for 10 minutes and 20 mL of nitrogen-purged 1, 4 dioxane was added. The solution was reacted at 65 °C for 48hrs.

For radical polymerized pNIPAAm controls, a 3.2 g mixture of 100:1 ratio of NIPAAm:AIBN was placed in a sealed 25 mL round-bottom flask equipped with a magnetic stir bar. The mixture was purged with nitrogen for 10 minutes and 20 mL of nitrogen-purged 1, 4 dioxane was added. The solution was reacted at 65 °C for 48 hrs.

A temperature shock radical polymerization control experiment was also conducted in which a 3.2 g mixture of 100:1 ratio of NIPAAm:AIBN was placed in a sealed 25 mL round-bottom flask equipped with a magnetic stir bar. The mixture was purged with nitrogen for 10 minutes and 20 mL of nitrogen-purged 1, 4 dioxane was added. The solution was reacted at 65 °C for 1 hour as a thermal initiation or temperature shock, and then removed from the heat to react at room temperature for 95 hrs.

A copolymer with 4% AAc, pNIPAAm-*co*-AAc, was also synthesized for comparison with the resulting polymers. This was done by reacting 1.5 g of NIPAAm with 37.9 μL of AAc and 2.18 g of AIBN in a sealed 25 mL round-bottom flask equipped with a magnetic stir bar. The mixture was purged with nitrogen for 10 minutes and 20 mL of nitrogen-purged 1, 4 dioxane was added. The solution was reacted for various lengths of time at 65 °C. An 8% AAc copolymer was also synthesized using the same method and incorporated 75.8 μL of AAc.

Upon completion of reactions, all pNIPAAm samples were precipitated in anhydrous diethyl ether and collected via filtration. The samples were then dissolved in nanopure water and dialyzed with a 2000 MWCO membrane. The water was changed at 1 hr, 3 hrs, and 20 hrs. The samples were then frozen and lyophilized. pNIPAAm and majority syndiotactic pNIPAAm polymerized by this method is hereafter denoted as pNIPAAm-**1** and pNIPAAm-**1**s respectively.

2.3.3 Characterization

Polymers were characterized using GPC, NMR, MALDI mass spectrometry, and UV-Vis spectrometry. GPC was conducted on a PL-GPC 50 with UV, RI, and ELS detectors (Agilent, Inc.) equipped with two Plgel 3μm MIXED-E columns. Filtered stabilized tetrahydrofuran was used as the polymer solvent and GPC eluent at a flow rate of 1 mL/min. Chromatograms were compared with those of polystyrene standards (Agilent Inc). ^{1}H NMR was conducted on a Varian Mercury Vx 400 spectrometer using chloroform-*d* as solvent for room temperature experiments or DMSO-*d*6 as a solvent at 90 °C. The high temperature was used to resolve the methine backbone peaks [125, 216, 101]. Mass Spectrometry was run on an Applied Biosystems 4700 Proteomics Analyzer with a 200 Hz Nd:YAG laser using CHCA matrix and reflecting detector. UV-Vis spectrometry was conducted using a Cary 50 UV-Vis Spectrophotometer (Agilent Inc.) with the single cell peltier thermostatted cell holder and accessory for temperature control. Temperature was ramped at a rate of 0.5 ° per minute and data points were taken every 0.1 °.

2.4 Results and Discussion

2.4.1 Molecular Weight Control

pNIPAAm was synthesized under various reaction times at room temperature. The initial reaction temperature of all polymers was 65 °C in order to thermally initiate the reactions. This was maintained for one hour and the reactions were then placed in room temperature baths to slowly polymerize over the course of seven days. This temperature shock treatment was used to form well-controlled low molecular weight pNIPAAm. The primary goal of using this method, rather than control using feed concentrations, is to allow for better tacticity control since it has been previously shown that reducing polymerization temperature increases the efficacy of bulky alcohols and Lewis bases as syndiotacticity-inducing agents [101, 106]. pNIPAAm synthesis was

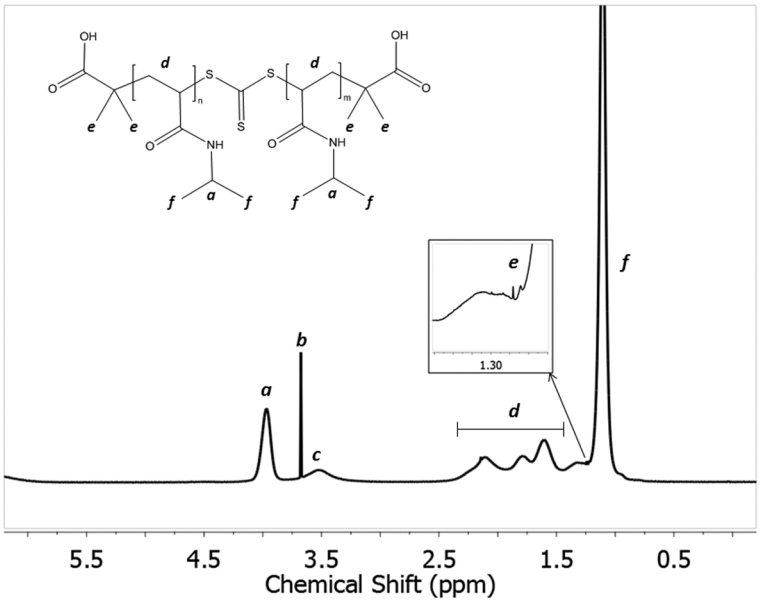

Figure 2.1: ^{1}H NMR spectra of pNIPAAm synthesized using **1** in chloroform-*d*. This polymer was synthesized at 65 °C for 48 hrs (pNIPAAm-**1**-HT; GPC M_n = 7500, PDI = 1.23). Peaks b and c corresponds to residual solvent peaks of 1,4 dioxane and water respectively. The peaks shown in d correspond to polymer backbone peaks in various configurations.

confirmed using ^{1}H NMR as shown in Figure 2.1.

Gel permeation chromatography (GPC) was conducted on pNIPAAm-**1** at various reaction times using a refractive index (RI) detector; traces are shown in Figure 2.2. Clearly the molecular weight continues to increase with time, indicating continued polymerization after reaching room temperature. The molecular weights and PDIs for the polymers are shown in Table 2.1. As expected for RAFT polymerization, the PDIs exhibited by the polymers are low, on the order of 1.1. This indicates good control despite the low conversion and overall molecular weight. Free radical polymerization, however, imparts a typically higher PDI (> 1.5). The table also indicates relatively consistent molecular weights regardless of polymerization times for free radical polymerization, indicating that within an hour of polymerization the reaction has already approached completion and further polymerization at room temperature did not affect conversion or final molecular weight.

Table 2.1: pNIPAAm was polymerized for varying periods of time at room temperature using 0.9 M NIPAAm solution in 1,4 dioxane. Thermal initiation was conducted by polymerizing in a preheated 65 °C oil bath for 1 hr and subsequent polymerization was conducted at room temperature. A high temperature control polymer (pNIPAAm-**1**-HT) was polymerized at 65 °C for 48 hrs.

	Feed molar ratio (NIPAAm:**1**:AIBN)	Total Reaction Time (hr)	M_n^a (NMR)	M_w (GPC)	M_n (GPC)	PDI[b]	Conversion (%)
pNIPAAm-**1**-1hr	100:1:0.5	1	3194	3800	3500	1.10	55.2
pNIPAAm-**1**-3hr	100:1:0.5	3	3316	4000	3700	1.09	57.3
pNIPAAm-**1**-6hr	100:1:0.5	6	3597	4000	3700	1.10	62.1
pNIPAAm-**1**-12hr	100:1:0.5	12	3815	4100	3700	1.12	65.9
pNIPAAm-**1**-1d	100:1:0.5	24	3974	4200	3800	1.10	68.6
pNIPAAm-**1**-2d	100:1:0.5	48	3981	4200	3800	1.10	68.8
pNIPAAm-**1**-3d	100:1:0.5	72	4122	4300	3900	1.10	71.2
pNIPAAm-**1**-4d	100:1:0.5	96	4127	4300	3900	1.10	71.3
pNIPAAm-**1**-7d	100:1:0.5	168	4150	4300	4000	1.09	71.7
pNIPAAm-r-1hr	100:0:1	1	10699	11300	6900	1.64	92.4
pNIPAAm-r-3hr	100:0:1	3	10732	14500	9600	1.51	92.7
pNIPAAm-r-6hr	100:0:1	6	10350	15300	9200	1.66	89.4
pNIPAAm-r-12hr	100:0:1	12	10330	16300	9200	1.77	89.2
pNIPAAm-r-1d	100:0:1	24	10668	16600	9400	1.77	92.1
pNIPAAm-r-2d	100:0:1	48	10466	19800	13200	1.50	90.4
pNIPAAm-r-3d	100:0:1	72	9958	19800	13200	1.50	86.0
pNIPAAm-r-7d	100:0:1	168	10946	7400	4700	1.56	94.5
pNIPAAm-**1**-HT	100:1:0.5	48	5762	9300	7500	1.23	97.0
pNIPAAm-**1**s-4d	100:1:0.5	96	-	4000	3800	1.06	-
pNIPAAm-**1**s-7d	100:1:0.5	168	-	4700	3900	1.22	-

[a]Theoretical molecular weight calculated by multiplying conversion and theoretical maximum molecular weight based on feed ratios. [b]PDI=M_w(GPC)/M_n(GPC)

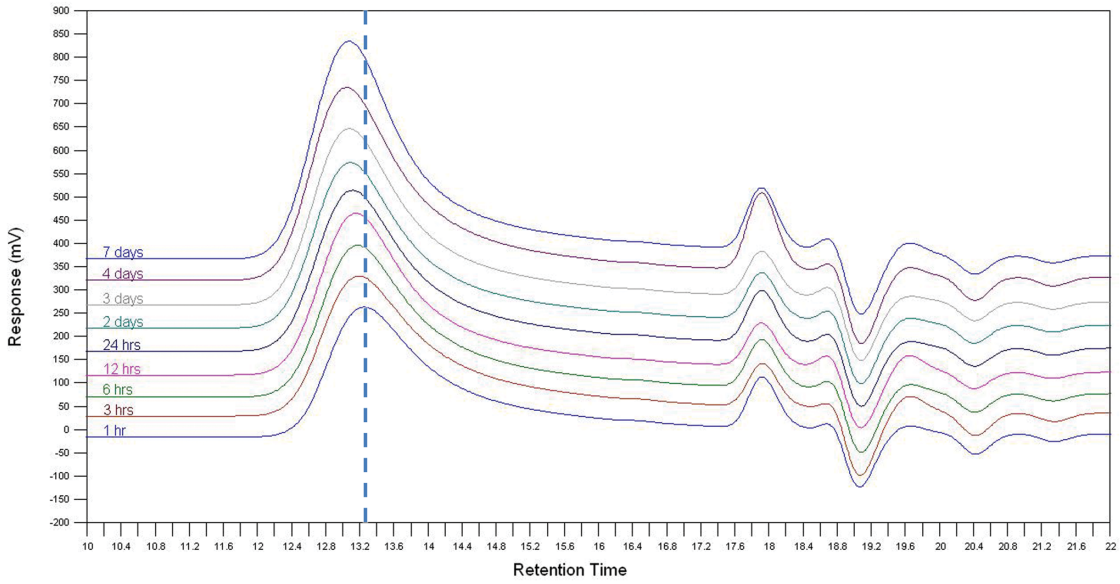

Figure 2.2: pNIPAAm-**1** polymerized for various lengths of time using a 100:1:0.5 ratio of NIPAAm:**1**:AIBN. The time indicated is the total reaction time with 1hr signifying a reaction for 1hr at 65 °C, 3hrs signifying reaction for 1hr at 65 °C and 2 hrs at room temperature, etc. As shown in the figure, molecular weight increases with increasing time with the dotted blue line representing the peak retention time for 1 hr of polymerization.

When the molecular weight of RAFT-polymerized pNIPAAm (the pNIPAAm-**1** series) was plotted against the conversion of the polymer, the approximation of a straight line was observed, as shown in Figure 2.3. This linear relationship, combined with the low PDIs of the polymers, are the hallmarks of CRP [48, 169] and confirm continued CRP at room temperature. In addition, while pNIPAAm polymerized for varying reaction times at a constant 65 °C reached 97% conversion within 4 hrs, the level of conversion only reached 71.1% after 7 days of polymerization at room temperature. This is to be expected due to the much higher glass transition temperature (T_g) of pNIPAAm (135 °C) when compared to the reaction temperature [237]. At moderate to high conversions, polymerization slows down considerably due to the vitrification effect, where the rate of propagation is hindered by the segmental diffusion of the polymer [77, 248, 174, 187]. As the polymer gets bigger, it becomes less soluble and coils more tightly. The polymerization rate then becomes diffusion

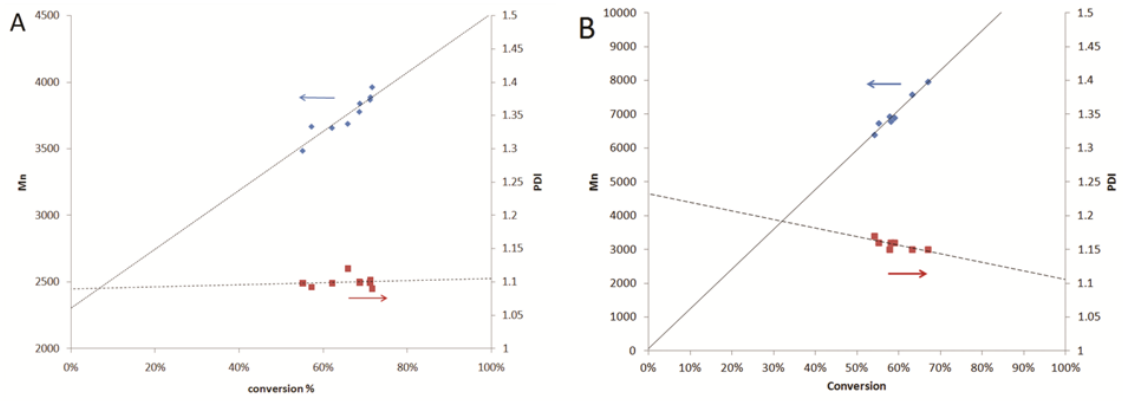

Figure 2.3: Molecular weight vs. conversion of A) pNIPAAm-**1** series and B) pNIPAAm-**1**s series. The solid line represents theoretical values. Linear correlations between conversion and M_n (R^2 values of 0.86 and 0.96 for pNIPAAm-**1** series and pNIPAAm-**1**s series, respectively) confirm living controlled radical polymerization. Nearly constant low PDI indicates that conversion is independent of PDI for these levels of conversion.

limited as the radicals must diffuse to the surface of the coil in order to propagate. This effect is more pronounced when pNIPAAm is polymerized at room temperature than when it's polymerized at 65 °C due to the larger temperature difference between T_g and the reaction temperature. Nearly complete conversion, such as that shown in the high temperature polymerization, is therefore not expected. Nevertheless, the values shown in Figure 2.3A indicate that reducing the reaction temperature, while slowing the reaction kinetics, did not change the characteristic linear increase of M_n as a function of conversion. It should also be noted that the PDI remained almost completely constant. We can therefore conclude that this method of polymerization does not affect the CRP while providing finer control over molecular weight.

In a separate experiment, the racemo diad promoting agent 3Me3PenOH was included in the polymerization process to confirm continued CRP behavior when synthesizing a majority syndiotactic polymer. The results of this experiment are shown in Table 2.2 and Figure 2.3B. As expected, the linear relationship between conversion and M_n continues to be observed. The PDIs of the system (on the order of 1.15) are also within the range of RAFT polymerization, although they are slightly

Table 2.2: pNIPAAm polymerization results in the presence of 3Me3PenOH. 0.9 M NIPAAm was reacted for varying periods of time in a 2:1 ratio of 3Me3PenOH to NIPAAm. Thermal initiation was conducted at 65 °C for 1.5 hrs.

	Polymerization Time at Room Temperature (hr)	Feed molar ratio (NIPAAm:**1**:AIBN)	M_n (NMR)[a]	M_n (GPC)	PDI	Conversion (%)
pNIPAAm-**1**s-a	0	100:1:0.5	6300	6400	1.17	54.1
pNIPAAm-**1**s-b	2	100:1:0.5	6400	6700	1.16	55.2
pNIPAAm-**1**s-c	5	100:1:0.5	6700	6900	1.15	57.8
pNIPAAm-**1**s-d	23	100:1:0.5	6700	6800	1.16	58.2
pNIPAAm-**1**s-e	47	100:1:0.5	6800	6900	1.16	59.0
pNIPAAm-**1**s-f	71	100:1:0.5	7300	7600	1.15	63.2
pNIPAAm-**1**s-g	95	100:1:0.5	7800	8000	1.15	67.0

[a]Theoretical molecular weight calculated by multiplying conversion and theoretical maximum molecular weight based on feed ratios

higher than those polymerized without the presence of 3Me3PenOH.

While both polymerization methods exhibited CRP, a direct comparison could not be made due to a longer thermal initiation time for the pNIPAAm-**1**s-a through pNIPAAm-**1**s-g series. Subsequently a new polymer (pNIPAAm-**1**s-4d, M_n=4100, PDI=1.15) was synthesized to directly compare pNIPAAm-**1**-4d with a majority racemo diad version of the same polymer (pNIPAAm-**1**s-4d). Both polymers were polymerized under the same conditions for four days and the GPC traces are shown in Figure 2.4. An ELS detector was used due to its higher sensitivity to low concentrations of polymer. As shown in Figure 2.4, pNIPAAm-**1**s-4d is slightly larger than the pNIPAAm-**1**-4d. This is as expected since the bulky alcohol acts as an accelerator during the polymerization process when used in conjunction with free radical polymerization [107]. It is therefore not surprising that it has a similar effect in RAFT polymerization. This acceleration may have also contributed to the slightly higher PDI of pNIPAAm-**1**s. In addition to having a larger polymer overall, pNIPAAm-**1**s shows a small peak at 12.5 minutes into the elution. This peak corresponds to higher molecular weight polymers and/or aggregates (15200 Da) that may have formed as a

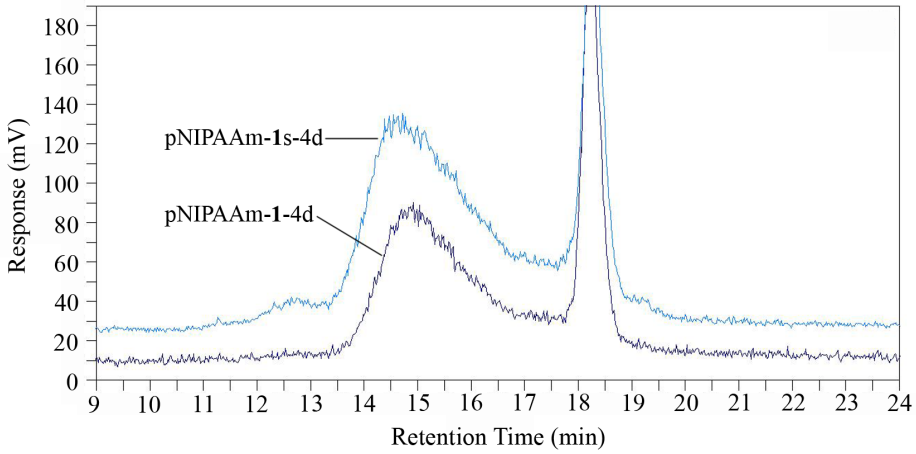

Figure 2.4: GPC traces using ELS detector of pNIPAAm-**1**-4d and pNIPAAm-**1**s-4d (M_n = 3700 and 4100, respectively)

result of termination reactions and represents 2.4% of the total polymers. The traces indicate that this sample of pNIPAAm-**1**-4d has a molecular weight of 3700 Da with a PDI of 1.13 while pNIPAAm-**1**s-4d has a molecular weight of 4100 Da with a PDI of 1.15.

2.4.2 MW and End Group Control Influence on LCST

The measured cloud point temperature (T_{cp}), indicative of the LCST, is taken in this thesis to be the temperature at which normalized transmittance drops to 50%. As expected, pNIPAAm polymerized through free radical polymerization shows a sharp T_{cp} at 32 °C in deionized water (Figure 2.5A). This is independent of the polymerization conditions and can be seen in long-term low temperature polymerization as well as short-term high temperature polymerizations. This temperature is shifted to 28 °C when measured in PBS (Figure 2.5A), the commonly accepted ion concentration and pH for physiological systems. The decrease in transition temperature is due to the destabilizing effects of the salt ions in an aqueous solution [312]. Both sodium chloride and sodium phosphate are known to decrease the LCST and even split it into two or more transitions depending on concentration [312]. While physiological concentrations of NaCl and NaH_2PO_4 are insufficient to induce the splitting of the

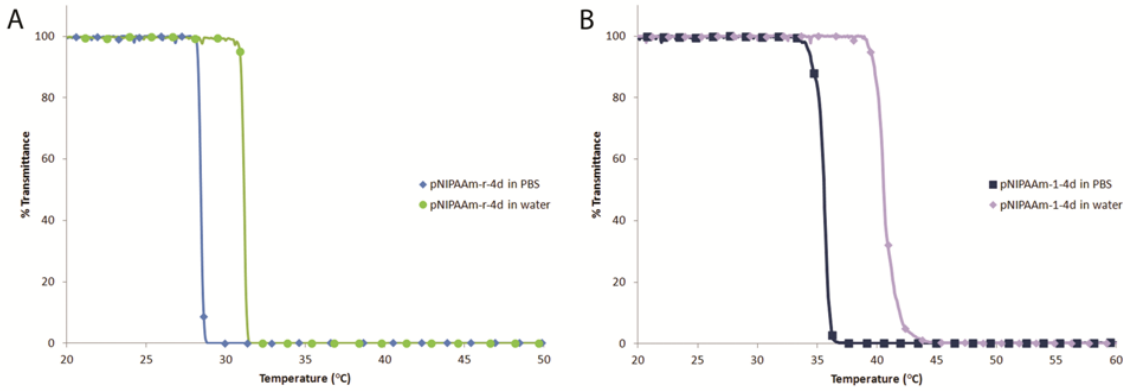

Figure 2.5: Changes in the T_{cp} of polymers assessed in deionized water (18 mΩ) and PBS. A) pNIPAAm-r-4d and B) pNIPAAm-**1**-4d. The T_{cp} changes from 32 °C to 28 °C and 40.5 °C to 35.5 °C for pNIPAAm-r-3d and pNIPAAm-**1**-4d respectively.

LCST, the reduction in LCST is still significant.

With the addition of **1** as the RAFT agent, the T_{cp} is significantly increased to 40.5 °C when measured in water (Figure 2.5B). The acetic acid end groups (from the RAFT agent) act in a similar manner to hydrophilic co-monomers, especially at low molecular weights [153].

To analyze this effect, pNIPAAm of several molecular weights was synthesized using RAFT polymerization with **1** at 65 °C. The T_{cp} was measured and is shown in Figure 2.6. As shown in the figure, the T_{cp} shifting effect of the end-groups decreases drastically with increased molecular weight. This data is in good agreement with the literature [286] and the effect appears to be linear between these molecular weights with a correlation coefficient of 0.94. When extrapolated to the molecular weight of pNIPAAm-**1**-4d, which has a molecular weight of 3900, we expect a T_{cp} of 40.4 °C, remarkably close to the actual observed T_{cp} of 40.5 °C.

To compare the end-group effect with analogous copolymer systems, we compared our sample of pNIPAAm-**1**-4d to pNIPAAm-*co*-AAc copolymers with a target degree of polymerization (DP) of 50 and an acrylic acid content of 4%. Such polymers should theoretically have approximately 2 AAc groups per polymer, similar to the 2 acid groups from the RAFT polymerization, and comparable molecular weights. Due

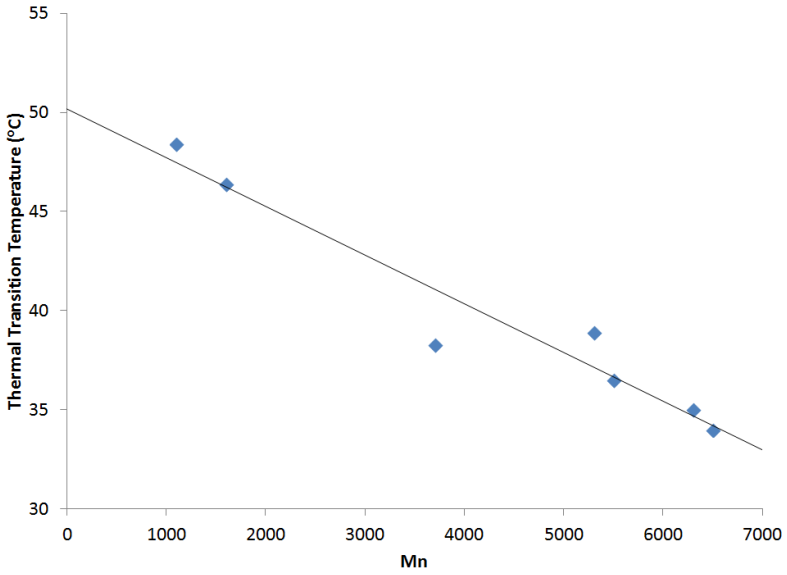

Figure 2.6: Molecular weight dependence of end-group efficacy. As M_n increases, the end-groups become less effective. The T_{cp} dependence on M_n is linear with an R^2 value of 0.94.

to the difficulty in achieving a specific target molecular weight using free radical polymerization, two different samples with number averaged molecular weights near that of pNIPAAm-**1**-4d are presented. The T_{cp} of the polymers are shown in Figure 2.7.

Compared to copolymers of comparable molecular weights, pNIPAAm-**1**-4d shows a higher T_{cp} than both the 4900 MW copolymer and the 6100 MW copolymer, with the higher molecular weight copolymer exhibiting a closer T_{cp} curve to pNIPAAm-**1**-4d than the lower molecular weight samples. Expected T_{cp}s of pNIPAAm polymerized with **1** based on the M_n vs T_{cp} correlation are 37.9 °C and 34.9 °C for 4900 and 6100 MW polymers, respectively. Observed T_{cp}s for the copolymer are 34.6 °C and 36.7 °C for 4900 and 6100 MW polymers, respectively, several degrees from the expected value for end-group effects. Clearly the use of copolymerization and the use of end-groups elicit different bulk behaviors of pNIPAAm, with the copolymer exibiting a contrary molecular weight vs T_{cp} trend from that of the end-group controlled polymers. It is interesting to note that sensitivity of the T_{cp} to molecular weight is not eliminated in the copolymers. Higher molecular weight copolymers have larger effects on the

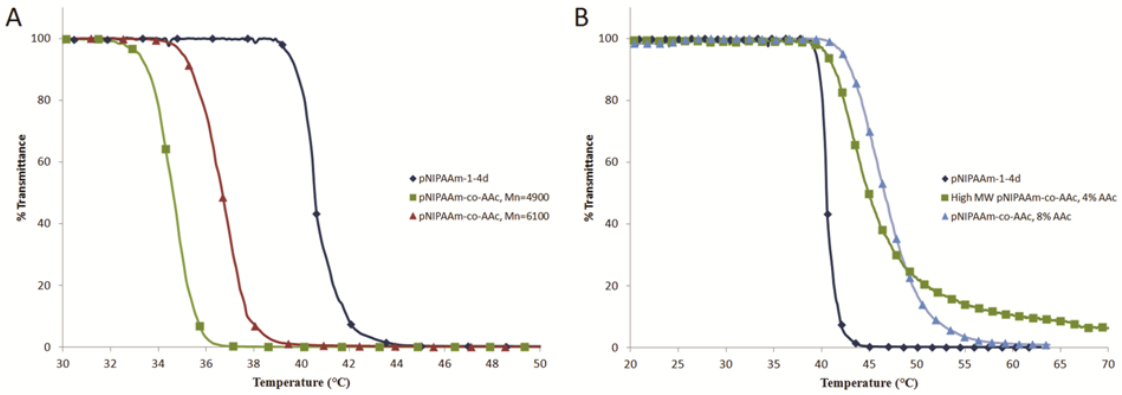

Figure 2.7: Normalized transmittance of 1wt% aqueous solutions of pNIPAAm-**1**-4d and pNIPAAm-*co*-AAc. A) pNIPAAm-*co*-AAc with 4% AAc content and similar molecular weights to pNIPAAm-**1**-4d (M_n of 4900 and 6100 with PDIs of 1.9 and 2.2 respectively) and B) higher MW 4% AAc content polymer (M_n=11800, PDI=1.7) as well as low molecular weight 8% AAc polymer (M_n = 5000, PDI = 1.9).

T_{cp} despite having the same theoretical percentage of AAc content. A proposed explanation for this can be that higher molecular weight pNIPAAm is more coiled in solution; therefore, the hydrophilic properties of AAc are more effective in raising the T_{cp} compared to the lower molecular weight polymers. In addition to this difference between the systems, the characteristic widening of the T_{cp} curve in these copolymers is small at these low molecular weights. Since these copolymers were formed through free radical polymerization and have high PDIs (>1.9), it is likely that many chains contain fewer than the anticipated number of hydrophilic groups. Due to the low number of expected acrylic acid groups per polymer (approximately 2), the variation can lead to lower thermal transition temperatures and the still somewhat sharp transitions exhibited.

When polymerized to higher molecular weight (M_n=11800, PDI=1.7) to reduce this effect, as shown in Figure 2.7B, the start of the thermal transition is almost identical to that of pNIPAAm-**1**-4d; however, the range of transition for pNIPAAm-**1**-4d was 2.3 °C, while the range for high MW pNIPAAm-*co*-AAc was greater than 10 °C. Furthermore, pNIPAAm-*co*-AAc did not reach a stable transmittance until

26 °C above the start of the transition. The T_{cp} for the two polymers are also quite different: 44.9 °C and 40.5 °C for pNIPAAm-*co*-AAc and pNIPAAm-**1** respectively. The similar starting temperatures for the transitions suggest that comparable ratios of hydrophilic groups were incorporated into both polymers, and the large difference in transition temperature ranges can again be attributed to the less well-defined nature of the copolymer. On the other hand, the exclusion or inclusion of one or two acrylic acid groups per polymer chain will not change the acrylic acid content as drastically as in the case of the lower molecular weight copolymers. In an effort to reproduce both the molecular weight and the thermal transition of pNIPAAm-**1**-4d, an 8% AAc copolymer with an M_n of 5000 was also synthesized (Figure 2.7B). As expected, this polymer showed a much higher thermal transition of 46.7 °C than the comparable 4% AAc copolymers. It also exhibited a broader transition, taking place over 13.5 °, indicative of more widespread incorporation of the acrylic acid co-monomer. The manipulation required to synthesize copolymers having thermal transition characteristics comparable to our RAFT homopolymer, a more or less iterative process involving multiple variables, confirms the superiority of our method of LCST modification over the traditional copolymerization method.

2.4.3 Tacticity Control Over LCST

A secondary effect of using **1** in the polymerization scheme is the increase of racemo diads in the overall pNIPAAm polymer. While the number of acetic acid groups is limited to the small amount of RAFT agent available during the polymerization and is inconsequential compared to the concentration of a solvent additive like 3Me3PenOH, the effect is still pronounced, as shown in Figure 2.8A and 2.8B.

As shown from the methine backbone peaks, there is a slight increase in the percentage of racemo diads when using **1**. The racemo content increases from 54.6%

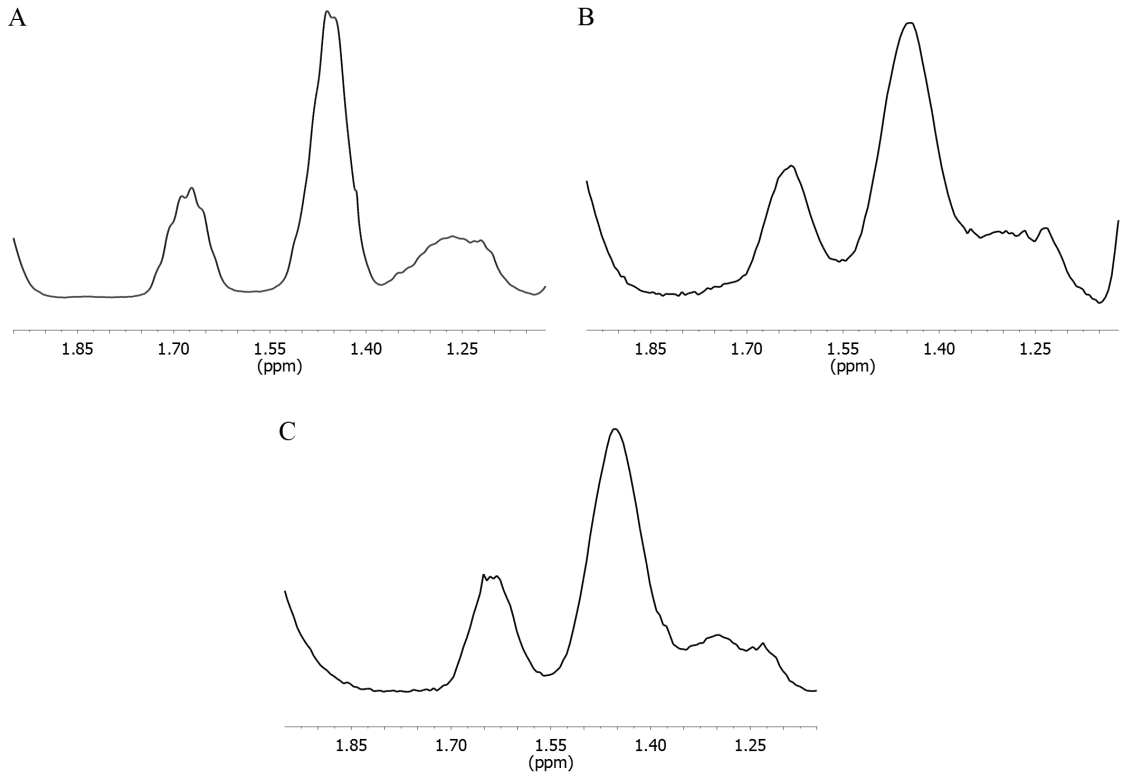

Figure 2.8: Methine backbone peaks of A) free radical polymerized pNIPAAm showing 54.6% racemo diads, B) pNIPAAm-**1**-4d showing 58.6% racemo diads, and C) pNIPAAm-**1**s-4d showing 61.1% racemo diads. The peaks at 1.67 ppm and 1.27 ppm correspond to meso diads while the peak at 1.46 ppm corresponds to racemo diads.

in free radical polymerization to 58.4% in polymerization with **1**. When polymerized with 3Me3PenOH however, the racemo content further increases to 61.1% (Figure 2.8C). Previous studies on the relationship between diad tacticity and racemo diad promoting agent properties have shown an inverse relationship between pKa and racemo diad content [292]. Therefore, it is not surprising that the RAFT agent has an outsized effect on the tacticity despite its low concentration, since the acetic acid groups on the end of the RAFT agent have a much smaller pKa than 3Me3PenOH. These tacticity changes, though small, have a significant effect on the observed T_{cp}s, which is consistent with previous work in which pNIPAAm having a higher percentage of racemo diads displays higher T_{cp}s [107].

Figure 2.9 shows the difference that a small change in tacticity can make in the T_{cp} of pNIPAAm. When polymerized for 4 days at room temperature, we see a transition temperature increase from 40.5 °C to 43.3 °C. When polymerized for 7 days at room temperature, we see a transition temperature increase from 39.7 °C to 42.2 °C. When polymerized normally at 65 °C for 48 hrs to insure completion, pNIPAAm polymerized with **1** has an T_{cp} at 33.7 °C, slightly higher than that of free radical polymerized pNIPAAm, but not high enough for applications in biotechnology. With the inclusion of 3Me3PenOH to induce stereospecific polymerization, the transition temperature is increased to 35 °C.

From this, we deduce that by polymerizing slowly for a long period of time the bulky alcohol has more opportunity to induce racemo diads. The T_{cp} shift stays constant at $\sim$ 2.7 °C for both the 4-day and 7-day polymerizations, while it decreases to a 1.3 °C difference with faster, 48 hr reactions at 65 °C. This is further confirmed using NMR, in which the methine backbone of the higher reaction temperature pNIPAAm with 3Me3PenOH shows a lower racemo diad content of 60% (see Figure B.2 in Appendix B).

The slight decrease in LCST between the 4-day and 7-day polymerizations can

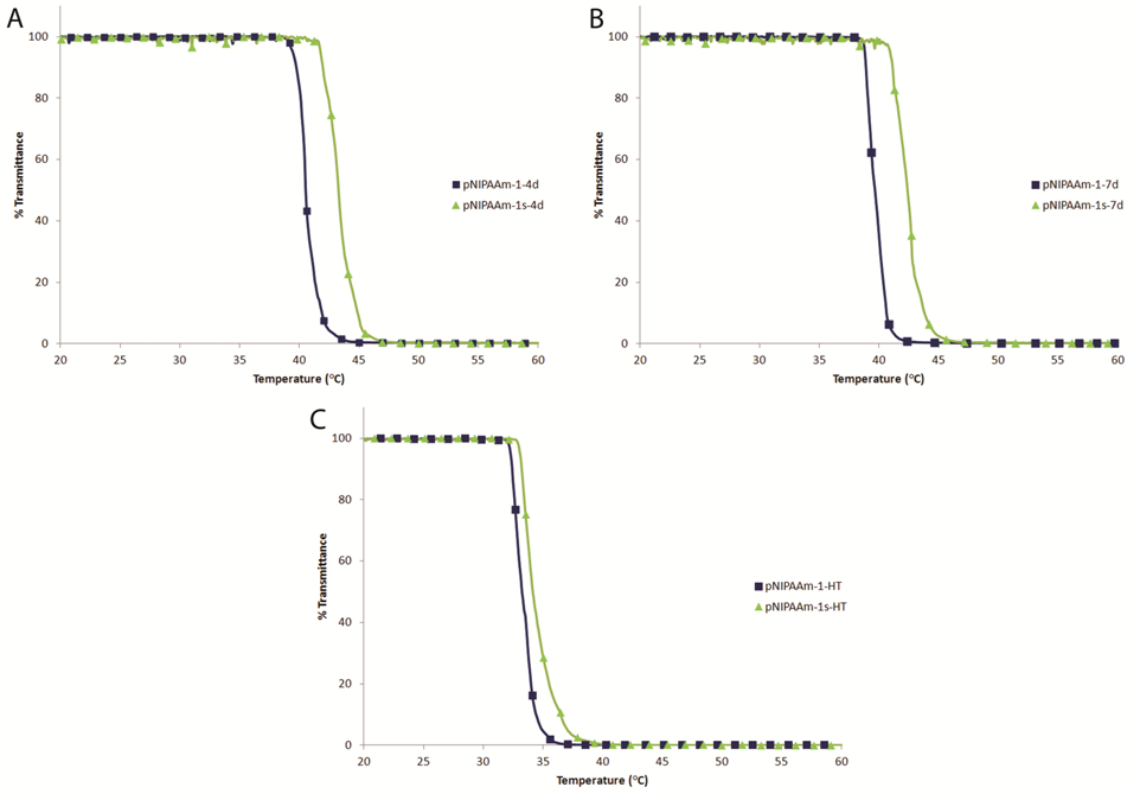

Figure 2.9: Normalized transmittance of 1 wt% aqueous solution of A) pNIPAAm-**1**-4d and pNIPAAm-**1**s-4d (T_{cp}=40.5 °C and 43.3 °C respectively), B) pNIPAAm-**1**-7d and pNIPAAm-**1**s-7d (T_{cp}=39.7 °C and 42.4 °C respectively), C) pNIPAAm-**1** polymerized to completion at 65 °C (T_{cp}=33.7 °C and 35.0 °C for pNIPAAm-**1** and pNIPAAm-**1**s respectively).

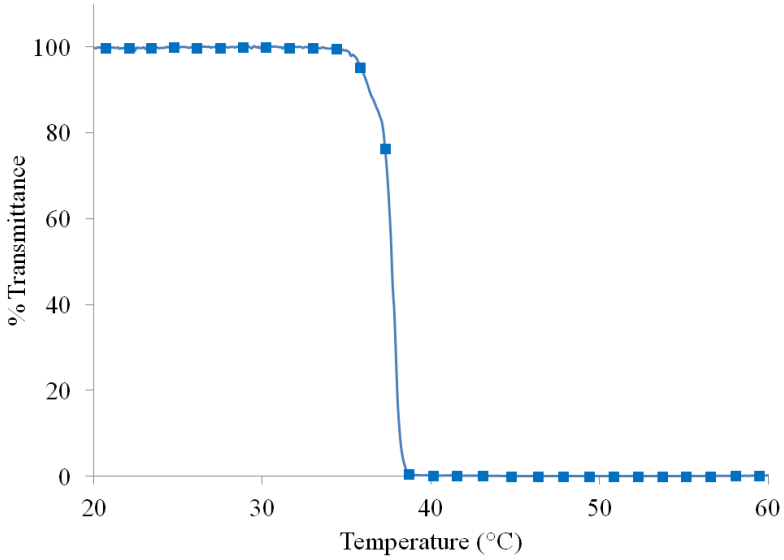

Figure 2.10: Normalized transmittance of 1wt% solution of pNIPAAm-**1**-4d polymerized with additional 3Me3PenOH in PBS.

be attributed to the larger size of the 7-day polymer, having a M_n of 4000 (PDI = 1.07) compared to an M_n of 3500 (PDI = 1.13) for chains polymerized for 4 days. As expected, the higher molecular weight slightly inhibits the effect of the acetic acid end groups.

Due to the further increase in T_{cp} by inducing a larger percentage of racemo diads, and the relative stability of that 2.7 °C increase, we are therefore able to combine tacticity control with the properties of **1** to produce a NIPAAm polymer that undergoes a sharp thermal transition temperature at 37.6 °C, exactly within physiological temperature range, in a solution of PBS as shown in Figure 2.10. This transition takes place 2.1 °C above the transition temperature of the pNIPAAm synthesized in the presence of 3Me3PenOH and occurs within a span of 2 °C. Such a polymer with its low PDI of 1.15 and lack of co-monomers can greatly improve the sensitivity to temperature that pNIPAAm copolymer systems for biological applications currently lack.

2.5 Conclusion

Successful applications of pNIPAAm for biological purposes have been limited in part due to the trade-off between having a temperature transition at physiological temperatures and having a very sharp transition. We have shown in this chapter that this problem can be overcome by implementing various polymerization methods and tools to modify the polymer structure. By polymerizing slowly with **1** over the course of four days while inducing racemo diad formation, we were able to synthesize well-defined pNIPAAm with a sharp LCST of 37.6 °C in a solution of PBS. This reaction scheme combines tacticity control with RAFT polymerization, molecular weight control, and end-group control. Such polymers can be used for more accurate transitions in drug delivery, diagnostics, BioMEMs, and other applications in biotechnology.

CHAPTER III

APPLICATION OF STRUCTURALLY CONTROLLED PNIPAAM IN HYDROGEL SYSTEMS

3.1 Summary

pNIPAAm hydrogels are often used in a variety of biomedical applications including drug delivery. The thermal transition characteristic of pNIPAAm causes dramatic macroscopic changes in pNIPAAm hydrogels. In order to explore transferable properties from single chains of pNIPAAm into more complex systems, we have applied the polymers formed with structural control (as described in Chapter 2) to pNIPAAm hydrogels. These gels exhibit far greater shrinking characteristics as well as higher LCSTs compared to traditionally formed pNIPAAm hydrogels. These characteristics are in line with the properties of pNIPAAm in solution. For example, modification of end-groups yields changes in the gelation properties and transition temperature. In addition, these gels also exhibit physiological mechanical properties. The gels demonstrate that structural transformations of pNIPAAm polymer chains carry over into hydrogel systems and with the proper optimization, a superior thermally-responsive hydrogel can be formed with potential applications in drug delivery.

3.2 Introduction

A major class of biomaterial used in many current biomedical applications is the hydrogel [200]. These versatile materials can act as cell scaffolds both *in vitro* [194, 251] and *in vivo* [27, 221] and have been applied in a variety of drug delivery applications [131, 200, 293, 236, 27]. Stimuli responsive (or 'smart') hydrogels in particular

have been of interest for these purposes [42, 200]. Thermally responsive and pH responsive hydrogels are often used in drug delivery constructs [43, 17, 90]. These often multi-responsive constructs, including microgels [203], nanogels [152, 178], and hybrid gel-nanoparticle drug releasing systems [59, 255], traditionally take advantage of the slight changes in conditions at various physiological locations to affect 'smart' release, although externally triggered gels is a rapidly advancing technology [135, 255].

pNIPAAm in particular is the most common thermally responsive material used in biologically relevant hydrogels [90, 159, 53]. The temperature transition and subsequent dehydration of pNIPAAm hydrogels at 32 °C has been used in applications as varied as LCST precipitated gel formation and cell encapsulation [33, 265], and temperature transition mediated cell sheet detachment [156, 273, 181], to temperature activated drug delivery nanoparticles [135]. The transition, however is exclusively mediated through copolymer incorporation and transition control based upon structural modifications of linear pNIPAAm chains is currently unexplored.

3.2.1 Shortcomings of traditional pNIPAAm hydrogels

Traditional pNIPAAm hydrogels are synthesized through polymerization of NIPAAm monomer in the presence of crosslinker (usually ethylene glycol dimethacrylate (EGDMA) or methylene bisacrylamide (MBAm)) [225]. Hydrogels synthesized in this way have poor architectural control and generally exhibit broad transition behavior (on the order of 5 °C) and a transition around 32 °C [197]. Since control of the LCST of pNIPAAm hydrogels is completely reliant upon copolymers, often -*co*-AAc. The resulting hydrogels generally have broader transitions, on the order of 15 °C [197], and therefore is no longer sensitive to small changes in temperature or suitable for the on-off type applications for which pNIPAAm is most commonly used [287, 273]. The broad transition tempers a key advantage of using pNIPAAm as the thermally responsive polymer, thereby reducing the efficacy of the hydrogel as a drug delivery vehicle. The

addition of significant acrylic acid groups to the hydrogel, while making the hydrogel pH responsive, also introduces complex ionic effects to the system [143].

As nanoconstructs become increasingly complex, pNIPAAm hydrogel synthesis has deviated significantly from traditional methods to include reversible crosslinking [167], interpenetrating networks [159, 94], and copolymers with functional side chains that crosslink [15]. These approaches provide additional functionality to hydrogels but do not address the temperature response or response rate. Instead, optimizing for response rate has been approached by the formation of more porous structures such as gelation above the LCST to form heterogeneous gels [252, 224, 133], gelation in the presence of porogens [315, 193, 44], gelation under freezing conditions [291, 290], and other porosity increasing methods [87, 16, 6]. Additionally, chemical strategies such as grafting hydrophilic copolymers [73, 64], bonding surfactants [185, 289], and using RAFT polymerization [158, 157] have been shown to be effective ways to accelerate shrinking kinetics. With the exception of using RAFT polymerization, these strategies rely upon macrostructures or chemical additives to achieve these results [311].

In this chapter, we use the optimized pNIPAAm synthesized in Chapter 2, as well as other RAFT polymerized pNIPAAm to form novel pNIPAAm hydrogels controlled by polymer chain architecture. The scheme uses re-initiation and chain extension of RAFT polymerized pNIPAAm, as shown in Scheme 3.1. While it is known that this RAFT chain extension crosslinking does change the swelling characteristics of the resulting hydrogel [158], to our knowledge this is the first usage of end-group and tacticity modified pNIPAAm in hydrogel systems. These hydrogels exhibit physiological LCSTs without copolymers, shrink to a greater extent than traditional gels, and exhibit mechanical properties comparable to human tissue.

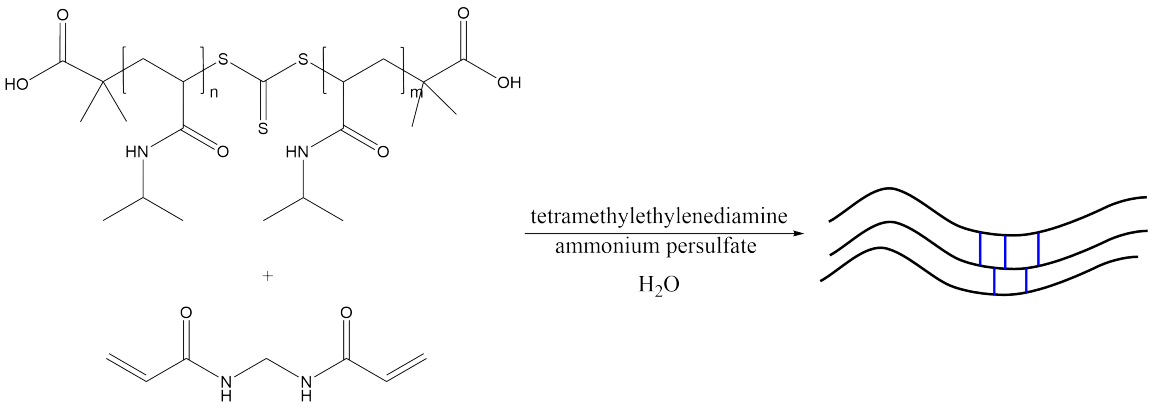

Scheme 3.1: pNIPAAm chain extension hydrogel synthesis.

3.3 Materials and Methods

N-isopropylacrylamide was purchased from TCI America and recrystallized in a 9:1 ratio of hexanes:benzene. Tetramethylethylenediamine (TEMED), methylene bisacrylamide, ammonium persulfate, cyanomethyl dodecyl trithiocarbonate, 1-dodecanethiol, Aliquat 336, carbon disulfide, hydrogen chloride, azobisisobutyronitrile, and 3Me3PenOH were purchased from Sigma Aldrich and used without further purification. Chloroform, methanol, and acetone were purchased from BDH Chemicals and used without further purification.

3.3.1 2-dodecylsulfanylthiocarbonylsulfanyl-2-methyl-propionic acid (DMP) Synthesis

DMP was synthesized as reported by Lai et al [146]. Briefly, 8.09 g of 1-dodecanethiol was reacted with 19.5 g of acetone, and 0.647 g of Aliquat 336 under nitrogen at 10 °C. 6 g of 50% sodium hydroxide solution was added dropwise to the reaction over 20 mins. The reaction was allowed to proceed for an additional 15 mins before a solution of 2.4 mL of carbon disulfide in 5.1 mL of acetone was added dropwise over 20 mins. The reaction was allowed to proceed for an additional 10 mins and 4.8 mL of chloroform was added in one shot. 10 g of 50% sodium hydroxide solution was added dropwise over 30 mins. The reaction was allowed to proceed overnight at 10 °C.

Upon completion, 60 mL of 17.5 MΩ nanopure water was added to the reaction mixture. The solution was then acidified with 25 mL of 6N HCl. The remaining acetone was evaporated by purging the reaction vessel with nitrogen for 20 mins while stirring at 500 rpm. The solution was then filtered. The filter cake was stirred into 100 mL of methanol. The resulting mixture was filtered again with the solid product discarded and the liquid left to crystallize. The resulting product was recrystallized in hexanes and characterized using ^{1}H NMR.

3.3.2 pNIPAAm synthesis

Atactic and syndiotactic pNIPAAm were synthesized as described in Chapter 2. High temperature polymerized atactic polymers, DMP controlled polymers, and cyanomethyl dodecyl trithiocarbonate controlled polymers were synthesized using typical RAFT polymerization techniques. Briefly, a 3.2 g mixture of 100:1:0.5 ratio of NIPAAm:RAFT agent:AIBN was placed in a sealed 25 mL round-bottom flask equipped with a magnetic stir bar. The mixture was purged with nitrogen for 15 minutes and 20 mL of nitrogen-purged 1, 4 dioxane was added. The solution was reacted at 65 °C for 48 hrs. The polymer was precipitated in chilled diethyl ether and collected via filtration. The samples were then dissolved in nanopure water and dialyzed with a 2000 MWCO membrane. The water was changed at 0.5 hr, 1 hr, 2 hrs, 3 hrs and 20 hrs. The samples were then frozen and lyophilized.

Polymers were characterized using GPC, NMR, MALDI mass spectrometry, and UV-Vis spectrometry. GPC was conducted on a PL-GPC 50 with UV, RI, and ELS detectors (Agilent, Inc.) equipped with two Plgel 3μm MIXED-E columns. Filtered stabilized tetrahydrofuran was used as the polymer solvent and GPC eluent at a flow rate of 1 mL/min. Chromatograms were compared with those of polystyrene standards (Agilent Inc). ^{1}H NMR was conducted on a Varian Mercury Vx 400 spectrometer using chloroform-*d* as solvent for room temperature experiments or DMSO-*d*6

as a solvent at 90 °C. UV-Vis spectrometry was conducted using a Cary 50 UV-Vis Spectrophotometer (Agilent Inc.) with the single cell peltier thermostatted cell holder and accessory for temperature control. Temperature was ramped at a rate of 1 ° per minute and data points were taken every 0.1 °.

3.3.3 pNIPAAm hydrogel synthesis

Six different pNIPAAm hydrogels were synthesized (see Scheme 3.2). Atactic and syndiotactic pNIPAAm as synthesized in Chapter 2 were used in pNIPAAm-A and pNIPAAm-S hydrogels, respectively. High temperature polymerized atactic pNIPAAm, DMP controlled pNIPAAm, and cyanomethyl dodecyl trithiocarbonate controlled pNIPAAm were used in pNIPAAm-A-HT, pNIPAAm-D, and pNIPAAm-C hydrogels respectively. Control hydrogels formed by traditional pNIPAAm hydrogel synthesis with NIPAAm monomer were also synthesized and labeled pNIPAAm-M. All hydrogels were synthesized using the following method. 200 mg of pNIPAAm, 77 mg of MBAm, and 25 μL of TEMED were dissolved in 2.5 mL of nanopure water. The solution was purged with nitrogen for 15 minutes. 57 mg of ammonium persulfate was then dissolved in 200 μL of water. The two solutions were then reacted in a 3 mL plastic syringe for ten minutes to form cylindrical gels. The gels were then removed from the plastic syringes and swelled in nanopure water for 24 hours prior to experimentation. Six gels were condition were used in the following studies.

3.3.4 Gel characterization

Gel properties were characterized using SEM and mechanical testing. SEM was conducted using a Hitachi S-3700N VP-SEM operating at 6 Pa. Uniaxial compression testing was conducted on a Bose Endura TEC ELF 3200 Uniaxial Testing System. Briefly, gels were cut into cylinders 10 mm long and 14 mm wide and a 100 N load cell was applied using a loading speed of 0.25 mm/s.

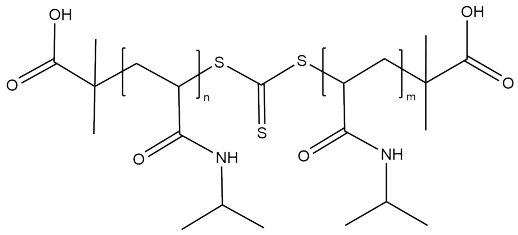

pNIPAAm-A, pNIPAAm-A-HT, pNIPAAm-S

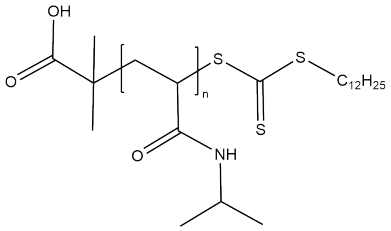

pNIPAAm-D

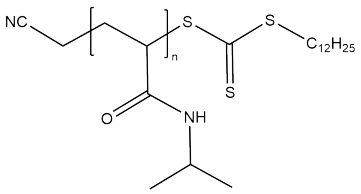

pNIPAAm-C

Scheme 3.2: pNIPAAm-A, pNIPAAm-S, and pNIPAAm-A-HT all have the same chemical formula but are polymerized under different conditions and have different tacticity. pNIPAAm-D was polymerized with DMP and pNIPAAm-C was polymerized with cyanomethyl dodecyl trithiocarbonate.

3.3.5 Gel shrinking

Gel shrinking was analyzed using two methods. First, the rates of gel shrinkage was tested. The gels were weighed and placed in fresh nanopure water. The solutions were heated up to 50 °C and the gels were removed from solution, dabbed dry, and re-weighed every minute for ten minutes.

The LCST of the gels was also determined through similar methods. Gels were placed in fresh nanopure water in poly(methyl methacrylate) cuvettes. The cuvettes were heated in a peltier controlled heater and allowed to stabilize at the set temperature for fifteen minutes. The gels were then removed, dabbed dry, and weighed. This was repeated every 2 °C from 25 °C to 50 °C.

3.4 Results and Discussion

pNIPAAm was synthesized using six different methods, and the resulting molecular weights are shown in Table 3.1. As shown, the low PDIs (near 1.1) indicate control

Table 3.1: pNIPAAm synthesized using various conditions and RAFT agents.

	M_n	M_w	PDI
pNIPAAm-A	6700	8800	1.3
pNIPAAm-S	5700	6700	1.1
pNIPAAm-A-HT	6000	7300	1.2
pNIPAAm-D	6200	8000	1.3
pNIPAAm-C	7500	8400	1.1

over the molecular weight and RAFT polymerization. Additionally, the molecular weights are comparable and therefore the differences shown in the hydrogels are not a function of molecular weight.

LCST data for the polymers in solution was also collected. As shown in Figure 3.1, the end-groups cause varying effects on the LCSTs of pNIPAAm. The more hydrophobic cyanomethyl dodecyl trithiocarbonate reduces the LCST to 29.3 °C. The amphiphilic DMP shows a sharp transition at 30.4 °C to half of its original value and gradually continues to decrease for more than 10 °. The high temperature polymerized atactic pNIPAAm (pNIPAAm-A-HT) shows a sharp transition at 32.8 °C, slightly above that of free radical polymerized pNIPAAm. pNIPAAm-A and pNIPAAm-S show higher transitions, as expected, at 35.5 °C and 36.6 °C, respectively.

The changes in the LCST of pNIPAAm-A, pNIPAAm-S and pNIPAAm-A-HT due to the end-groups are comparable to those shown in Chapter 2. pNIPAAm-C and pNIPAAm-D, however, show more nuanced results. pNIPAAm-C has a highly lipophilic dodecane end, which has a calculated octanol-water partition coefficient (logP) of 6.1, and a slightly hydrophilic nitrile group with an logP of -0.02 [257]. The nitrile group is a weak hydrogen bond acceptor but is not charged at neutral pH and does not significantly distort the structured water dissolving the pNIPAAm. Because of this, the nitrile group does not play a significant role in the LCST behaviour of pNIPAAm. The dodecane group, however, is of intermediate length and

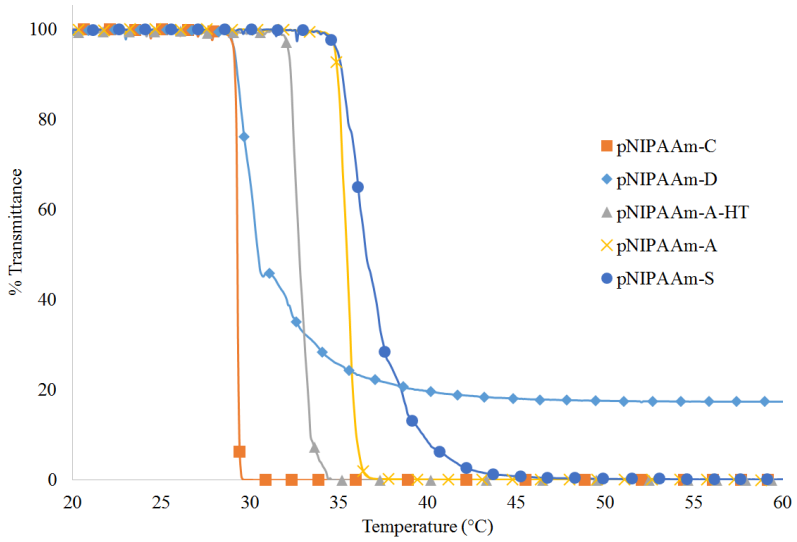

Figure 3.1: LCSTs of different pNIPAAm polymers. pNIPAAm-C, pNIPAAm-A-HT, pNIPAAm-A, and pNIPAAm-S show LCSTs at 29.3, 32.7, 35.5, and 36.6 °C, respectively. pNIPAAm-D shows a partial transition at 30.4 °C.

exists between linear and U-shaped chains [34], potentially significantly distorting the surrounding structured water, and therefore causing a 2.7 °C shift toward lower temperatures. By comparison, pNIPAAm-D, also has a dodecane chain end on one side, but has a highly hydrophilic propionic acid chain end on the other side, with a logP of -0.7 for the acid group [148]. The transition curve shows the result of both of these end-groups with a sharp initial transition at 29.3 °C and a gradual decrease thereafter. Propionic acid has a pK_a of 4.87 and is therefore charged at neutral pH, causing stabilization in the surrounding structured water. It is speculated that the difference between these two end groups and their locations on opposite ends of the chain causes partial chain collapse until sufficient energy is provided, resulting in the profile shown in Figure 3.1.

3.4.1 Hydrogel synthesis and characterization

RAFT-mediated chain extension hydrogel formation was optimized using pNIPAAm-A. As shown in Table 3.2, a polymer to crosslinker ratio of 5:1 did not consistently form hydrogels; a 10:1 ratio was needed. While under ideal conditions, only a 2:1 ratio

Table 3.2: pNIPAAm-A hydrogels synthesized with varying amounts of crosslinker (n=6)

	Ratio of polymer to crosslinker to initiator	Time to polymerize
pNIPAAm-A	1:5:1	No gelation
pNIPAAm-A	1:5:3	Partial gelation
pNIPAAm-A	1:5:5	Partial gelation
pNIPAAm-A	1:10:1	16 h
pNIPAAm-A	1:10:3	25 s
pNIPAAm-A	1:10:5	15 s
pNIPAAm-A	1:15:1	120 s
pNIPAAm-A	1:15:3	45 s
pNIPAAm-A	1:15:5	8 s

is strictly necessary for chemical crosslinking to form hydrogels, the chain extension system only allows for incorporation at the CTA locations. The requisite proximity of these groups for reaction promotes multiple links between the same polymers and therefore greater ratios are required for proper crosslinking.

A 1:10:5 ratio of polymer to crosslinker to initiator was chosen for subsequent experiments due to the ease of synthesis. Comparable systems and their gelation times are shown in Table 3.3. As shown, systems behaved very differently depending upon the RAFT agent and the polymer synthesis conditions. Traditionally formed comparable pNIPAAm (pNIPAAm-M) exhibits drastically different results from all of the other systems, forming a stiff, opaque hydrogel within one second. Other systems formed between 10 s and 15 mins.

Of particular interest is the difference between pNIPAAm-A-HT, pNIPAAm-A, and pNIPAAm-S. All three are synthesized using the same RAFT agent and are of similar molecular weight, but pNIPAAm-A-HT takes 60 times as long to form compared to the other two gel types. Prior work describes gels forming with different properties due to diverse sets of reaction conditions including crosslinking temperature

Table 3.3: pNIPAAm hydrogels synthesized with different pre-polymerized pNIPAAm under the same conditions (n=6).

	Ratio of polymer to crosslinker to initiator	Time to polymerize
pNIPAAm-A	1:10:5	15 s
pNIPAAm-M	100:10:5	$>$ 1s
pNIPAAm-S	1:10:5	10 s
pNIPAAm-A-HT	1:10:5	12 $\pm$ 4 mins
pNIPAAm-D	1:10:5	15 $\pm$ 5 mins
pNIPAAm-C	1:10:5	2 mins

and mold geometry [84]; however, pNIPAAm-A-HT, pNIPAAm-A, and pNIPAAm-S gels were all synthesized using the same mold and temperature. Since the only difference between these polymers is the pre-polymerization temperature, the only conclusion is that polymerization temperature affects the gelation properties.

For additional characterization, mechanical testing was conducted on pNIPAAm-M, pNIPAAm-A, and pNIPAAm-S hydrogels. As shown in Figure 3.2 and Figure 3.3, the mechanical properties between the three types of hydrogels are significantly different. pNIPAAm-S gels have a Young's modulus 2.4 times that of pNIPAAm-A gels and is comparable to cardiac tissue [149]. pNIPAAm-A gels have a Young's modulus comparable to skeletal muscle [149]. pNIPAAm-M control gels were also tested and exhibited a Young's modulus of 151 kPa; 4.8 times that of pNIPAAm-S gels and 11.8 times that of pNIPAAm-A gels.

The differences in the mechanical properties are interesting due to the fact that the chemical composition of all three gels are the same except for a small amount of CTA ($<$1%) present in the pNIPAAm-A and pNIPAAm-S gels. This drastic difference of up to 11.8 fold is completely due to the architectural properties of the polymer. We propose that this difference is due to the freedom of the pNIPAAm chains to rearrange to a greater extent as compared to the control. Similarly, due to greater

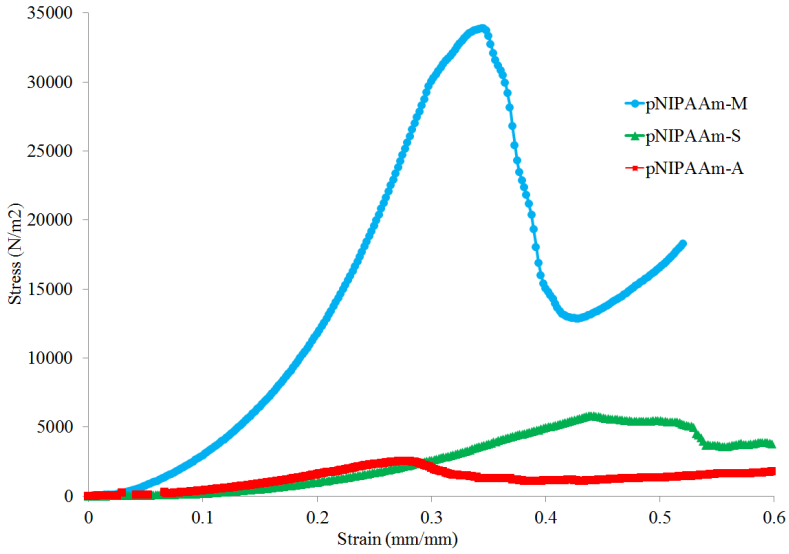

Figure 3.2: Mechanical properties of pNIPAAm-M, pNIPAAm-A, and pNIPAAm-S hydrogels.

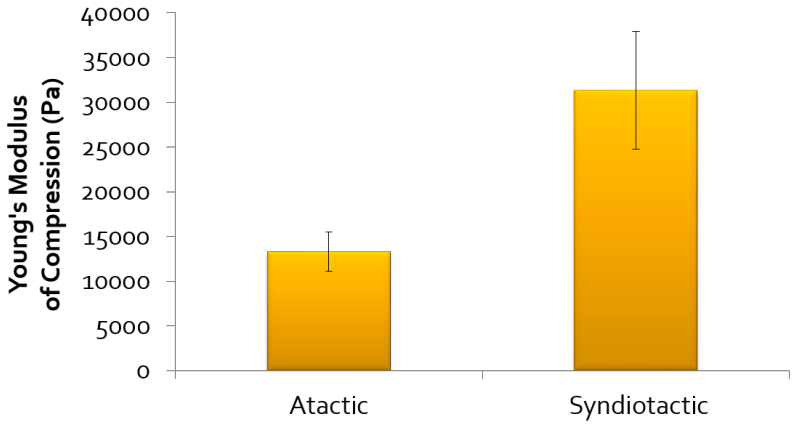

Figure 3.3: Young's modulus of compression for pNIPAAm-A and pNIPAAm-S gels, which are 13.3 and 31.3 kPa respectively. By comparison, pNIPAAm-M has a Young's modulus of 151 kPa (n=8, $p<0.01$).

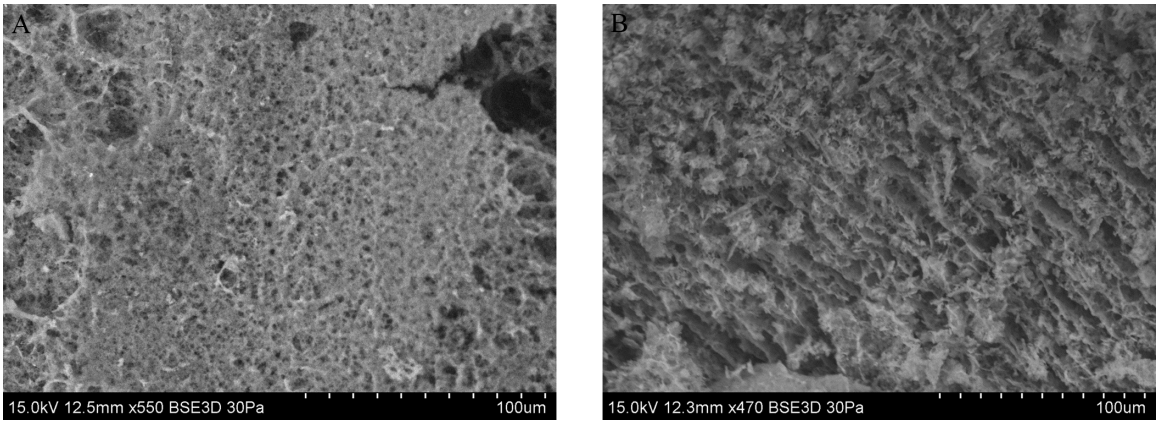

Figure 3.4: SEM of A) pNIPAAm-M, B) pNIPAAm-A. Random patterning of pNIPAAm-M suggest random cross-linking while striations in pNIPAAm-A suggest more ordered polymer structure.

tacticity control in pNIPAAm-S gels, the pNIPAAm chains are likely preferentially stacked such that reconfiguration would be difficult, thereby increasing the stiffness of the gels. This theory is corroborated by the failure stresses of the gels. pNIPAAm-M gels have a high failure stress at 30 kPa. pNIPAAm-A and pNIPAAm-S gels have much lower failure stresses at 3 kPa and 6 kPa respectively. With a much lower barrier to molecular motion, pNIPAAm-A gels quickly reach the limit of elastic deformation. Similarly, pNIPAAm-S gels have a higher yield strength but it is still much lower than that of pNIPAAm-M, the hydrogel with the least amount of molecular motion.

To further confirm the order of the pNIPAAm hydrogels, SEM was conducted on pNIPAAm-M and pNIPAAm-A hydrogels, as shown in Figure 3.4. pNIPAAm-M hydrogels have a much more crosslinked structure compared to pNIPAAm-A and lacks the striations of the long polymer chains. pNIPAAm-A exhibits polymer striations and far greater order as expected from pre-polymerized hydrogels.

3.4.2 Gel shrinking kinetics and volume transition

pNIPAAm hydrogel shrinking kinetics were measured over the time it takes for full shrinkage of the gels, as well as at various temperatures for temperature responsiveness. To measure gel response to a sudden change in temperature, pre-swollen gels

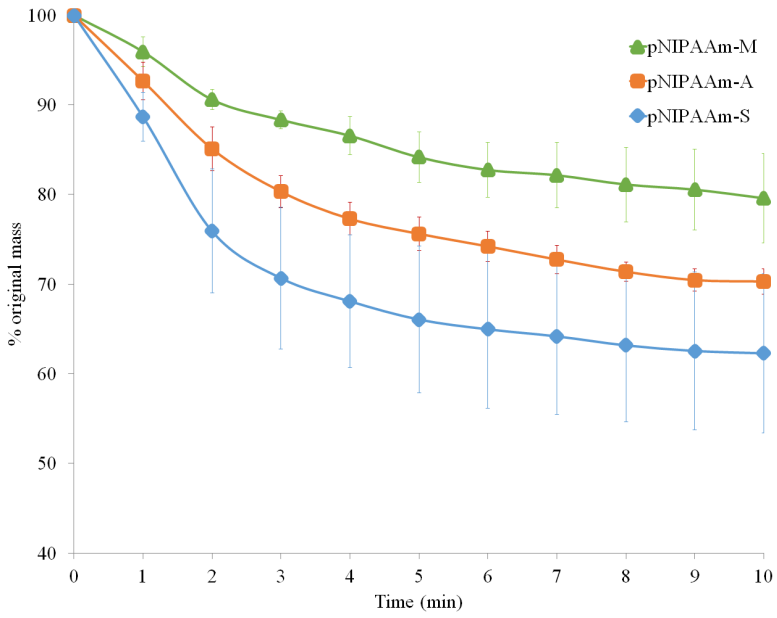

Figure 3.5: Shrinking behavior of different pNIPAAm hydrogels when exposed to temperature above the LCST. pNIPAAm-A and pNIPAAm-S shrank significantly more than pNIPAAm-M (n=6).

were placed in nanopure water at 50 °C and the mass was measured every minute. The results are shown in Figure 3.5. As shown, the temperature response is immediate and over the course of ten minutes, all gels reached their final mass.

pNIPAAm-M gels exhibited significantly less shrinkage compared to the pNIPAAm-A and pNIPAAm-S gels. This further confirms the hypothesis that hydrogels formed from pre-polymerized pNIPAAm have greater chain mobility and therefore exhibit more drastic changes upon transition. Additionally, as shown in the figure, the biggest differences between the three gels occur within the first two minutes. The difference in the rate of mass decrease between the three gels is greatest before 3 mins. After 5 mins, the shrinking rates are comparable.

In addition to a faster initial shrinking rate and overall more shrinkage, pNIPAAm gels formed from pre-polymerized pNIPAAm also exhibited higher LCSTs than the control. LCSTs for pNIPAAm hydrogels here are defined as the temperature resulting in the greatest change in mass, as per convention [273]. As shown in Figure 3.6, the

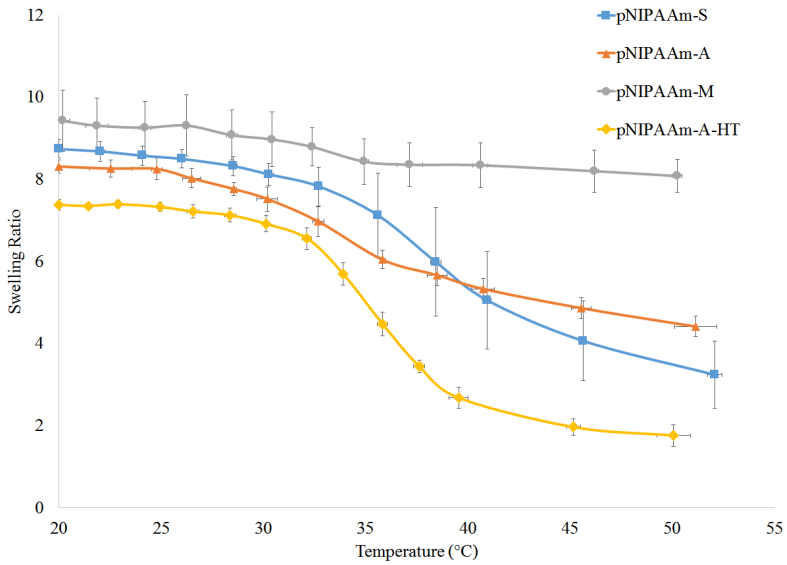

Figure 3.6: LCST of pNIPAAm hydrogels formed under various conditions. As shown, pNIPAAm-M shows an LCST of 32 °C. pNIPAAm-A shows an LCST of 35 °C. pNIPAAm-S shows an LCST of 37 °C. pNIPAAm-A-HT also shows an LCST of 35 °C (n=5).

LCST of pNIPAAm-M is at the expected temperature of 32 °C while the LCST of pNIPAAm-A and pNIPAAm-S hydrogels are at 35 °C and 37 °C, respectively. This is expected since they are comparable to the LCSTs exhibited by the polymers before hydrogel synthesis, as shown in Chapter 2, and confirms the transfer of properties from linear free-floating polymer to hydrogels. Surprisingly, pNIPAAm-A-HT exhibited a sharper transition profile than pNIPAAm-A at approximately the same temperature. This may be due to the differences in gelation as described previously. Qualitatively, pNIPAAm-A-HT formed translucent hydrogels while all other hydrogels were opaque. This may indicate lower crosslink levels than other hydrogels and therefore a larger temperature response.

pNIPAAm-M hydrogels had a high crosslink density which formed a 'skin' of collapsed polymers around the core of the hydrogels. This caused the small decrease in swelling ratio upon thermal activation instead of a large one. This is much less of a problem with pNIPAAm-A, pNIPAAm-A-HT, and pNIPAAm-S hydrogels

since despite having the same amount of crosslinker, the crosslinks are localized at specific areas. Shrinking kinetics analysis was also conducted on pNIPAAm-C and pNIPAAm-D hydrogels but they showed no significant change in mass upon heating (see Figure B.3 in Appendix B). This is speculated to be the result of the asymmetric polymer architecture of these polymers and the subsequent localization of crosslinking chemistry although further analysis into crosslink density should be conducted to confirm this hypothesis.

3.5 Conclusion

End-groups and tacticity play a large role in macroscopic properties as shown by the different hydrogels synthesized in this chapter. Hydrophobic and amphiphilic RAFT agents cause a dramatic decrease in the thermal response while hydrophilic RAFT agents increase the response in both magnitude and temperature. pNIPAAm hydrogels capable of transitioning within the physiological range were synthesized by chain-extension crosslinking of pre-polymerized majority racemo diad pNIPAAm. These gels and their atactic counterparts exhibit physiological mechanical properties and transition temperatures. They also exude more water than their monomeric counterparts. These differences indicate that chain architecture of pNIPAAm can greatly affect intermolecular interactions and can be used in the design of hydrogel based drug delivery devices. With further characterization, pNIPAAm-S gels can potentially be optimized as an implantable controlled release drug delivery device due to its physiological transition temperature, large bulk response to temperature change, and physiological mechanical properties.

CHAPTER IV

STRUCTURAL OPTIMIZATION OF HIGHLY BRANCHED THERMALLY RESPONSIVE POLYMERS AS A MEANS OF CONTROLLING TRANSITION TEMPERATURE

4.1 Summary

pNIPAAm is at the forefront of stimuli-responsive polymers; however, few transition temperature modification methods of linear pNIPAAm have been explored in highly branched systems. In this study, the three primary techniques of transition temperature modification of linear pNIPAAm are investigated for their efficacy on highly branched polymers and optimized for drug delivery applications. Of these LCST modification techniques, co-solvent-mediated tacticity control demonstrates an effect opposite of that which is expected. Temperature transition control via end-group modification shows a marked decrease in efficacy in highly branched systems, despite highly branched systems having more end-groups per polymer. Copolymerization with hydrophilic co-monomers exhibits varying changes in efficacy compared to linear analogues, lending insights into the specific effects on the structured water surrounding the copolymer. While copolymerization proved to be most versatile in changing the transition temperature, all of the techniques showed interesting secondary effects.

4.2 Introduction

Three dimensional polymer architecture has been the subject of much research in recent years. From star polymers to dendrimer-like polymers, architecture has played a crucial role in developing new properties in polymeric materials [95, 171, 11, 12].

This has been especially true for stimuli-responsive polymers such as the thermally responsive pNIPAAm, where modifications in the architecture have opened up new possibilities in bio-processes [31, 285, 294]. Changing the three dimensional architecture to highly branched pNIPAAm continues the trend of using topology to modify properties. The resulting polymer exhibits a globular structure that can be exploited for controlled drug delivery, a subject of much current research [114, 160, 298]. This structure combined with the near physiological LCST of the polymer provides the basis of a controlled-release drug delivery system, which can provide clinicians with the ability to control when drugs are delivered, and therefore better monitor their patients dosages. This ability, along with the potential of targeting these delivery systems, may prove especially important in the realm of chemotherapy for cancer treatment, establishing a means to limit the harsh side effects of chemotherapeutic drugs [298]. Due to the sensitivity of such a system, deviations in transition temperature of even a few degrees can lead to significant failure. Therefore, understanding the effects of branching on this type of system can not only lead to optimally designed drug delivery constructs, but also provide insights into the variety of controls that need to be in place to successfully modify responsive highly branched polymer systems.

In this study, we explore three different techniques employed in LCST manipulation: tacticity control, end-group control, and copolymerization, and investigate their utility and limitations in the highly branched architecture. Incorporation of tacticity control into polymerization schemes for highly branched polymers through solvent interactions introduces new areas of complexity, and to the best of our knowledge, such control has not previously been explored. End-group effects on the transition properties of highly branched pNIPAAm are also largely unknown. Due to the effects exhibited by the end-groups on linear pNIPAAm [35], it is expected that this form of T_{cp} control is even more effective for highly branched pNIPAAm since there

are more end-groups available for highly branched polymers. While copolymerization of pNIPAAm with various comonomers in highly branched systems has been briefly explored [32, 269], comparisons to linear models have not been done. By exploring these three models of LCST control on highly branched pNIPAAm, we demonstrate that these methods not only have different efficiencies in controlling the LCST, but can also have unexpected effects on the polymer product.

4.2.1 Highly branched pNIPAAm

As discussed in Chapter 1, highly branched polymers have many of the benefits of dendrimers while maintaining a one-pot synthesis reaction [95, 30, 32]. The controlled synthesis of a stimuli-responsive highly branched polymer system such as pNIPAAm is not trivial. There are three key issues when synthesizing such a polymer: 1) control over the polymer molecular weight distribution, 2) branching, and 3) the effects on the response mechanism, which in this case is the LCST, represented by the T_{cp}. Molecular weight control of highly branched polymers has been attempted through various polymerization schemes such as ATRP [83, 168] and RAFT polymerization [155, 31, 269] to varying degrees of success. Mathematical models of such polymerization schemes conclude that such systems can produce macromolecules of low PDIs of around 1.1, with individual branch segments having PDIs of less than 1.4 (see Appendix A) [308]; however, PDIs greater than 2.0 are commonly observed in such systems [168, 30]. Controlling the degree of branching has been attempted through careful monomer selection and reaction condition control [230, 228, 99] as well as the use of different polymerization schemes [92, 99]; however, these attempts are primarily focused upon the hyperbranching of AB_x type monomers and not the branching of long polymer chains in a dendrimer-like structure. The effects of branching on the stimulus response of smart polymers are an important consideration since the change in polymer topology can have a significant impact on the magnitude of the

response. For example, highly branched pNIPAAm shows a significant decrease in the T_{cp} compared to its linear counterpart (∼2-5 °C) [268, 269].

4.2.2 RAFT agents as branching agents

In this work, highly branched polymer synthesis was conducted using RAFT polymerization. In the past decade, CTAs have been designed to promote a variety of architectures from star polymers to brushes [14, 304, 171]. Of note are the CTAs that cause highly branched polymer formation as pioneered by Yang et al. and extend by various groups [276, 30, 32, 269]. These CTAs combine RAFT polymerization with Self Condensing Vinyl Polymerization (SCVP) to form long chain highly branched structures [71]. In this study, branching of pNIPAAm was induced using the well-characterized branching CTA, 4-vinylbenzylimidazoledithioate [30]. The vinyl group attached to the chain transfer agent makes it possible to induce polymerization along two directions concurrently (see Scheme 4.1). This secondary direction of polymerization induces the branching effect [32, 155, 269].

As shown in Scheme 4.1, the chemistry of using CTAs as branching agents in this fashion dictates that the CTAs also double as end-groups for the overall polymer. This provides the opportunity for facile end-group modification through cleavage of the CTA to form a thiol, which can then be utilized in standard bioconjugation techniques.

4.2.3 RAFT agent cleavage

The thiocarbonylthio from the RAFT agent can be cleaved through a variety of methods including aminolysis [171, 259, 278], radical induced reduction [50], thermolysis [175] and UV irradiation [58]. These methods have different advantages, not only in efficiency and ease of use, but also in the end-group left on the polymer, as shown in Scheme 4.2. Aminolysis leaves a thiol end-group while thermolysis yields an -ene and radical reduction leaves a hydrocarbon. Of these methods, aminolysis is the most

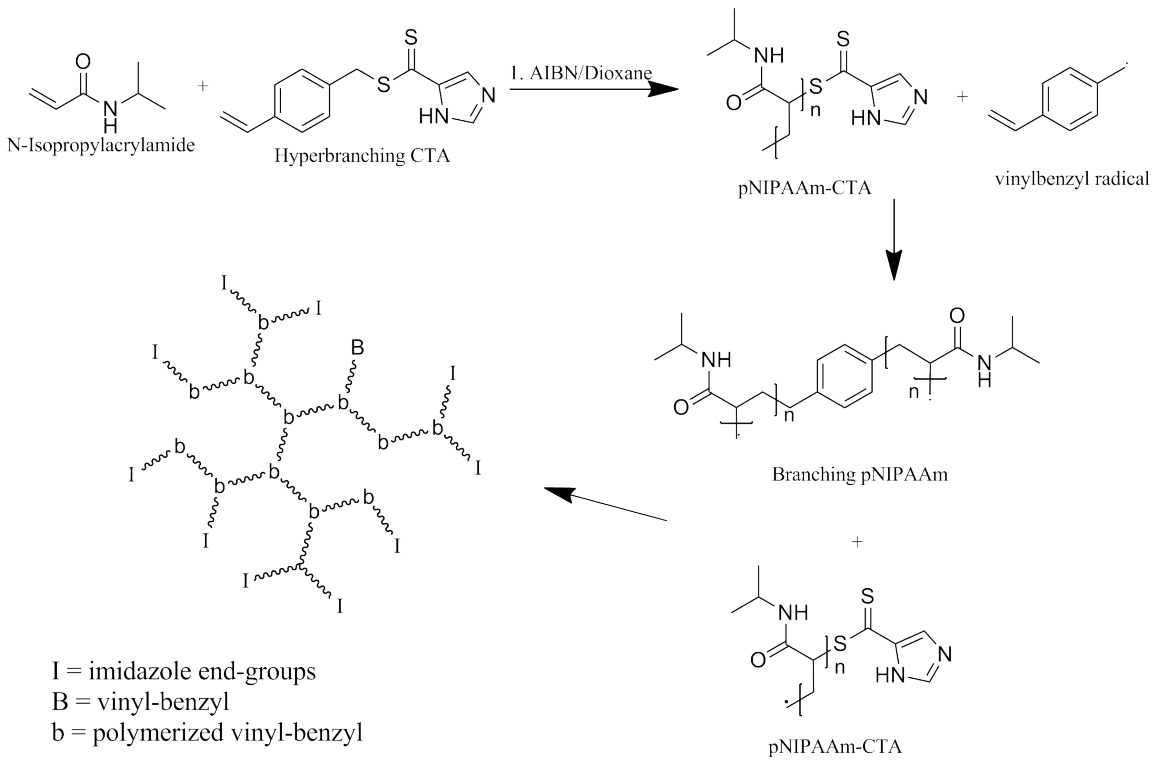

Scheme 4.1: Polymerization of highly branched pNIPAAm using the branching chain transfer agent, 4-vinylbenzylimidazoledithioate.

versatile for end-group modification due to the reactive thiol left after the cleavage and is used to modify the end-groups of the synthesized HB pNIPAAm.

4.2.4 Thiol click chemistry: thiol –ene and thiol –Michael addition

Once cleaved to a thiol, the end-groups can easily be modified. The thiol functional group is one of the most basic and best studied functional groups in organic chemistry. As such, there is a multiplicity of reactions associated with thiols. In bioconjugate chemistry where efficiency and orthogonality are extremely important, 'click' chemistry techniques that prioritize modularity, high atom economy, stereospecificity, and high chemical yields are currently the best-suited techniques for functional group modifications [140]. Current thiol 'click' chemistry schemes are described in a detailed review by Hoyle and coworkers [118] and have been integrated into the synthesis of

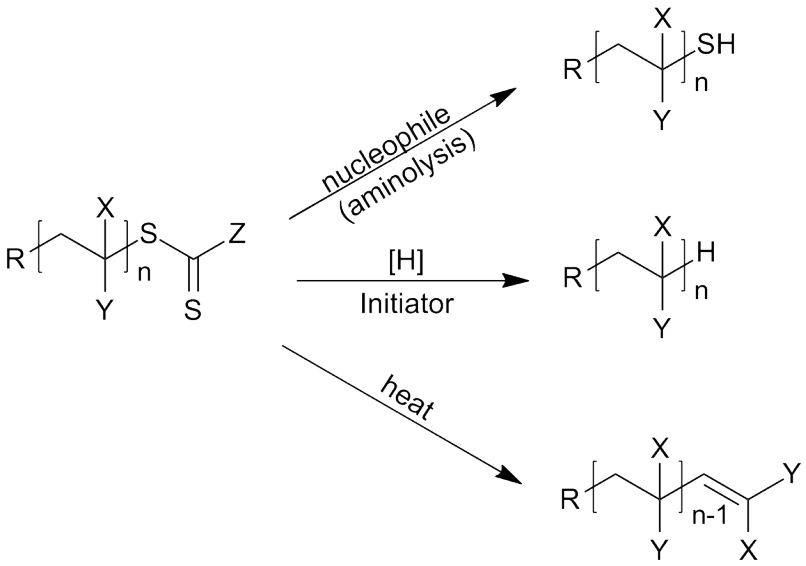

Scheme 4.2: Chain transfer agents can be cleaved via a variety of methods, each leaving different end-groups depending on the method.

new materials to great success [296, 234, 5]. The main chemistries for thiol click reactions are thiol –ene click chemistry [63, 116, 117, 245], thiol –isocyanate chemistry [151], and thiol –Michael addition [121, 57]. All of these are highly efficient reactions with broad possibilities which add to the versatility of having a thiol end-group. In this chapter we use thiol –Michael addition due to the ability to easily click on an –ene without the potential for further polymerization.

4.3 Materials and Methods

N-isopropylacrylamide was purchased from TCI America and recrystallized in 9:1 hexanes:benzene. 4(5) imidazole dithiocarboxylic acid, cesium carbonate, dimethyl acrylamide, acrylamide, acrylic acid, 1-hexylamine, 2,2-dimethyl-2-phenylacetophenone, 5,5-dithiobis(2-nitrobenzoic acid), tributylphospine, N-vinylpyrrolidone, 1, 4 dioxane, 3-methyl-3-pentanol (3Me3PenOH) were purchased from Sigma Aldrich and used without further purification.

4.3.1 4-vinylbenzylimidazoledithioate (2) synthesis

Synthesis of **2** was modified from the procedure set forth by Carter et al. [32] Briefly, 2.2 g of 4(5) imidazole dithiocarboxylic acid and 15.4 g of cesium carbonate was dissolved in 45 mL of dimethylformamide (DMF). The solution was purged with nitrogen and stirred for 30 min. 1.69 mL of 4-vinylbenzyl chloride was added to the reaction vessel and was reacted for 70 h. The raw product was then filtered to remove excess cesium carbonate. The filtrate was diluted with 500 mL of nanopure water and extracted with 200 mL of dichloromethane twice. The DCM mixture was subsequently concentrated using a rotary evaporator to reduce the volume to approximately 50 mL. The mixture was then passed through a silica column with 2.5% methanol in DCM and then again through an alumina column with 2% methanol in DCM. The appropriate fraction was collected and the resulting product was dried, yielding bright orange crystalline product. **2** was confirmed using ^{1}H NMR (400 MHz, CDCl3, δ): 7.8 (d, 2H); 7.3 (d, 2H); 6.6 (q, 1H); 5.6 (d, 1H); 5.15 (d, 1H); 4.5 (s, 1H) (see Figure B.4 in Appendix B).

4.3.2 Tacticity control

Polymerization of NIPAAm was carried out with **2** in the presence and absence of 3Me3PenOH to control tacticity. Two ratios of 3Me3PenOH were tested: 4:1 and 10:1 of 3Me3PenOH:NIPAAm. For example, under the 4:1 condition, a 1.03 g mixture of 100:1:0.5 ratio of NIPAAm:1:AIBN and 4 mL of 3Me3PenOH was placed in a sealed 25 mL round-bottom flask equipped with a magnetic stir bar. The mixture was purged with nitrogen for 15 min and 10 mL of nitrogen-purged 1,4 dioxane was added. The solution was reacted at 65 °C for 48 h and was quenched by exposure to air. The pNIPAAm was precipitated in diethyl ether and collected via filtration. The pNIPAAm was then dissolved in nanopure water, and dialyzed with a 2000 MWCO membrane dialysis cassette. During dialysis the water was changed every hour for

the first 4 h and then allowed to proceed overnight. The samples were then frozen and lyophilized.

4.3.3 End-group modification

pNIPAAm was synthesized similarly to the methods described above. For instance, a 10.3 g mixture of 100:1:0.5 ratio of NIPAAm:1:AIBN was placed in a sealed 25 mL round-bottom flask equipped with a magnetic stir bar. The mixture was purged with nitrogen for 15 min and 10 mL of nitrogen-purged 1,4 dioxane was added. The solution was reacted at 65 °C for 48 h and was quenched by exposure to air. The pNIPAAm was precipitated in diethyl ether and collected via filtration. The pNIPAAm was then dissolved in nanopure water, and dialyzed as previously described with a 2000 MWCO membrane dialysis cassette. The sample was then frozen and lyophilized.

The freeze-dried pNIPAAm was then was then subjected to aminolysis using hexylamine. Thiol functionality was maintained using tributylphospine. Briefly, 1 g of pNIPAAm was reacted with 660 L of 1-hexylamine and 247 L of tributylphosphine in 25 mL of 1, 4 dioxane under nitrogen for 2 hrs. The product was precipitated in cold ether, filtered, and dried in vacuo. An Ellmans assay was conducted to confirm the presence of thiols [70]. In brief, 100 L of 100 M solution of lysed pNIPAAm in 0.1 M Tris buffer, pH 8 was reacted with 100 L of 4 mg/mL of 5,5-dithiobis(2-nitrobenzoic acid) in Tris buffer. The absorbance was measured at 410 nm on a Beckman DTX 880 Multimode Plate Reader and was compared to standards made with known concentrations of L-cysteine.

End-groups were introduced using thiol-Michael addition. A 1:1.2 ratio of thiols to -enes were conjugated using 1-hexylamine as the base. In a typical reaction, 300 mg of cleaved pNIPAAm was dissolved in 5 mL of THF and 60 L of dimethylacrylamide (DMA) or 40 L of acrylic acid (AAc) was added along with 50 L of 1-hexylamine. The solutions were reacted at 40 °C overnight and dried in a vacuum oven. They were then

re-dissolved in nanopure water, dialyzed as previously described using 2000 MWCO dialysis cassettes, and lyophilized. Conjugation was confirmed using GPC and ^{1}H NMR (see Figures B.6-B.8 in Appendix B).

4.3.4 Random copolymer synthesis

Copolymerization of NIPAAm was carried out with **2**. Copolymers of pNIPAAm with DMA, AAm, and AAc were synthesized with varying amounts of comonomer. For example, a 1.03 g mixture of 90:10:1:0.5 ratio of NIPAAm:AAc:**2**:AIBN was placed in a sealed 25 mL round-bottom flask equipped with a magnetic stir bar. The mixture was purged with nitrogen for 15 min and 10 mL of nitrogen- purged 1, 4 dioxane was added. The solution was reacted at 65 °C for 48 h and was quenched by exposure to air. The copolymers were precipitated in diethyl ether and collected via filtration. Successful copolymerization was confirmed using ^{1}H NMR.

4.3.5 Characterization

Characterization was performed using gel permeation chromatography (GPC), NMR, matrix assisted laser desorption ionization (MALDI) mass spectrometry, and UV-Visible spectrometry. GPC was conducted on a GPC-50 Plus (Agilent, Inc.) equipped with two PLgel 3μm MIXED-E columns with UV, RI, and viscosity detectors. Tetrahydrofuran (THF) was used as the polymer solvent and eluent. A flow rate of 1 mL/min was used. Chromatograms were compared with those of polystyrene standards (Agilent Inc). ^{1}H NMR was conducted on a Varian Mercury Vx 400 spectrometer using chloroform-d as a solvent. High temperature ^{1}H NMR (150 °C) was conducted on a Bruker DMX 400 spectrometer using dimethylsulfoxide *d*-6 as solvent. Mass Spectrometry was run on an Applied Biosystems 4700 Proteomics Analyzer with a 200 Hz Nd:YAG laser using CHCA matrix and reflecting detector. Turbidity was measured using UV-Vis spectrometry conducted at constant pH (7.0 $\pm$ 0.1) using a Cary 50 UV-Vis Spectrophotometer (Agilent Inc.) with a single cell peltier thermostatted cell

holder and accessory for temperature control. Scans were conducted every 0.1 °C, and the temperature was ramped at 1 °C/min.

4.4 Results and Discussion

4.4.1 Effects of Using a Bulky Alcohol Co-Solvent

In the past few years, several publications have discussed the use of stereocontrol as a method of modifying LCST [107, 103, 100, 102]. According to Hirano et al., pNIPAAm polymers that are predominately syndiotactic have higher LCSTs than atactic pNIPAAm [107]. Similarly, isotactic pNIPAAm has a lower LCST than atactic pNIPAAm [217]. Not only does the transition temperature change, but the profile also changes, with syndiotactic pNIPAAm having sharper transitions than atactic pNIPAAm [107]. Lewis acids and bulky alcohols in particular have been used to induce majority isotactic or majority syndiotactic poly(acrylamides) [107, 216]. 3Me3PenOH has been shown to be a particularly effective racemo diad-inducing agent, increasing the racemo diad content to up to 70% in linear systems, while being a more mild additive than similar Lewis bases [107, 105].

In order to explore the feasibility of using solvent-mediated tacticity control as a LCST modifying agent, highly branched pNIPAAm was synthesized using a branching RAFT agent as shown in Scheme 4.1. The polymers displayed a slight orange tint, a residual effect from the orange coloration of the RAFT agent used in the polymerization. Branching was confirmed via GPC, with the polymers exhibiting Mark-Houwink values on the order of 0.13, which is well within the realm of highly branched pNIPAAm (see Figure B.5 in Appendix B) [30]. Three ratios of 3Me3PenOH were used in this study. The polymer weights and PDIs are shown in Table 1 and the GPC chromatograms are shown in Figure 4.1. The molecular weight trend indicates that even under the same polymerization conditions (65 °C, 48hrs), the polymers form larger highly branched structures compared to the control reaction that did not contain the

Table 4.1: pNIPAAm synthesized with various 3Me3PenOH amounts.

3Me3PenOH to Monomer Ratio	M_n [a]	M_w [a]	PDI[a]	DB[b]	ANB[b]
0	12,800	22,500	1.8	0.30	0.09
4:1	14,200	25,300	1.8	0.26	0.09
10:1	14,700	26,000	1.8	0.26	0.09

[a] M_n, M_w and PDI were calculated via GPC using polystyrene standards. [b] Degree of Branching (DB) and Average Number of Branches (ANB) were obtained via NMR using equations 1 and 2.

bulky alcohol. This increase in molecular weight is likely due to increased branching and is supported by the branching data.

The degree of branching (DB) and average number of branches (ANB), a measure of branching density, were calculated using ^{1}H NMR using the equations put forth by Frechet et al. (Equation 1) [95] and Frey et al. (Equation 2) [110]

$$DB = \frac{D + T}{D + T + L} \tag{1}$$

$$ANB = \frac{D}{D + L} \tag{2}$$

T, D, and L represent terminal, dendritic, and linear groups respectively. DB and ANB are commonly used to describe the branching properties of highly branched polymers [261, 177, 230, 269, 254]. ANB was calculated to be the average number of branches per non-terminal, non-linear unit and the results of both parameters are shown in Table 4.1 [110].

The DB values decreased with increasing amounts of 3Me3PenOH; however, the branching density remained constant. This provides several insights into the polymer characteristics. First, the average linear segment length remains unchanged due to the constant ANB. This means that the overall change in size is not due to individual segments becoming longer during the polymerization. Second, the proportion of linear

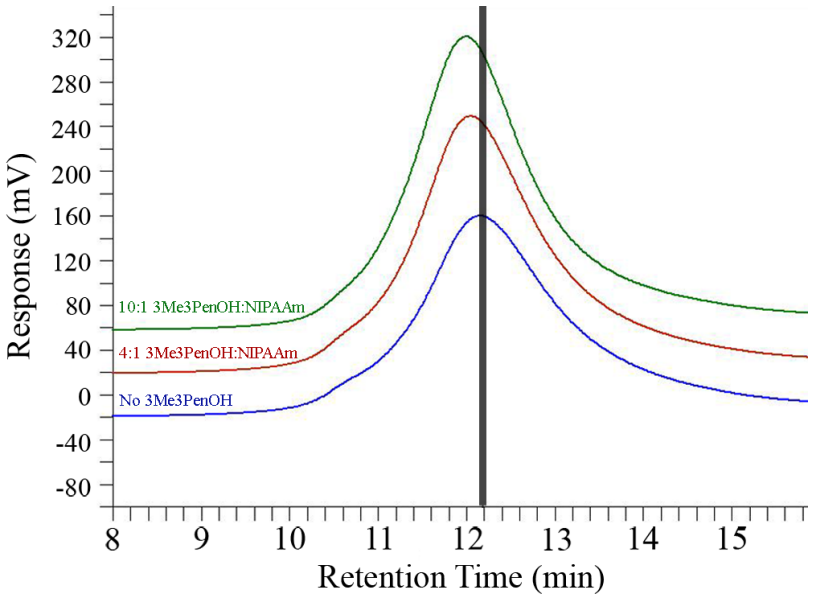

Figure 4.1: GPC traces showing the molecular weight as the amount of 3Me3PenOH increases. The vertical line indicates retention time of the main polymer peak synthesized without 3Me3PenOH. The molecular weight increases significantly with increasing 3Me3PenOH.

chains in the overall polymer is increasing. This is consistent with increased polymer size. Taken together, the data clearly indicates that the increased size of the polymer is due to more branches per polymer. Statistically, the segments remain at ∼10 linear units per branch unit but the number of branches increases with the solvent ratio.

The increase in the number of branches, combined with the constant PDI, paints an interesting picture of the state of the polymer. Despite having more branches and therefore more chances of variability, the polymer does not become more polydisperse.

4.4.2 Characterization of Tacticity Effects

The tacticity of the polymers were confirmed using high temperature ^{1}H NMR spectrometry as shown in Figure 4.2. Interestingly, the amount of racemo diads decreased from 56% in the control to 52% in the polymer with a 10:1 ratio of 3Me3PenOH:NIPAAm. This change in racemo diad content is contrary to that of linear polymers run under similar conditions, which show an increased racemo diad content of 61% [35]. While this initially seems counterintuitive for this system considering the molecular weight

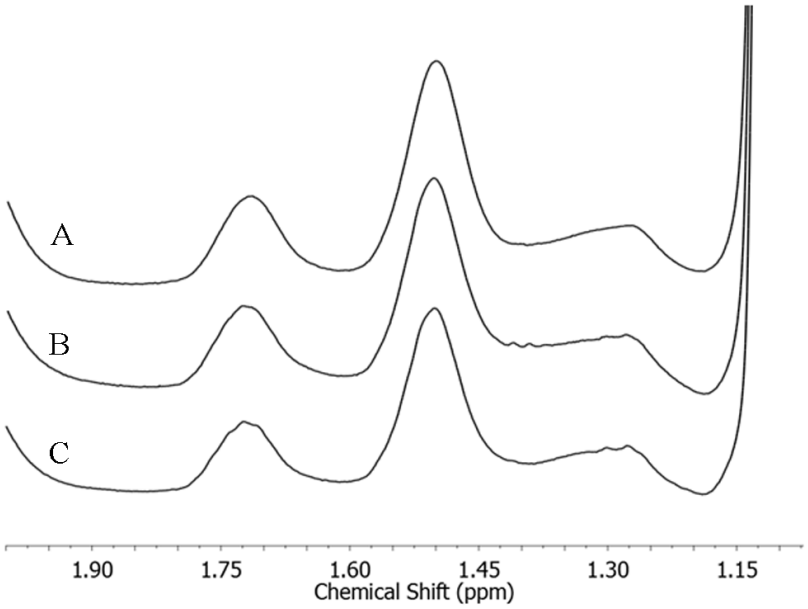

Figure 4.2: ^{1}H NMR Spectra of methine backbone peaks conducted at 150 °C. A) 10:1 3Me3PenOH:NIPAAm showed 52% racemo diads, B) 4:1 3Me3PenOH:NIPAAm showed 55% racemo diads, C) control pNIPAAm showed 56% racemo diads. Racemo diads are indicated by the peak at 1.50 ppm while meso diads are indicated at 1.28 and 1.73 ppm.

effects observed in the polymer through the use of this co-solvent, it may be a confirmation of accelerated polymerization induced by 3Me3PenOH, a process known to occur in radical polymerization in polar protic solvents [111, 107, 35]. The accelerated polymerization reduces any preferential backbone configuration.

Racemo diad formation using bulky alcohols is caused by hydrogen bonding between the alcohols and the acrylamide group, which sterically hinders polymerization in the meso diad form [104]. Since proper hydrogen bonding for this effect is temperature-dependent, preferring low temperatures, racemo diad formation was already weak at the polymerization temperature. Lower temperature polymerizations including high temperature initiated room temperature polymerization and UV-initiated room temperature polymerization were attempted. However, despite successful polymerization in the absence of the RAFT agent, these attempts failed in the scheme of interest due to the reaction kinetics of the RAFT agent used. At the

normal polymerization temperature, any nominal racemo diad preference may have been quenched by the acceleration effect of the co-solvent, since the increased reaction rate favored atactic polymerization. Since this effect was not seen in the linear counterpart [35], even at high polymerization temperatures, it can therefore be attributed to the branching architecture of the polymer and a factor in its polymerization.

UV-Vis spectroscopy was used to assess the T_{cp} of highly branched pNIPAAm, as shown in Figure 4.3A. T_{cp} is defined as the point where the transmittance drops to 50% of the initial value. The results are consistent with the observed increase in meso diad content. It is well known that increasing the racemo diad content of linear pNIPAAm increases the T_{cp}, while increasing the meso diad content decreases the T_{cp}. [217] In this case, the T_{cp} decreased from 28.4 °C without 3Me3PenOH to 28.0 °C with a 4:1 ratio of 3Me3PenOH:NIPAAm to 27.9 °C with a 10:1 ratio of 3Me3PenOH:NIPAAm. These differences, while small, are statistically significant as assessed by an ANOVA test with Tuckey's post-hoc analysis ($n=3$, $p<0.05$). They are also consistent with theory and suggest that with stronger tacticity controls, significant changes in the T_{cp} may be achieved.

As a matter of comparison, similar molecular weights of highly branched pNIPAAm were prepared using differing molar ratios of monomer to RAFT agent as the controlling factor for the molecular weight, and the opposite relation between molecular weight and T_{cp} was observed. As shown in Figure 4.3B, in the absence of 3Me3PenOH, increasing molecular weight increases the T_{cp}. This is due to the increased aggregation caused by the polymerization process. The high molecular weight shoulder increases in intensity as degree of polymerization and molecular weight increase, indicating a more bimodal distribution with a significant number of higher molecular weight particles, as shown in Figure 4.4.

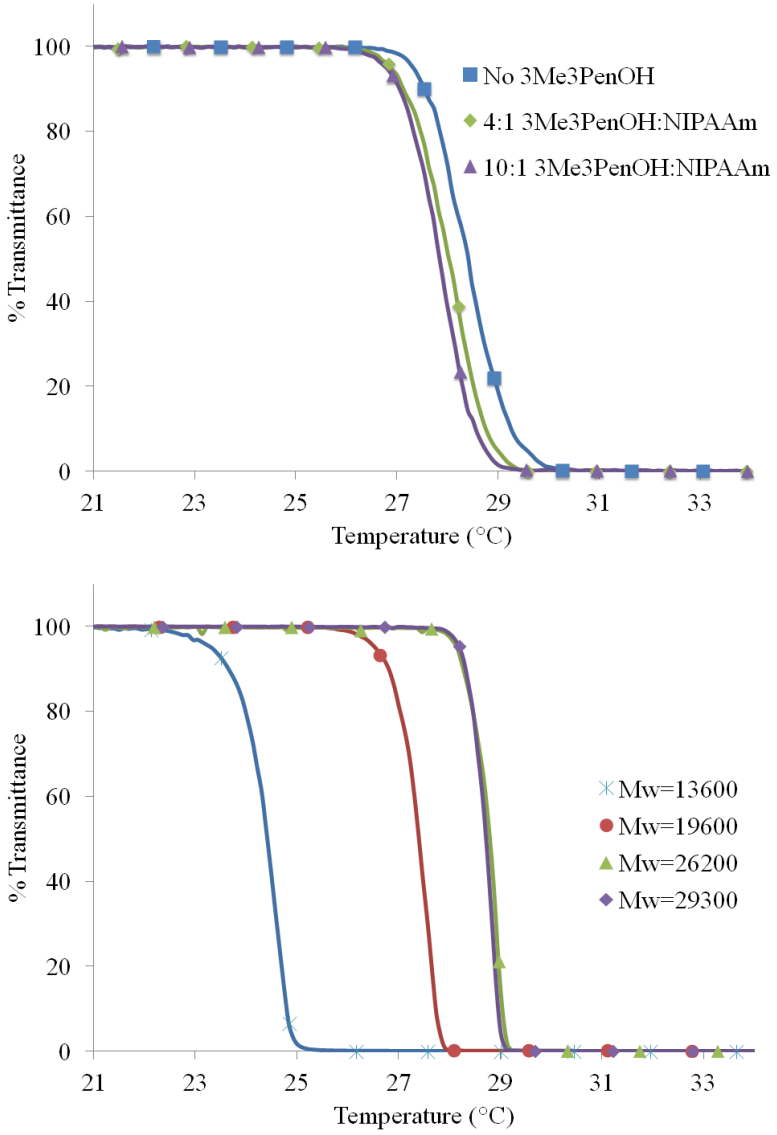

Figure 4.3: Turbidity measurements with readings taken every 0.1 °C. A) T_{cp} of pNIPAAm with varying amounts of 3Me3PenOH as cosolvent. T_{cp} decreases with increasing 3Me3PenOH content. B) T_{cp} of pNIPAAm of varying molecular weights without the use of 3Me3PenOH. T_{cp} increases with increasing molecular weight.

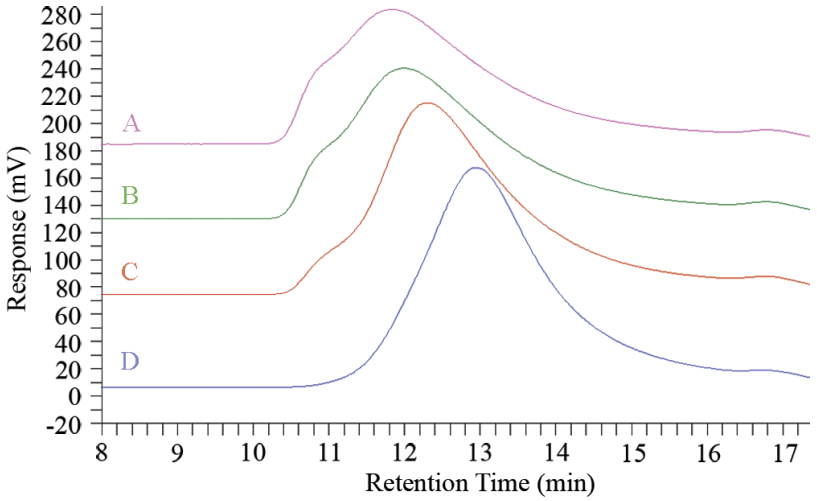

Figure 4.4: GPC traces of different molecular weight hyperbranched pNIPAAm synthesized without 3Me3PenOH. From top to bottom the weight average molecular weights were 29,300, 26,200, 19,600, and 13,600, respectively. The PDIs were 1.7, 1.8, 1.9, and 1.8 respectively.

4.4.3 End-group control

Previous studies have shown that end-groups have significant effects on the transition temperature of linear pNIPAAm [286, 35]. In our system, the RAFT groups double as the chain ends in our branching scheme and can be easily cleaved via aminolysis [245, 254]. The remaining thiols can then be modified through thiol Michael addition [150, 208, 172, 241].

Due to the increased number of end-groups in a highly branched polymer, it is expected that the end-groups will play an even greater effect on these polymers. In order to test this, the RAFT agent was cleaved to leave a thiol, and thiol-ene click chemistry was used to attach two different hydrophilic end-groups, DMA and AAc, as shown in Scheme 4.3.

In the initial cleavage of the polymer, the molecular weight decreased from M_w = 30,000 g/mol to M_w = 25,800 g/mol. This indicates a removal of approximately thirty-seven 1-imidazole-5-carbothialdehyde groups per polymer. The removal of

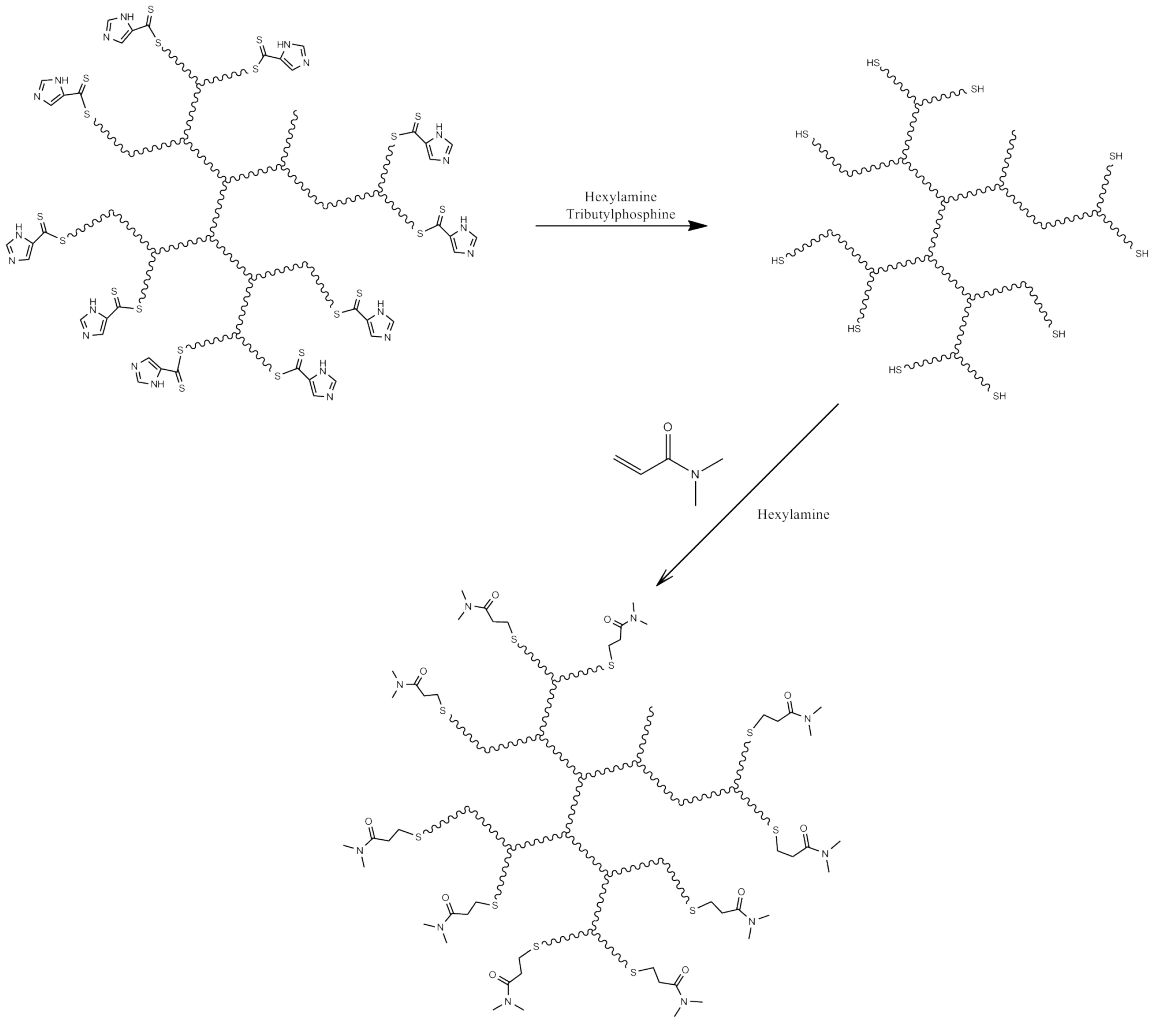

Scheme 4.3: DMA end-group attachment to hyperbranched pNIPAAm. RAFT imidazole dithioate end-groups were cleaved via aminolysis using hexylamine, generating thiol end-groups. DMA was clicked onto the thiol end-groups via thiol-Michael addition.

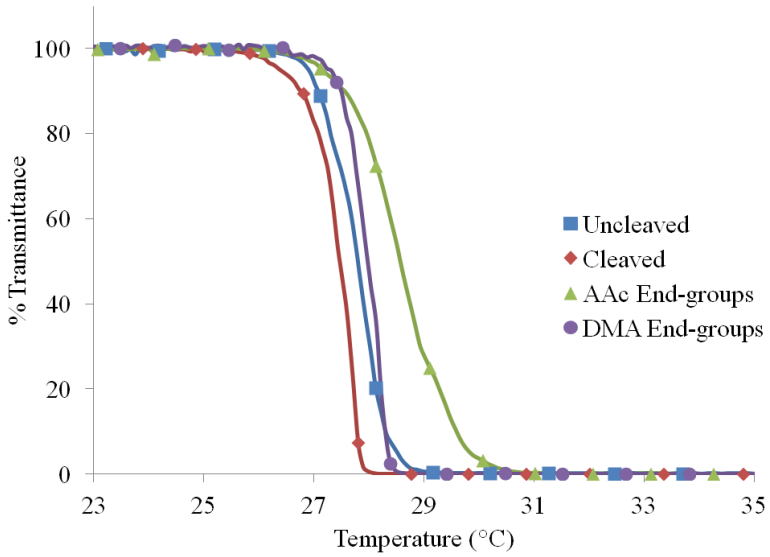

Figure 4.5: T_{cp} of highly branched pNIPAAm with various end-groups. The uncleaved pNIPAAm shows a T_{cp} of 27.8 °C while the cleaved pNIPAAm shows a T_{cp} of 27.4 °C. The AAc end-groups ncreased the T_{cp} to 28.6 °C while the DMA end-groups increased the T_{cp} to 28.0 °C.

these slightly hydrophilic end-groups does change the T_{cp} slightly as shown in Figure 4.5, but the 0.3 ° difference is small compared to the changes observed in linear pNIPAAm [286, 153, 35].

Upon inclusion of AAc and DMA end-groups the M_w increased to 29,300 g/mol, indicating >90% conjugation. ^{1}H NMR analysis further confirmed 7.5% end-group content for the AAc system and 10% end-group content for the DMA system (see Figure B.8 in Appendix B). The combination of the MW and NMR data indicates between 7 and 12 repeat units per end-group, which is comparable to linear systems of 900-1400 g/mol with one modified end-group. Previous discussions on the effect of end-groups on linear pNIPAAm systems show increases in transition temperature of more than 5 °, even at molecular weights of >10,000 g/mol for amine- and ether-terminated polymers [286]. As shown in Figure 4.5, incorporating DMA end-groups only increased the T_{cp} by 0.5 ° while incorporating AAc end-groups increased the T_{cp} by 1.2 °. This discrepancy suggests that the branching architecture interferes with the

efficacy of the end-groups as LCST-modifying agents. Recent studies on the segmental mobility of various pNIPAAm end-groups suggest a correlation between the two, with hydrophobic end-groups exhibiting limited segmental mobility and hydrophilic end-groups exhibiting enhanced segmental mobility [220]. The short chains of 8-10 repeat units between branching segments naturally inhibit segmental mobility in highly branched pNIPAAm, thereby limiting the effects of the hydrophilic end-groups attached to these polymers [192]. The data therefore suggests that a decrease in end-group mobility may strongly affect the ability of the end-group to change the LCST of the polymer. In fact, the lack of mobility makes highly branched polymers extremely resistant to end-group based LCST modification despite the large number of end-groups and the small adjusted equivalent linear size.

Even with the small overall change in LCST, the larger of the increases was caused by AAc end-groups and is consistent with the literature [74]. In addition, both end-groups increased the T_{cp} beyond the un-cleaved state. This indicates that the degree of hydrophilicity does have an effect on the transition properties of highly branched pNIPAAm, although much diminished compared to linear systems.

4.4.4 Copolymerization

Since the inclusion of tacticity control decreased the LCST and end-group control had a minimal effect on the LCST, the traditional method of copolymerization with hydrophilic monomers is the most promising method to induce the large LCST increase necessary for sufficiently high transition temperatures. In order to quantify the effectiveness of this method, three different common pNIPAAm copolymers were synthesized. The three different highly branched copolymers, pNIPAAm-co-DMA, pNIPAAm-co-AAm, and pNIPAAm-co-AAc, show drastically different temperature transition profiles from a highly branched homopolymer of pNIPAAm. As shown in Figure 4.6, even with a constant 10% copolymer content, the effects on the final

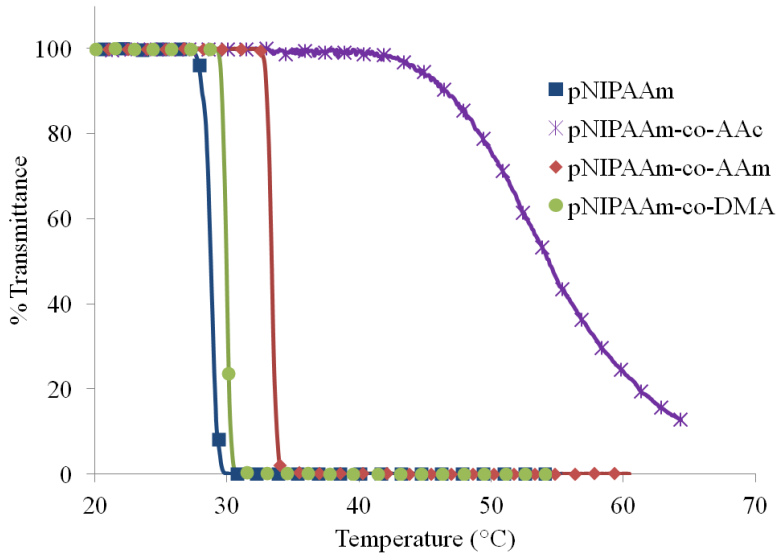

Figure 4.6: Temperature transition profiles for different copolymers. All copolymers contained 10% copolymer content. Highly branched pNIPAAm exhibited a sharp transition at 28.8 °C. AAc exhibited a broad transition at 54 °C. AAm and DMA exhibited sharp transitions at 33.4 °C and 29.9 °C, respectively.

polymer exhibited varied dramatically.

A closer study of the effects of varying percentages of each copolymer on the overall transition temperature further revealed the differences between these systems. As shown in Figure 4.7, the co-DMA system required a large amount of copolymer in order to significantly change the transition temperature; a shift of 13.5 ° required a copolymer content of 35%. Despite needing a large copolymer percentage in order to effect significant T_{cp} change, the transitions were relatively sharp, even at high copolymer content, with a transition range of 4.3 ° even at 50% copolymer content.

Similarly, as shown in Figure 4.8, the co-AAm system also required a large copolymer content in order to effect significant T_{cp} change, with a 19.3 ° increase requiring 30% copolymer content. While AAm was a more efficient copolymer than DMA for modifying the T_{cp}, it also increased the transition range to a greater degree, with 60% AAm showing a transition range of 10.8 °.

Compared to the other two copolymers, the co-AAc system was drastically more

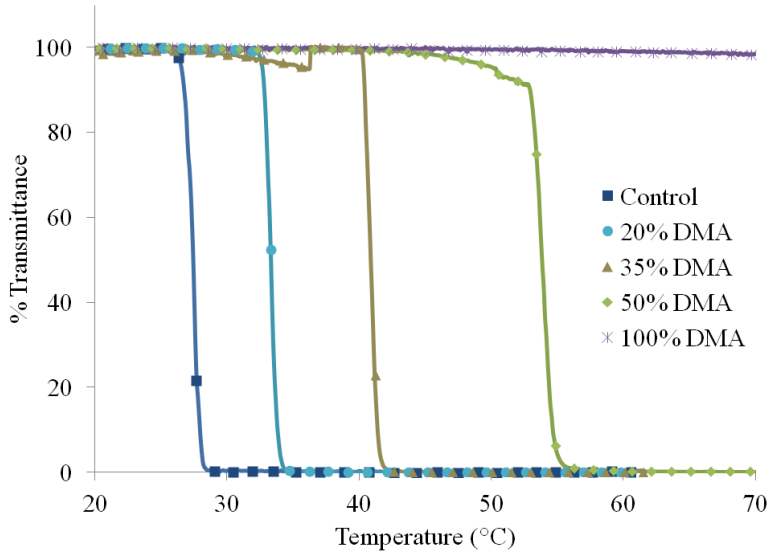

Figure 4.7: pNIPAAm-co-DMA copolymers and their T_{cp}s. Transitions were narrow and occurred at 33.3 °C, 40.9 °C, and 53.9 °C for 20%, 35%, and 50% copolymer content, respectively.

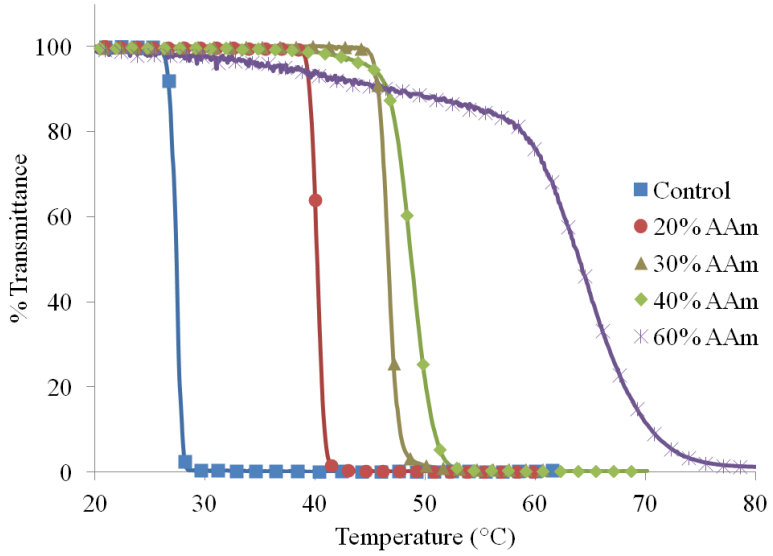

Figure 4.8: pNIPAAm-co-AAm copolymers and their T_{cp}s. Transitions were narrow and occurred at 40.2 °C, 46.7 °C, 48.8 °C, and 63.9 °C for 20%, 30%, 40% and 60% copolymer content, respectively.

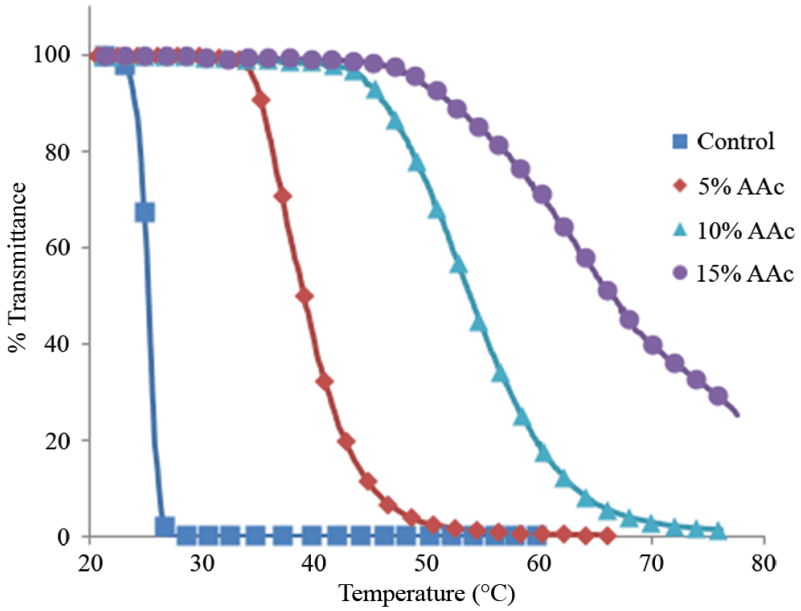

Figure 4.9: pNIPAAm-co-AAc copolymers and their T_{cp}s. Transitions were rather broad and occurred at 39.0 °C, 54.0 °C, and 66.4 °C for 5%, 10%, and 15% copolymer content, respectively.

effective at changing the T_{cp}, as shown in Figure 4.9. A mere 5% copolymer content raised the T_{cp} by 11.6 °. This efficacy was coupled with a dramatic broadening of the transition, with 15% AAc requiring more than a 30 ° range to fully transition.

The effect of hydrophilic and charged copolymers on the LCST of pNIPAAm has previously been explored in linear systems and concluded to be a result of fewer hydrophobic groups and greater polymer-water interactions [74]. While this was likely still true for highly branched polymers, the branched architecture enforced closer packing of polymer chain segments and reduced their degrees of freedom, yielding lower transition temperatures. When compared to a linear system, as shown in Figure 4.10A, the branched architecture for co-AAc demonstrated greater deviations as related to copolymer content. This indicated that in closer proximity, the additional acrylic acid groups in highly branched systems were more effective at stabilizing hydrophilic interactions with structured water and disrupting hydrophobic interactions than in linear systems. The opposite effect was shown in Figure 4.10B, with the linear

DMA system being more effective at raising the LCST. This was due to the DMA having a similar hydrophilic/hydrophobic imprint as pNIPAAm, with hydrophobic dimethyl groups protruding from the hydrophilic acrylamide fragment. The reduced degrees of freedom and close packing of the highly branched system therefore encouraged hydrophobic interactions with these chains and reduced the effectiveness of DMA as an LCST modifying agent.

In addition to raising the LCST, clearly copolymer content has a broadening effect on the polymer transition, as shown in Table 4.2. The most effective system, -co-AAc, also exhibits the broadest transitions, while the least effective system, -co-DMA, has the sharpest transitions regardless of whether the copolymers are compared at the same copolymer content or at the same transition temperature. Furthermore, regardless of copolymer, transition ranges increased with copolymer content. While the increase in transition range with copolymer content can be explained by the inclusion of more non-pNIPAAm monomers in the polymer chains, the dependence on copolymer type cannot. Since these are likely random copolymers, the implication is that the hydrophilicity of the copolymer drastically alters the hydrogen-bonding structure of the surrounding pNIPAAm and thus, its responsiveness. Since the transition range is not conserved based on the percentage of copolymer, the sharpness of the transition is not exclusively dependent upon the statistical placement of copolymer in the polymer backbone.

We propose that this effect is due to the hydrophobic properties of the comonomers. The methyl pendant groups on DMA can be co-opted into the hydrophobic structures generated by pNIPAAm, yielding a stronger and more definitive response. In fact, it is not until 50% copolymer is incorporated, that the range significantly deviates from the control. AAm lacks these pendant groups but is compact, behaving like a void space in terms of hydrophobic side groups, and is therefore unlikely to disrupt the hydrophobic structures significantly. The ability of the pNIPAAm hydrophobic

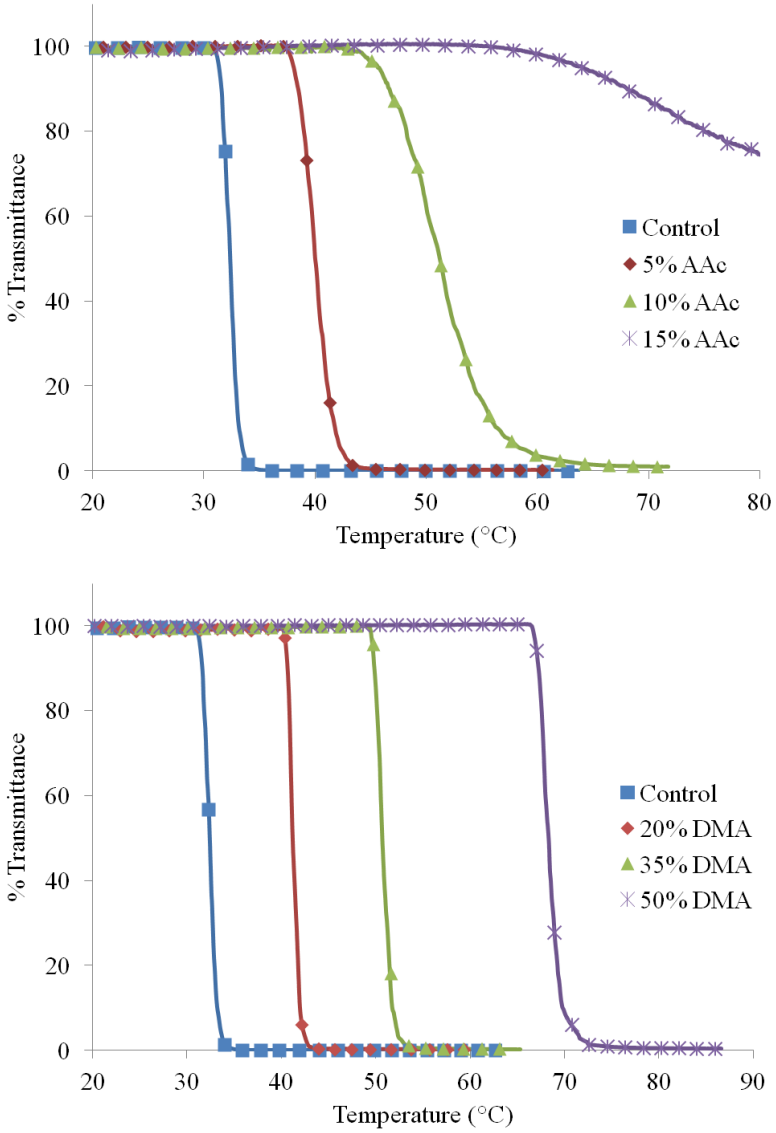

Figure 4.10: A) Linear pNIPAAm-co-AAc copolymers and their T_{cp}s. Transitions occurred at 40.0 °C and 51.2 °C for 5% and 10% copolymer content respectively. 15% AAc content started transitioning at 62 °C but did not complete its transition. B) Linear pNIPAAm-co-DMA copolymers and their T_{cp}s. Transitions occurred at 41.2 °C, 50.6 °C, and 68.3 °C for 5%, 10%, and 15% copolymer content respectively.

Table 4.2: pNIPAAm copolymer content, transition temperature and range. Copolymer content calculated via ^{1}H NMR. T_{cp} and transition range increase with copolymer content.

	Alpha[c]	Feed Ratio[e]	Composition[e]	T_{cp} (°C)	Deviation	Range (°C)
pNIPAAm	0.15	100/0	100/0	27.4	26.6-28.1	1.5
5% AAc[a]	0.17	95/5	96/4	39	34.5-48.5	14
10% AAc[a]	0.16	90/10	91/9	53.8	43.5-66.1	22.6
15% AAc[a]	0.13	85/15	83/17	66.6	49.2-80+	30+
20% DMA[b]	0.15	80/20	81/19	33.3	32.7-34.1	1.4
35% DMA[b]	0.04	65/35	64/36	40.9	40.2-41.9	1.7
50% DMA[b]	0.03	50/50	49/51	53.9	52.8-55.2	2.4
100% DMA[b]	0.08	0/100	0/100		No Transition	
20% AAm[a]	0.02	80/20	74/26	40.2	38.8-41.3	2.5
30% AAm[a]	NS[d]	70/30	68/32	46.7	44.1-48.6	4.5
40% AAm[a]	NS[d]	60/40	60/40	48.8	45.3-51.5	6.2
60% AAm[a]	NS[d]	40/60	37/63	64.9	59.9-70.7	10.8
pNIPAAm-linear		100/0	100/0	32.4	31.2-33.9	1.7
5% AAc-linear[a]		95/5	95/5	40	37.4-43.4	6
10% AAc-linear[a]		90/10	90/10	51.2	45.0-58.5	13.5
20% DMA-linear[b]		80/20	78/22	41.2	40.4-42.8	2.4
35% DMA-linear[b]		65/35	63/37	50.6	49.7-53.5	3.8
50% DMA-linear[b]		50/50	48/52	68.3	66.7-70.7	4

[a]NIPAAm content calculated from 1H NMR by dividing the integral of the isopropyl peak (∼4 ppm) from the proton adjusted integral of backbone polymer peaks (∼1.2-3.5 ppm). [b]NIPAAm content calculated from ^{1}H NMR by dividing the integral of the isopropyl peak (∼4 ppm) with the sum of the integral of the isopropyl peak and the proton adjusted integral of the dimethyl peak (∼2.8 ppm). [c]Alpha values calculated using GPC with a universal calibration. Linear polymers were analyzed using a linear calibration and model which did not produce alpha values. [d]Higher co-AAm copolymers were not soluble (NS) in THF for this analysis. [e]Ratio presented as (NIPAAm/Comonomer).

groups to compensate for these voids, however, is strongly dependent on copolymer content. Therefore, as shown in Figure 4.10, the transition range increases non-linearly with AAm content. AAc, on the other hand, is charged at neutral pH and strongly hydrogen bonds to multiple water molecules. While it is also compact like AAm, the number of bound water molecules and configuration of these strongly favored bonds disrupts the surrounding hydrophobic system. This disruption inhibits polymer collapse to varying degrees depending upon location and number of acrylic acid groups present in a particular chain. A broad transition is therefore observed in these copolymers, even at low AAc content.

To further confirm this theory and to extend the findings into physiological systems, the T_{cp}s of highly branched pNIPAAm copolymers were found when the polymers were dissolved in PBS, as shown in Figure 4.11. As expected, the T_{cp}s were significantly lower due to the ionic content of the buffer. However, typical drops in the transition temperature for linear polymers with low copolymer content are 4-5 °C [35]. In the branched samples, the transition temperature drop is 2.5-3.5 °C for up to 40% copolymer content in the case of AAm. The smaller drop in T_{cp} due to the ionic content of the solvent can be attributed to the more crowded architecture. The normal drop is caused by decreased water surface tension surrounding the hydrophobic pendant groups on pNIPAAm and the polarization of the surrounding water molecules [312]. With a more dense system, the disruption has a less pronounced effect.

The other difference of note between using water as the solvent and using PBS as the solvent is the dramatic sharpening of the T_{cp}s of co-AAc polymers. This is explained by the stabilization of the charges from the AAc groups with the cations in the solution. This stabilization removes some of the outsized effects of the negatively charged AAc groups on the temperature transition behavior. Indeed, the T_{cp} drops are significantly higher for AAc copolymers as compared to DMA and AAm copolymers. This sharpening of the transition for pNIPAAm-co-AAc in isotonic conditions

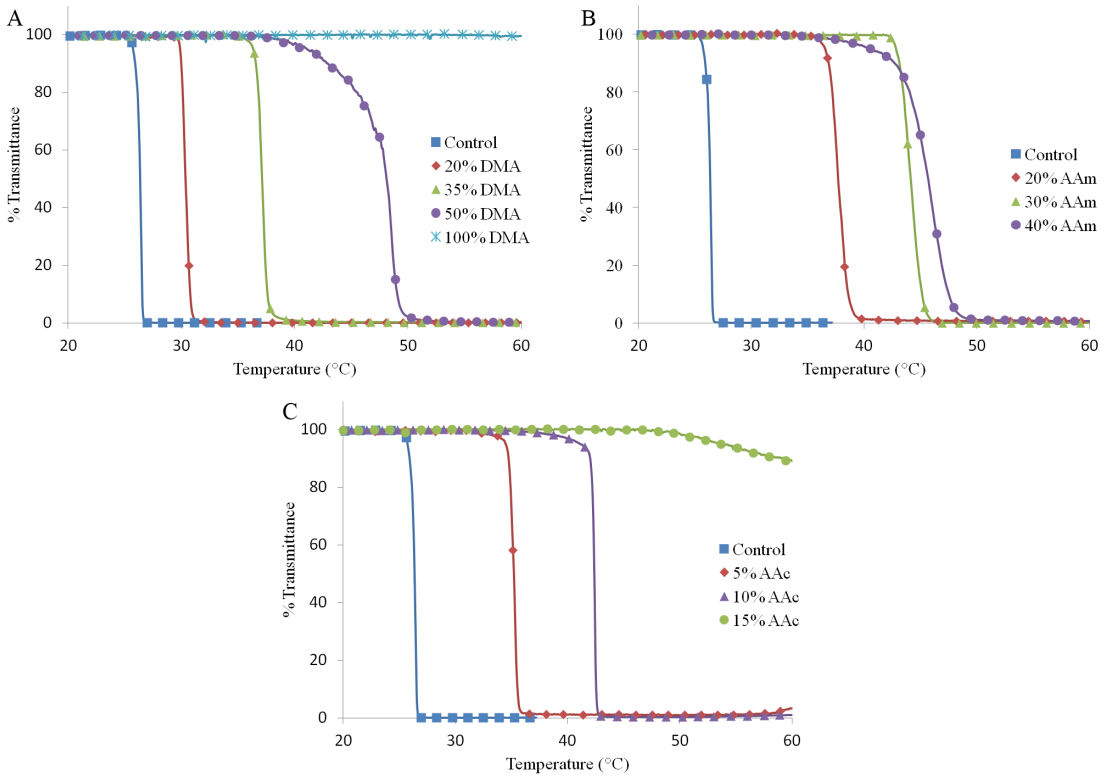

Figure 4.11: A) Highly branched pNIPAAm-co-DMA copolymers and their T_{cp}s in PBS. Transitions occurred at 26.3 °C, 30.4 °C, 37.1 °C, and 48.2 °C for 0%, 20%, 35%, and 50% copolymer content respectively. 100% DMA did not transition. B) Highly branched pNIPAAm-co-AAm copolymers and their T_{cp}s. Transitions occurred at 26.3 °C, 37.7 °C, 44.0 °C and 45.7 °C for 0%, 20%, 30% and 40% copolymer content respectively. C) Highly branched pNIPAAm-co-AAc copolymers and their T_{cp}s. Transitions occurred at 26.3 °C, 35.1 °C, and 42.3 °C for 0%, 5%, and 10% copolymer content respectively. 15% AAc content started transitioning at 50 °C but did not complete its transition.

confirms the superioriority of AAc copolymers for drug delivery applications.

4.5 Conclusion

Highly branched pNIPAAm is at once more sensitive and more robust than its linear counterpart. The synthesis of this polymer is robust since its most biologically relevant bulk property, the LCST, is resistant to changes based upon solvent interactions during polymerization and end-group modification. This resistance, especially to end-group modification, allows for the use of this polymer in a variety of constructs without the need to re-optimize the LCST every time. Additionally, it allows for end-group functionalization, providing a scaffold for small molecule targeting systems for targeted drug delivery, for example. As a result of this robust synthesis however, the only way to significantly raise the LCST of highly branched pNIPAAm is to use large amounts of copolymer. The other methods are useful in fine-tuning the transition, but by themselves are not effective enough to induce large changes in the LCST as necessary in applications such as controlled drug delivery. The choice of copolymers in this branched system is even more important than in a linear system due to the close packing of branched pNIPAAm chains. For biological applications, which use buffered solvents like PBS, AAc copolymers provide the greatest change in LCST with the smallest copolymer content.

CHAPTER V

SYNTHESIS AND CHARACTERIZATION OF HIGHLY BRANCHED PNIPAAM-GOLD NP SYSTEM

5.1 Summary

Nanoparticle drug delivery systems have seen a tremendous increase in interest in the past decade, especially biological applications and drug delivery in particular. As an example of the utility of polymer structural optimization, highly branched pNIPAAm was attached to gold nanoparticles to form pNIPAAm-gold NP complexes that can encapsulate small molecule drugs and release them upon thermal stimulus. These NPs continue to exhibit the characteristic properties of HB pNIPAAm such as the LCST. Additionally they absorb wavelengths in the nIR range due to the tuned response of the gold nanoparticles (AuNPs). When combined, the NPs exhibit greater drug loading than comparable dendrimers and superior burst drug release characteristics upon activation.

5.2 Introduction

The increasing interest in nanotechnology and in particular nanomedicine has revealed many promising materials that can be exploited in drug delivery [154]. One of the most promising is the AuNP [24, 243]. As described in Chapter 1, the localized surface plasmon resonance (LSPR) of AuNPs can be tuned based on the shape, size, and composition of the AuNPs and heat significantly upon activation [161, 162, 129, 41, 40]. Even single NPs can heat localized areas up to 10 °C using a 1 mW laser [113]. LSPRs in the near-infrared (nIR) range can produce AuNPs with externally-activated cancer cell thermolysis capabilities [41, 162]; however, the depth of tissue

penetration of nIR lasers is on the order of centimeters and cannot properly destroy deep tissue tumors. While nIR wavelengths can pass through up to 10 cm of tissue [277], attenuation weakens the signal to such an extent that cell lysis have not been achieved under current conditions beyond one or two centimeters [61, 162]. To help extend the effective range of this type of therapy, hybrid polymer-NP materials can be synthesized with complementary properties between the polymers and the NPs.

5.2.1 pNIPAAm-NP conjugates

pNIPAAm, the quintessential thermally responsive [69, 86], biocompatible [266, 164] polymer, has the potential to use the heat generated by nIR activation of AuNPs to provide controlled release of encapsulated drugs. The temperature transition, normally at 32 °C, can be increased using a variety of methods to facilitate a transition in the physiological range. A coating of pNIPAAm on AuNPs can therefore be manipulated using nIR lasers [113]. The resulting change in conformation can be used to release drugs as shown in Scheme 5.1.

Indeed, several groups have created pNIPAAm-gold nanoconstructs in attempts to exploit these properties [135, 212]. These include coated nanorods, coated nanocages, and nanogels encapsulating gold nanoparticles [135, 299]. While some constructs have demonstrated controlled release, the majority of methods only demonstrate increased release rate over normal diffusion upon LCST rather than burst release.

To account for this limitation, we conjugated highly branched pNIPAAm to AuNPs. As described in detail in Chapters 1-4 of this thesis, pNIPAAm can be synthesized into varying architectures, both in backbone architecture and branching architecture. The polymer transition can be tuned using these mechanisms for sharp transitions at a variety of temperatures. Highly branched polymers exhibit many similar properties with dendrimer-like polymers and can be used to encapsulate or load small-molecule drugs such as the anti-cancer drug doxorubicin (DOX). As shown in Chapter 4,

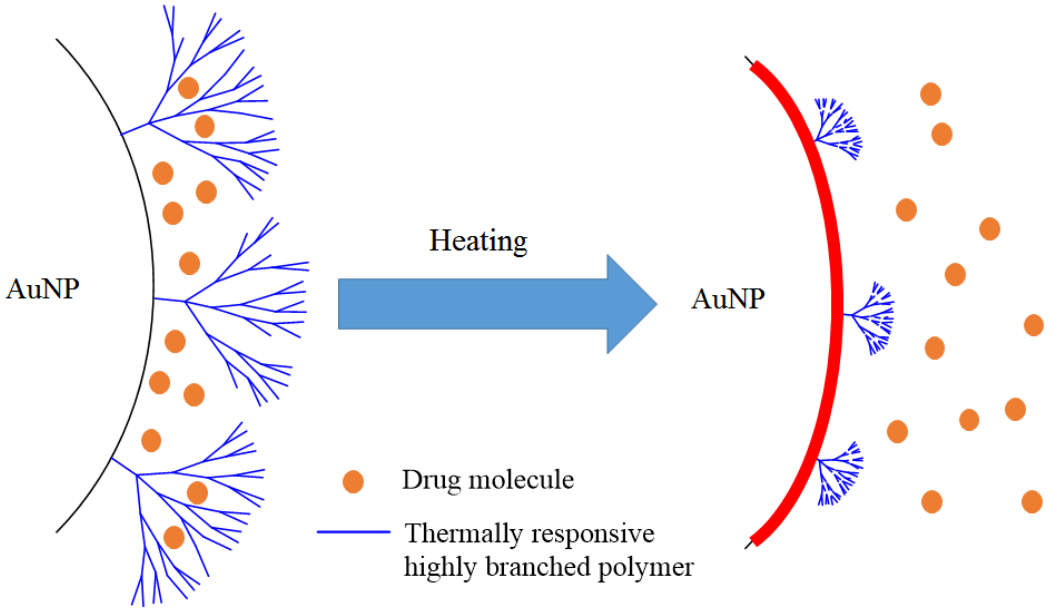

Scheme 5.1: Drug release from a AuNP coated with highly branched pNIPAAm. The nIR laser is absorbed by the AuNP, causing conformation change in the pNIPAAm, thereby squeezing out the entrapped drug molecules.

highly branched pNIPAAm can be synthesized with a variety of properties including an LCST between 40 °C and 50 °C under isotonic conditions. A highly branched pNIPAAm-AuNP construct has the potential to provide superior drug-loading and release capabilities using the thermal activation provided by the AuNPs, as shown in Scheme 5.1. The release temperature is much lower than that required for cell ablation; therefore, it is potentially suitable for deep tissue tumors.

In this chapter we describe conjugation of highly branched pNIPAAm to AuNPs, adjust the transition temperature, and characterize the drug release profiles. As shown in Scheme 5.2, HB pNIPAAm is conjugated onto AuNPs to provide dense surface structures in which encapsulated small-molecule drugs can be encapsulated. Upon heating, the hydrated pNIPAAm will collapse three-dimensionally, squeezing out encapsulated drug.

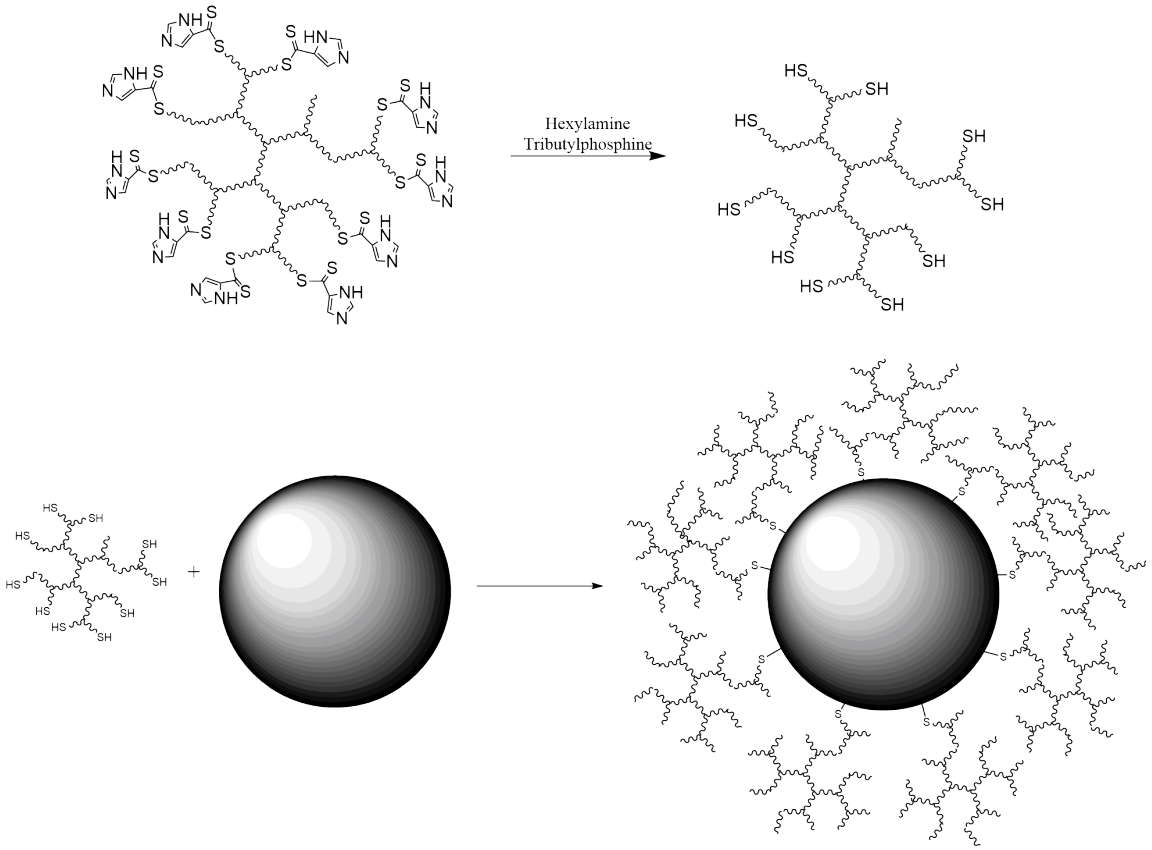

Scheme 5.2: pNIPAAm-NP conjugation. Highly branched pNIPAAm synthesized using RAFT polymerization was cleaved yielding terminal thiols. Thiols were then reacted with the gold on AuNPs, forming thiol-gold bonds to coat the NPs.

5.3 Materials and Methods

N-isopropylacrylamide was purchased from TCI America and recrystallized in a 9:1 ratio of hexanes:benzene. Hydrogen tetrachloroaurate(III) trihydrate was purchased from Alfa Aesar. Sodium thiosulfate, 1-hexylamine, 5,5-dithiobis(2-nitrobenzoic acid), and tributylphospine were purchased from Sigma Aldrich and used without further purification. Doxorubicin hydrochloride was purchased from Alfa Aesar and used without further purification.

5.3.1 Highly branched pNIPAAm copolymer synthesis and characterization

Highly branched pNIPAAm-*co*-AAc of varying copolymer content was synthesized similar to that described in Chapter 4 [36]. Briefly, a 1.03 g mixture of 93:7:1:0.2 ratio of NIPAAm:AAc:**2**:AIBN was placed in a sealed 25 mL round-bottom flask equipped with a magnetic stir bar. The mixture was purged with nitrogen for 15 min and 10 mL of nitrogen- purged 1, 4 dioxane was added. The solution was reacted at 65 °C for 48 h and was quenched by exposure to air. The copolymers were precipitated in diethyl ether and collected via filtration. Successful copolymerization was confirmed using NMR and GPC. GPC was conducted on a GPC-50 Plus (Agilent, Inc.) equipped with two PLgel 3μm MIXED-E columns with UV, RI, and viscosity detectors. Tetrahydrofuran (THF) was used as the polymer solvent and eluent. A flow rate of 1 mL/min was used. Chromatograms were compared with those of polystyrene standards (Agilent Inc). ^{1}H NMR was conducted on a Varian Mercury Vx 400 spectrometer using chloroform-d as a solvent. The turbidity of pure polymers was measured using UV-Vis spectrometry conducted at constant pH (7.0 ± 0.1) using a Cary 50 UV-Vis Spectrophotometer (Agilent Inc.) with a single cell peltier thermostatted cell holder and accessory for temperature control. Scans were conducted every 0.1 °C, and the temperature was ramped at 1 °C/min.

5.3.2 AuNP Synthesis

Gold-gold sulfide nanoparticles were obtained from our collaborator Dr. André Gobin at the University of Louisville and was synthesized according to Gobin et al. [247] Briefly, 3 mM $Na_2S_2O_3$ solution was directly added into 1.7 mM $HAuCl_4$ solution with the volumetric ratio of 2.8 ($HAuCl_4$:$Na_2S_2O_3$) and gently shaken for 15 sec. The mixture was then reacted for 1 h. The AuNPs were then centrifuged at 1200 g for 20 min to remove most of the gold colloid by-products and increase purity of the nIR absorbing fraction of nanoparticles. The pellets were collected and the corresponding supernatants were spun down again to increase yield. This method of purification by centrifugation was performed three times. Particles were characterized using UV-Vis spectrometry, DLS and TEM.

5.3.3 pNIPAAm-NP Synthesis

The chain transfer agent on the highly branched pNIPAAm cleaved via aminolysis using hexylamine. Thiol functionality was maintained using tributylphospine. Briefly, 1 g of pNIPAAm was reacted with 230 L of 1-hexylamine and 247 L of tributylphosphine in 25 mL of 1, 4 dioxane under nitrogen for 2 hrs. The product was precipitated in cold ether, filtered, and dried *in vacuo*. Dried samples were stored at $-80\,^{\circ}\mathrm{C}$. An Ellmans assay was conducted to confirm the presence of thiols [70]. In brief, 100 L of 100 M solution of lysed pNIPAAm in 0.1 M Tris buffer, pH 8 was reacted with 100 L of 4 mg/mL of 5,5-dithiobis(2-nitrobenzoic acid) in Tris buffer. Absorbance was measured at 410 nm on a Beckman DTX 880 Multimode Plate Reader and was compared to standards made with known concentrations of L-cysteine.

Cleaved pNIPAAm-*co*-AAc was reacted with AuNPs to form pNIPAAm-NPs. Briefly, 20 mg of cleaved pNIPAAm-*co*-AAc was dissolved in 1 mL of nanopure water. 4.8×10^{11} AuNPs were added to the solution and reacted in the dark overnight. The pNIPAAm-NPs were centrifuged at $5000 \times g$ for 15 mins. The supernatant was

discarded and the particles were resuspended in 1 mL of nanopure water. This wash process was repeated two times and after the third centrifugation, the pNIPAAm-NPs were resuspended in 1 mL of PBS.

5.3.4 pNIPAAm-NP Characterization

General characterization was performed using UV-Vis spectrometry, DLS, and SEM. DLS was conducted on a Malvern Zetasizer Nano ZS. SEM was conducted on a Zeiss Ultra60 FE-SEM.

Chemical conjugation of pNIPAAm onto the NPs was confirmed by the following. 10 mg of cleaved pNIPAAm was dissolved in 1 mL of nanopure water. 2.4×10^{11} AuNPs was added to the solution and reacted in the dark overnight. The pNIPAAm-NPs were then centrifuged at 5000 $\times$ g for 15 mins and the supernatant was removed. The pNIPAAm-NPs were then resuspended in nanopure water and 5 μL or 50 μL of propanethiol was added to the suspension. The suspension was incubated at room temperature for 1 hr, 6 hrs, or overnight, then centrifuged at 5000 g for 15 mins and the supernatant was removed. The pellet was resuspended in nanopure water and the NP size was taken using DLS.

The LCST of pNIPAAm-NPs was also observed using DLS. 1.2×10^{11} particles were suspended in 1 mL of PBS. Size versus temperature readings were conducted at a ramp rate of 1 °C every five minutes. Between 12 and 20 scans were taken per temperature point depending on the quality of the data and the average sizes are reported.

5.3.5 Model drug loading

Doxorubicin hydrochloride (DOX) was encapsulated in pNIPAAm-NPs via diffusive loading. Briefly, 36 μL of 8.3 μM solution of DOX was added to the pNIPAAm-NP suspension. The suspension was then vortexed and kept at 4 °C for 60 hrs. The pNIPAAm-NPs were then centrifuged at 5000 $\times$ g for 15 mins, the supernatant

was removed, and the pellet was resuspended in 1 mL of PBS. The supernatant concentration was then compared to controls of DOX with only Au-NPs, only PBS, and only polymer to determine pNIPAAm-NP drug loading.

5.3.6 Drug release

DOX release was measured using a Beckman DTX 880 Multimode Plate Reader and was compared to standards made with known concentrations of DOX. Readings were conducted at 485 nm. Since different buffers are known to affect the relation between between concentration and absorbance [246], different calibration curves were generated for PBS and water.

DOX passive release was quantified using two different methods. First, DOX loaded pNIPAAm-NPs were centrifuged at various time points. The supernatants were then collected and compared to standards in order to calculate DOX concentration. Second, DOX loaded pNIPAAm-NPs were dialyzed using 3.5K MWCO Spectra/Por 3 dialysis tubing in 40 mL of water or PBS and the concentration of DOX in the bath was measured at various time points.

Active drug release was also quantified using the same methods. First, microcentrifuge tubes of DOX loaded pNIPAAm-NPs were placed in 65 °C for thirty minutes. They were then centrifuged at 5000 g for 15 mins and the supernatant was collected and compared to unheated DOX loaded pNIPAAm-NPs, (n=6). Second, DOX loaded pNIPAAm-NPs were dialyzed in 50 °C water or PBS as maintained by an Ika C-Mag HS 7 thermostatted hot plate and the bath DOX concentration was measured at various time points, (n=4). Statistical significance was measured using an ANOVA test with Tuckey's post-hoc analysis.

Table 5.1: Bare AuNP sizes in suspension. 3 distinct species exist. While the majority of the mass is in the larger NPs, the smallest NPs exist in far greater quantity.

Diameter	% Mass	% NPs
69.29 ± 3.47	$80.87 \pm 1.37\%$	0.09%
9.44 ± 1.43	$11.09 \pm 0.94\%$	4.9%
2.70 ± 0.24	$5.07 \pm 0.59\%$	95%

5.4 Results and Discussion

5.4.1 pNIPAAm-NP characterization

AuNPs obtained from Dr. Gobin contained a mixture of three different sizes of particles: Larger, 69 nm in diameter particles, small 9 nm in diameter particles, and very small 3 nm in diameter particles. Previous studies have shown that the NPs with LSRPs in the nIR range are the 69 nm NPs [247]. These NPs generally have triangular plate morphology and strongly absorb wavelengths in the nIR range.

DLS measurements of the samples revealed that 81% of the mass correlated to the 69 nm size while 11% correlated to the 9 nm size and 5% correlated to the 3 nm size, as shown in Table 5.1. Due to the size discrepancy between the larger and smaller NPs, the larger NPs constitute $< 1\%$ of NPs in the suspension. Upon multiple centrifugation and resuspension steps, the 3 nm nanoparticles were removed from the mixture; however, the 9 nm NPs remain in suspension, making up 98% of the NPs.

HB pNIPAAm was coated onto AuNPs using thiol-gold chemistry. SEM was conducted on the resulting NPs, as shown in Figure 5.1. The SEM shows aggregates of AuNPs for bare particles but discreet particles for the coated NPs. Figure 5.1b also shows polymeric halos surrounding many AuNPs in addition to a few discreet bare AuNPs of both 69 nm size and 9 nm size.

DLS measurements of the NPs showed that the pNIPAAm indeed coated the NPs. As elaborated in Table 5.2, there was a size difference of over 20 nm between the AuNPs and the pNIPAAm-NPs for the larger NPs. This is in line with theoretical

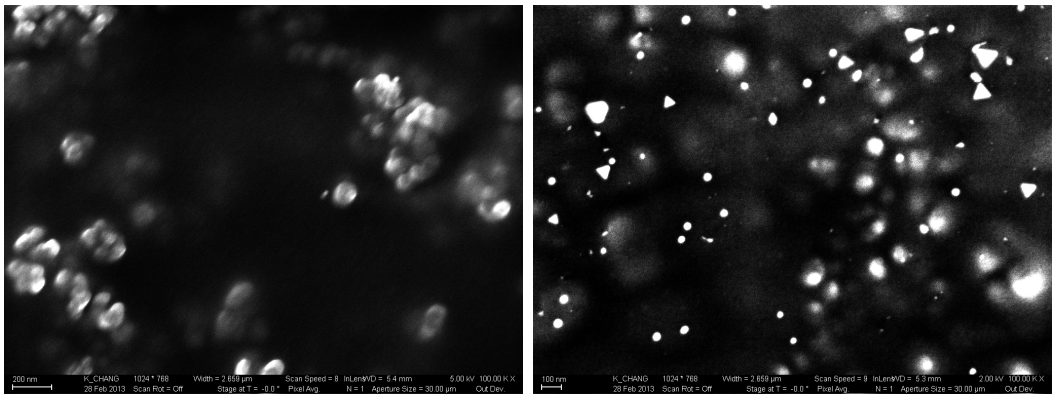

(a) Bare AuNPs (b) pNIPAAm-NPs

Figure 5.1: SEM of bare AuNPs and pNIPAAm-NPs. NPs formed clusters when bare but were discreet when coated. pNIPAAm-NPs showed NPs with polymer halos as well as discreet, uncoated, high contrast triangular plate 69 nm NPs and a population of small 9 nm NPs.

Table 5.2: pNIPAAm conjugated onto AuNPs: Particle diameter, absorption, and zeta potential.

	Larger NP Diameter (nm)	Smaller NP Diameter (nm)	nIR Absorption Wavelength	Zeta Potential
Bare AuNPs	69.29 ± 3.47	9.44 ± 1.43	958	-22.63 ± 0.252
pNIPAAm-NPs	90.37 ± 0.83	12.80 ± 1.92	957	-7.27 ± 1.20

values based upon molecular weight and branching calculations of the polymer. The smaller NPs also appeared to increase in size but the increase was not statistically significant indicating little if any polymer coating on the smaller NPs. There was also a significant change in the zeta potential between AuNPs and pNIPAAm-NPs, indicating that the surface charge of the NPs changed significantly upon coating with pNIPAAm. Combined, the data indicated that the coating was successful. The LSPR was also not greatly affected, as shown by the change in maximum absorption wavelength of only 1 nm.

Since the most desired property of AuNPs for drug delivery in conjunction with pNIPAAm is the LSPR at ∼900 nm, further studies were conducted to ensure LSPR stability. Conjugation of HB pNIPAAm onto the AuNPs slightly red-shifted the LSPR of the nanoparticles, as shown in Figure 5.2. In addition, the polymer amide bands at ∼290 nm were still observed after several washes of the NPs. This combined with the shift in the LSPR, continued to affirm successful conjugation between the polymers and the NPs. In addition to conjugation, the absorbance spectrum indicated that the presence of the polymer, whether in excess or not, had minimal effect on the LSPR and the pNIPAAm-NPs exhibited an LSPR still in the nIR range.

Although coating of the NPs was confirmed through sizing and zeta potential measurements, a separate experiment was conducted to confirm that the coating was a chemical conjugation and not just association. To confirm chemical conjugation of the pNIPAAm to the NPs, a DLS experiment was conducted. Figure 5.3 shows that uncleaved polymer without the thiol terminal groups did not significantly associate with the AuNPs, but the cleaved polymer caused a significant increase in size from 72 nm to 90 nm. Additionally, a small molecule thiol, propanethiol, was added to the conjugated NPs to displace the conjugated polymer and confirm that the bond formed was indeed a thiol-gold bond. As shown in Figure 5.3, at sufficiently high concentrations, propanethiol was able to displace the pNIPAAm from the AuNPs,

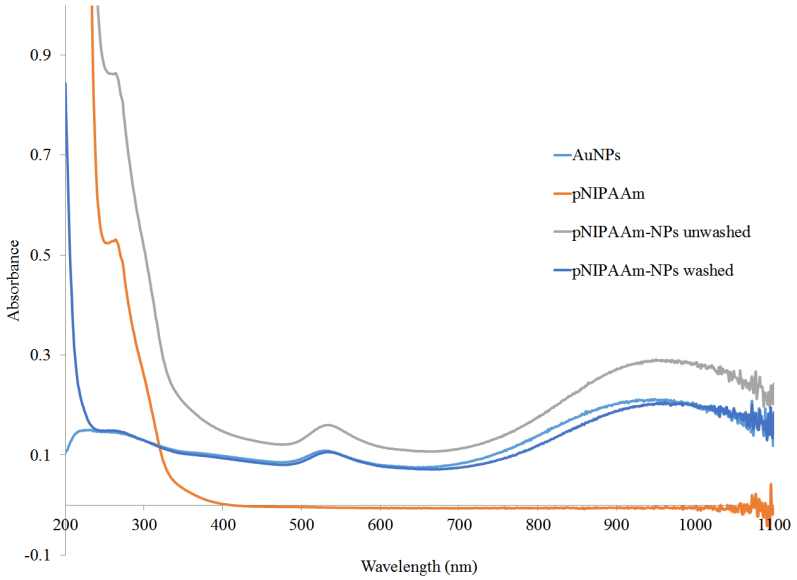

Figure 5.2: UV-Vis absorbance of pNIPAAm-NPs and controls. The amide band of the polymers is seen at 295 nm. The gold bands are seen at 530 and 950 nm.

resulting in smaller particles. With a lower concentration of propanethiol, however, the change in size was not statistically significant although a decreasing size trend can be seen with increasing incubation time. The final size of the propanethiol conjugated NPs was similar to that of the bare nanoparticles as expected, confirming that the cleaved HB pNIPAAm was chemically conjugated to the AuNPs through a gold-thiol bond.

In addition to confirming gold-thiol bond formation, Figure 5.3 also showed strong indications that these NPs would not be affected by serum concentrations of thiols. Plasma is estimated to have thiol concentrations between 324 μM and 510 μM [2, 3]. The tested thiol concentrations are 55 mM and 525 mM for 5 μL and 50 μL of propanethiol, respectively. Since there was more than two orders of magnitude difference between expected concentrations and tested concentrations, we do not expect serum thiol concentrations to play a significant destabilizing role for the pNIPAAm-NPs. Since pNIPAAm is known to be biocompatible, with 100% viability in cell studies for concentrations up to 10 mg/mL [266], and thiol concentrations *in vivo*

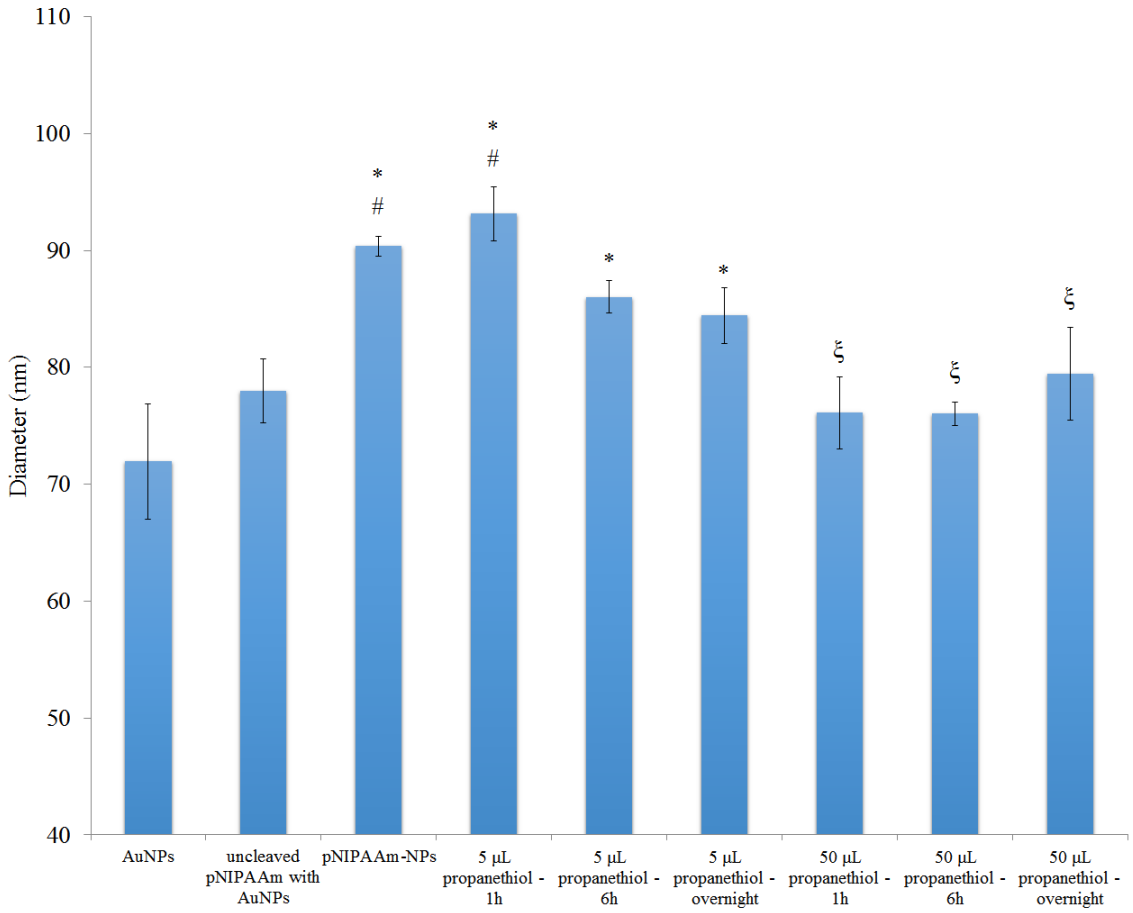

Figure 5.3: NP sizes as measured using DLS. Uncleaved pNIPAAm with imidazole ends do not cause NP sizes to increase. Cleaved pNIPAAm conjugated onto the AuNPs (pNIPAAm-NP) increases the size significantly, by 20 nm, as compared to AuNPs(*, $p<0.05$) and uncleaved pNIPAAm (#, $p<0.05$). Subsequent substitution by high concentrations of propanethiol reduces the size significantly as compared to the pNIPAAm-NPs (ξ, $p<0.05$) to near bare AuNP levels (n=3).

are not high enough to degrade the constructs, we expect the pNIPAAm-NPs to be tolerated *in vivo* at least from a toxicity perspective.

Previous data shown in Chapter 4 suggested that pNIPAAm-*co*-AAc copolymers with slightly greater than 10 % copolymer content would exhibit temperature transitions near 45 °C in PBS. However, in an attempt to increase branching, a lower initiator concentration was used in the polymerization (a molar ratio of 100:1:0.2). As a result, higher transition temperatures are produced, as shown in Figure 5.4.

pNIPAAm without copolymers now transitions at 25.4 °C, as opposed to 26.3 °C from a 100:1:0.5 polymerization ratio. This is consistent with more branching since there is a greater reduction in the degrees of freedom with greater branching. This affects the structured water dissolving the side chains of pNIPAAm and lowers the LCST.

Surprisingly, the the AAc copolymers increase in LCST. Figure 5.4 shows that 5% AAc copolymer now transitions at 40.2 °C as opposed to 35.1 °C, and the 10% AAc copolymer transitions only partway, with still $>$ 50% transmittance at 55 °C as opposed to a complete transition and LCST of 42.3 °C. The reason for this seemingly contradictory increase in LCST, as opposed to a continuing of the trend of decreasing LCST, is also explained by greater branching. Increased branching causes a more dense structure; therefore, the water stabilizing effect of the AAc affects more chains, causing greater increase in LCST than otherwise expected. This effect is great enough that 10% AAc no longer turns opaque due to the flocculation upon its transition, an effect not seen until 15% AAc content in less-branched polymers. The polymer properties and composition are shown in Table 5.3.

As shown, 5% AAc copolymers exhibited LCSTs closest to 45 °C. When combined with the nanoparticles the LCST changes only slightly. The transition temperature was measured for pNIPAAm-NPs using DLS and the transition temperature was taken as the temperature at which aggregation started occurring, or when the size

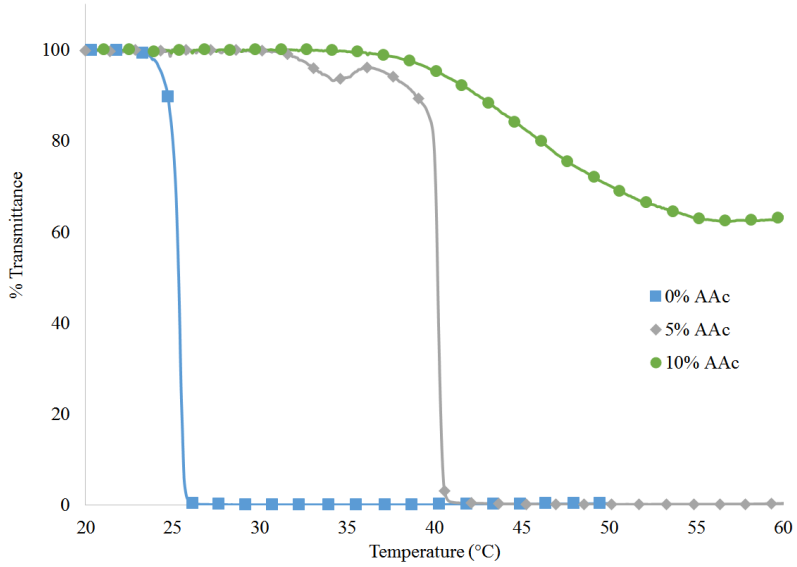

Figure 5.4: UV-Vis cloud point measurements of pNIPAAm copolymers. 0%, 5%, and 10% pNIPAAm-co-AAc copolymers show 25.4 °C, 40.2 °C, and 55 °C transitions respectively.

Table 5.3: pNIPAAm for conjugation onto AuNPs: Molecular weight, polydispersity index, alpha values, and composition

	M_n [a]	M_w [a]	PDI[a]	Alpha	Composition[b] (NIPAAm:AAc)
0% AAc	9,800	16,200	1.7	0.12	100:0
5% AAc	8,300	13,100	1.6	0.12	95:5
10% AAc	9,200	15,100	1.6	0.12	90:10

[a] Molecular weights and polydispersity indexes calculated from GPC using a universal calibration with RI and viscometer detectors. [b] Copolymer composition was measured using ^{1}H NMR.

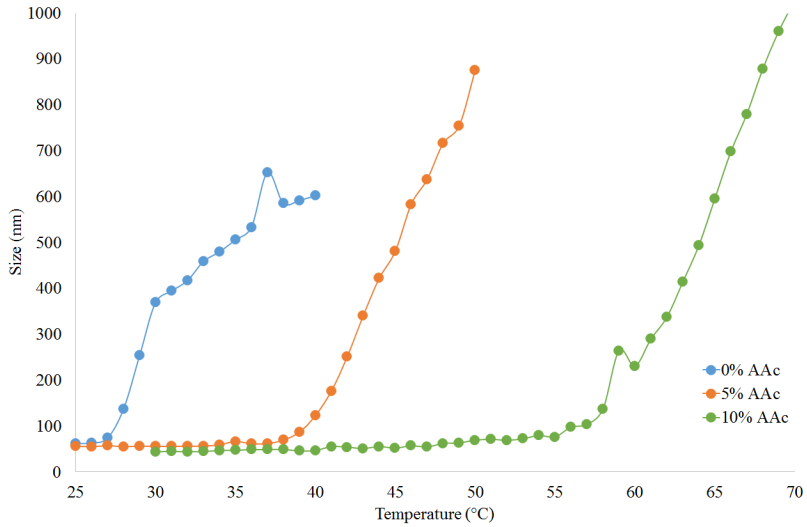

Figure 5.5: LCSTs of pNIPAAm-NPs. 0% AAc transitioned at 27 °C. 5% AAc transitioned at 39 °C. 10% AAc transitioned at 58 °C.

dramatically increases. Figure 5.5 shows transition temperatures of 27 °C, 39 °C, and 58 °C for 0%, 5%, and 10% AAc respectively.

To ensure that there was no discrepancy in measured LCST due to measurement technique, a sample was also measured using UV-Vis spectrometry. As shown in Figure 5.6, similar concentrations of free-floating polymer and conjugated polymer show a 3.5 °C difference in LCST. Of note here is that the transitions start at nearly the same temperature but the NPs display a wider curve. This could be due to fact that while both samples have the same overall concentration of pNIPAAm, the NPs have areas of high concentration (next to the NPs themselves) and areas of low concentration (everywhere else). In this case, pNIPAAm transition may occur at the same temperature but the low concentration of NPs prevent a sharp change in opacity due to flocculation. Dilute NP conditions contributed to the small difference in transmittance for the NP sample. Higher concentrations of NPs were tried but exhibited poor transparency in suspension.

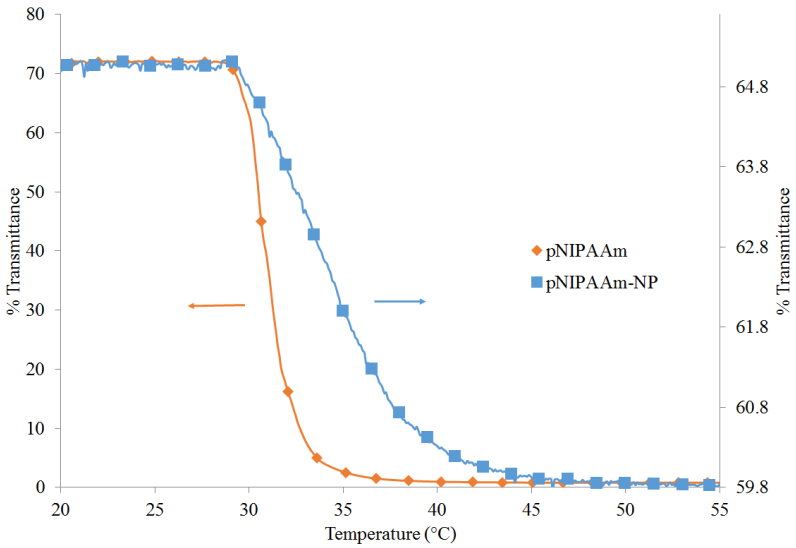

Figure 5.6: LCSTs of pNIPAAm and associated pNIPAAm-NP. pNIPAAm transitioned at 31.1 °C while pNIPAAm-NP transitioned at 34.3 °C.

5.4.2 Drug Loading and Release

Drug loading and release was conducted on linear and HB pNIPAAm conjugated to AuNPs. DOX was used as the model drug and loading was conducted via diffusion in the hydrated state. Loading was confirmed through the measuring of the difference in DOX concentration between samples and controls. While it is common for drug loading of polymer constructs to be characterized by drug loading efficiency (DLE) and drug loading content (DLC) [283, 246, 10, 1, 9], DLC is misleading in this circumstance due to the high comparative mass of the solid AuNP. DLE is commonly calculated using Equation 4; however, it is also misleading in that it is only comparable among drug loading systems that synthesize the nanoparticle in the presence of drug. In the case of diffusive loading, it would be extremely dependent upon the concentration of the NPs. High DLE can be achieved using massive amounts of pNIPAAm-NPs compared to the concentration of drug while the actual loading efficiency of the construct is not accurately measured.

$$DLC = \frac{Weight\ of\ encapsulated\ drug}{Weight\ of\ polymer} \tag{3}$$

$$DLE = \frac{Weight\ of\ encapsulated\ drug}{Weight\ of\ feed\ drug} \tag{4}$$

In order to more accurately measure the drug loading of the construct, the construct loading efficinecy (CLE) was calculated by taking the loading percentage of the theoretical maximum (see Equation 5). The theoretical maximum loading was calculated by dividing the free volume of the polymer construct by the volume of DOX. The mean drug molecules per NP was calculated by using the concentration of DOX remaining in the water after drug loading.

$$CLE = \frac{Mean\ drug\ molecules\ per\ NP}{Theoretical\ max\ drug\ molecules\ per\ NP} \tag{5}$$

Figure 5.7 shows the average loading of pNIPAAm-NPs. The calculated CLE is 39% with an average of 38,000 DOX molecules per pNIPAAm-NP. This is an 8.4% w/v loading for the polymer and approximately 885 drug molecules per polymer. Such loading is far greater than that of similar molecular weight commercially available dendrimers [39].

As shown in Figure 5.7, when incubated over 3 days in the dark at 4 °C, the pNIPAAm-NPs reduce the free DOX concentration by 27.6 μM in a 1 mL solution. The bare nanoparticles, however, showed no significant difference from the control after undergoing the same processing, indicating that the drug is in fact entrapped by the polymer on the surface of the particles and not associating with the nanoparticle surface.

After drug loading, release studies were conducted using both centrifugation and

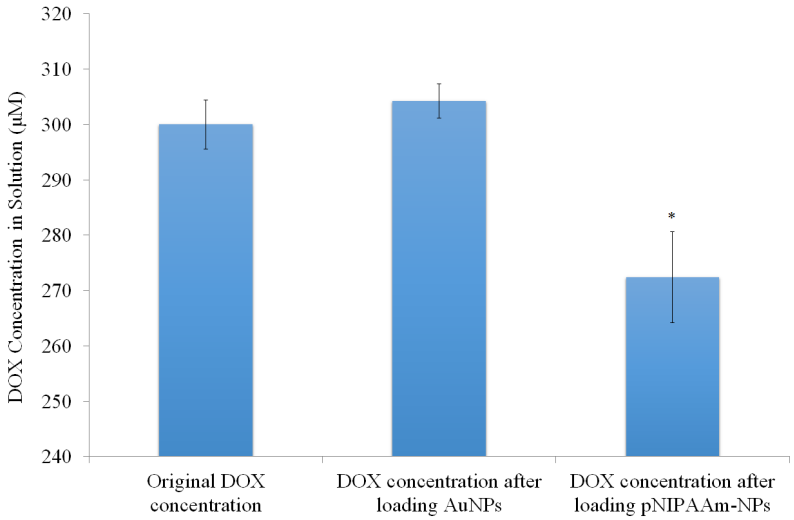

Figure 5.7: Diffusive loading of DOX into the pNIPAAm-NPs. After 3 days of incubation, no DOX was loaded onto bare AuNPs while 27.6 nmol of drug was loaded into 4.8×10^{11} pNIPAAm-NPs (n=6, p<0.01).

dialysis. Dialysis is the predominant method of measuring drug release from nanoparticles [231, 246, 307, 9]; however, it does not differentiate between the drug release rate and the diffusion rate across the membrane [307]. The measurements have to be taken from outside the dialysis tubing due to the NPs inside the tubing interfering with the readings. As such, the measurements are aggregate numbers that contain both NP drug release rates and membrane diffusion rates. Therefore, while a linear profile from such a study does indicate release, it may not be evidence of steady release. While the diffusion constant can be calculated and release rates back-calculated, serious assumptions are necessary about the mechanism of action and the calculations will only be as accurate as these assumptions.

As shown in Figure 5.8, in which 310 μM DOX in water was dialyzed against nanopure water, the dialysis membrane did not allow for complete release even after 24 h, due to the DOX becoming bound to the membrane. The drug release profile also shows that it takes up to 3 h before maximum release is achieved, indicating DOX release measurements are heavily diffusion limited under established release measurement methods. In addition, the temperature of the water bath significantly

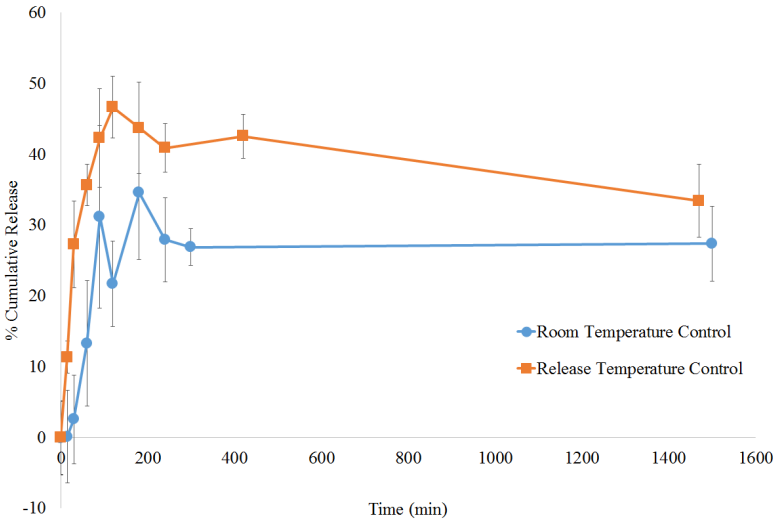

Figure 5.8: Release of DOX from dialysis tubing. Release was complete within 3 h with the cumulative release depending upon the temperature. Room temperature (20 °C) dialysis released 27% while release temperature (50 °C) dialysis released 42.5% (n=4)

affects the final cumulative release.

Figure 5.9 shows the diffusion release and the activated release of pNIPAAm-NPs as compared with NPs coated with linear pNIPAAm. Activation was conducted by placing the dialysis tubing into water above the LCST. As shown, approximately 10% of the loaded DOX was exuded from the pNIPAAm-NP system after 1 day of dialysis at room temperature with no additional release after 2 h. After 24 h without additional release, the system was activated in 50 °C water and the release immediately increased to 40% of the loaded DOX within 5.5 h. As a comparison, DOX has a maximum cumulative release of 42.5% $\pm$ 3%, as shown in Figure 5.8 due to DOX adhering to the membrane. This allows us to reasonably conclude that nearly all of the loaded DOX was released from the pNIPAAm-NPs upon activation. Since the release took 2.5 h longer than that of the control shown in Figure 5.8, release was probably not instantaneous although this method does not allow for proper quantification of the pNIPAAm-NP release profile.

When compared to pNIPAAm-NPs, the linear control in Figure 5.9 shows a much

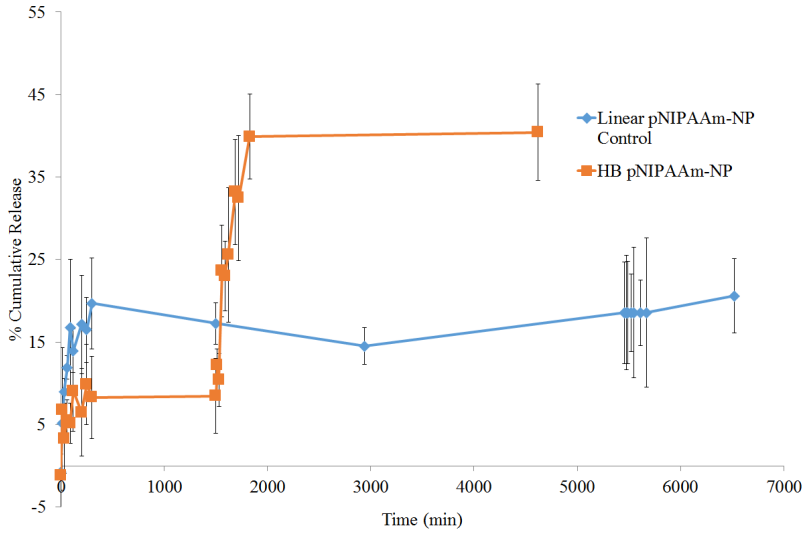

Figure 5.9: Release of DOX from pNIPAAm-NPs and linear pNIPAAm coated NPs as observed by dialysis. Activation of pNIPAAm-NPs was conducted at 25 h. Activation of linear pNIPAAm coated NPs was conducted at 91 h (n=4).

higher initial burst release at room temperature but no significant additional release upon activation after 3 days. The cumulative release of the linear pNIPAAm coated NPs is approximately 20%, which is only slightly less than the maximum release at room temperature of DOX from the dialysis tubing, as shown in Figure 5.8. The fact that the increase in temperature did not produce any additional release not only indicates that additional loaded DOX was not released, but it also shows that membrane-entrapped DOX is not freed upon increasing the temperature. As such, we can conclude that linear pNIPAAm does a poor job containing the associated DOX and the majority is released in solution even without activation.

To better quantify release rates, centrifugation studies were conducted. Centrifugation has also been used in the literature to quantify drug release [246]. While centrifugation does not have membrane based mass transfer limitations, it requires extensive processing which contributes to significant nanoparticle loss. In addition, centrifugation exerts force upon the NPs and can cause premature drug release.

As shown in Figure 5.10A, 20% of the loaded DOX diffuses from the pNIPAAm-NPs within 4 hours, with $>$ 90% of the diffusion occurring within the first hour. The

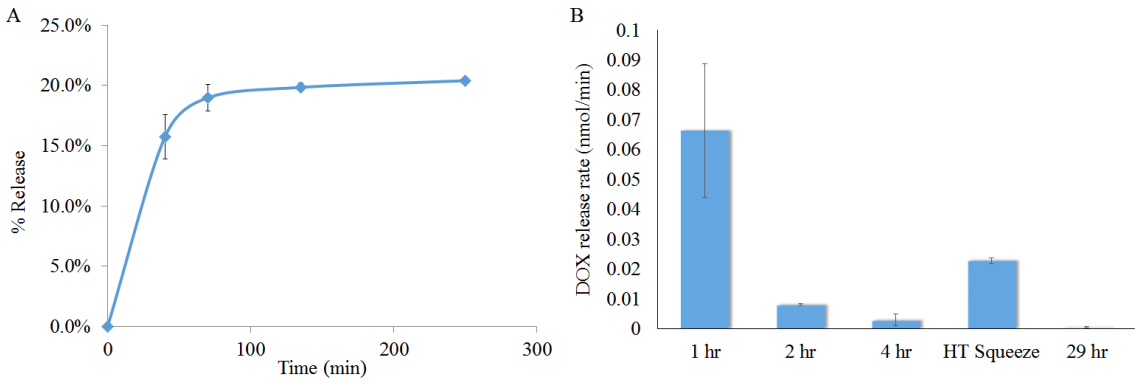

Figure 5.10: DOX release as measured using centrifugation. A) Cumulative diffusion release of DOX from pNIPAAm-NPs as measured from centrifugation (n=6). B) Release rate of DOX from pNIPAAm-NPs as measured from centrifugation (n=6). Diffusive release shows the majority of release within an hour. Release rates show decreasing release rates until activation.

time averaged release rates are shown in Figure 5.10B. After 4 hours, the NPs were heated in a 65 °C oil bath for 30 min. When heated above the LCST, the release rate significantly increased from its steady diffusion rate at 4 h, increasing from 0.003 nmol/min to 0.023 nmol/min, an increase of almost an order of magnitude. While the data indicates a dramatic increase in the release rate upon heating, it is difficult to ascertain the extent of this behavior due to the significant particle loss due to repeated centrifugation.

The combination of the centrifugation and dialysis data indicates a strong drug release response due to pNIPAAm heating. This data conclusively proves the superiority of engineered HB pNIPAAm as a coating for AuNPs for encapsulating and releasing drug molecules such as DOX in this configuration as compared to linear coatings. The HB polymers are able to suppress diffusive release beyond the initial burst and effect step-wise release upon activation.

5.5 Conclusion

Highly branched pNIPAAm coated nanoparticles show great potential as a controlled release drug delivery device. Polymer and nanoparticle properties were mostly conserved upon conjugation with pNIPAAm-NPs showing only a marginal shift in LSRP and LCST for compared to bare AuNPs and free-floating polymer, respectively. In addition, large quantities of doxorubicin can be loaded into these NPs with a loading efficiency of 39%. After an initial burst release of loosely associated DOX, HB pNIPAAm retains 80% of the loaded drug without further leaching for long periods of time. The drug can then be released upon thermal activation of the pNIPAAm-NPs with exceptional burst release properties. The drug retention and release properties of the HB polymer-NP construct are far superior to that of the linear polymer-NP control, demonstrating the advantage of structural modified pNIPAAm in this application of nanomedicine.

CHAPTER VI

CONCLUSIONS

6.1 Results and Implications

The work described in this thesis demonstrates the efficacy of architectural modification of pNIPAAm in the optimization of its bulk properties. The theoretical work of Ono and coworkers [190, 191] were expanded into their practical implications in which the tools of polymer architectural modification were used in the synthesis of biologically relevant pNIPAAm. Through changing the tacticity, modifying the end-groups, and controlling the molecular weight, homopolymer pNIPAAm can be synthesized to transition at physiological temperature under physiological conditions. Furthermore, branching was demonstrated to reduce the efficacy of end-groups as a way to modify LCST despite the increase in number of end-groups per polymer.

The implications of the linear pNIPAAm work led to insights into the compatibility of combinations of end-group, molecular weight, and tacticty control on the LCST of pNIPAAm. These three methods can work together using thermally initiated room temperature polymerization and maintain controlled characteristics even after long periods of polymerization time. The resulting polymers have majority racemo diads, well-controlled molecular weight, and defined end-groups. This translated into modified LCSTs that can be tuned to $> 37\,^{\circ}\mathrm{C}$ even in the chaotropic solvent of PBS. LCST manipulation in this manner had the added benefit of not broadening the temperature transition caused by many copolymers. From this, the power of architectural manipulation of pNIPAAm is demonstrated on its macroscopic property, the LCST.

The implications of architectural modifications on HB pNIPAAm are more varied.

HB pNIPAAm, with its shorter segment lengths, does not support racemo diad preferential polymerization in the same way that linear pNIPAAm does. Additionally, end-groups are much less effective tools for LCST manipulation. Nevertheless, copolymers can easily manipulate LCST, albiet differently depending on the side chains of the copolymers. The comparison between HB and linear copolymer pNIPAAm systems also lends insight into how the copolymer choice may effect the structured water systems surrounding these pendant groups. This, in turn, shows why certain copolymers are more effective than others at raising the LCST and why efficacy is linked with the breadth of the transition range.

These results led to examples of applications of both the linear polymer and the HB polymer. Biologically optimized linear pNIPAAm was synthesized into hydrogels with physiological mechanical properties and transitions. HB polymers were attached to AuNPs to produce step-release drug delivery nanoparticles. Both of these examples are biomedically relevant and should be further explored for their many applications.

6.1.1 Hydrogels

Hydrogels synthesized using the linear polymer demonstrated several interesting characteristics. First, they show the same influence due to end-groups as the linear polymers themselves. Since HB polymers do not show this susceptibility to end-group influence, it further implies that the HB polymers are almost uniquely resistant to end-group LCST manipulation, as shown in Scheme 6.1.

Furthermore, the hydrogels showed that tacticity manipulations, effective in linear polymer LCST modifications, carry over its efficacy into hydrogels in three important ways. First, increasing racemo diad content of the linear chains raises the LCST of the hydrogel, meaning that the structured water surrounding the pendant groups that was stabilized through increasing the racemo diad content continues to do so in a crosslinked system. Second, these majority racemo diad hydrogels respond faster

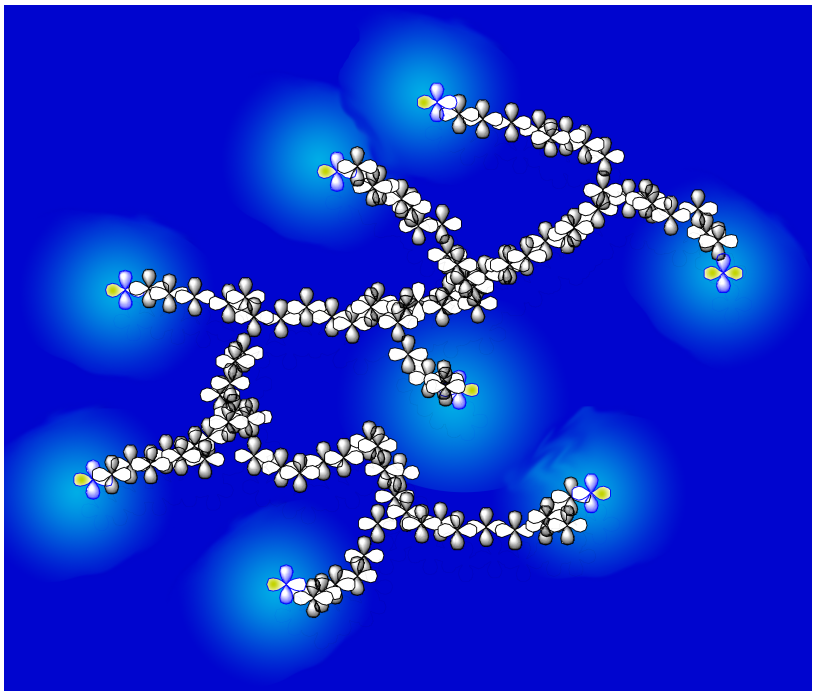

Scheme 6.1: HB pNIPAAm with hydrophilic end-groups. As shown, end-groups are forced to be more separated than in typical coils or cross-linked chains, providing a buffer against the effects of the end-groups.

and more dramatically than their comparable atactic counterparts. While additional experiments are necessary to explore the extent of the role of tacticity in hydrogel systems, preliminary indications suggest that racemo diads and the structured water in these configurations can cause additional lubrication in the system similar to that of hydrophilic copolymers or grafted surfactants. Third, these polymers show greater Young's moduli and fracture stresses than comparable atactic polymers. These properties suggest that tacticity also plays a role in chain entanglement, leading to changes in the elasticity of the material.

pNIPAAm hydrogels also have complications not seen in linear free-floating analogues. Specifically, at high concentrations necessary for stiff, physiological mechanical properties in hydrogels, the LCST can cause irreversible chain entanglement, especially at higher temperatures. This phenomenon, which has been used in a number of applications, may introduce confounding variables in the properties of pNIPAAm

hydrogels and should be investigated further.

6.1.2 pNIPAAm-NPs

HB pNIPAAm was conjugated onto AuNPs resulting in a drug delivery system that can release doxorubicin upon activation. HB pNIPAAm conjugation does not significantly shift the LSPR of the nanoparticle and coated NPs are seen to be more discreet than bare NPs. The LCSTs also remain largely unchanged due to NP conjugation. Upon diffusive loading, the loading efficiency was calculated to be 39%. Drug release from these constructs showed that after an inital burst release of approximately 20% of the loaded drug, diffusive release stops. Upon activation, nearly complete release of DOX from the NPs was observed. These properties show a highly effective drug release mechanism that overcomes one of the chronic problems of 'smart' drug delivery; that of leaky vesicles.

pNIPAAm-NPs show promise as an efficient way to overcome some of the current problems in drug delivery. Significant future work must be done however, to make this a viable drug delivery vehicle. Logical next steps include testing the release mechanism using a nIR laser and demonstrating efficacy in *in vitro* studies. Optimization of the construct in terms of circulation time, biocompatability, and toxicity must also be conducted for eventual *in vivo* trials.

While the continual developments in polymer chemistry will continue to provide new tools in the control over polymer chains, this thesis demonstrates that, in polymers that exhibit complex behavior like pNIPAAm, small changes in the polymer system can precipitate large changes in the bulk polymer behavior. Particularly for pNIPAAm, changing the end-group, tacticity, or solvent properties can be enough to provide the desired properties of the polymer. Deliberate engineering of these properties in the ever increasing numbers of branching architectures can lead to better optimized constructs. The hydrogels and nanoparticles synthesized in this thesis

provide an advanced glimpse into some of these possibilities. Their properties, as described previously, show tremendous promise because of the optimized pNIPAAm architecture and should be pursued for biomedical applications.

APPENDIX A

MATHEMATICAL MODELING OF HIGHLY BRANCHED WATER-SOLUBLE POLYMERS WITH APPLICATIONS IN DRUG DELIVERY

A.1 Summary

Although the method of moments has been used to determine the properties of copolymerizations, accounting for branching has either been ignored or required multiple dimensions to simulate. In this work, we extend our previous modeling efforts to account for hyperbranching, a form of polymerization that is particularly useful in the synthesis of targeted delivery vehicles capable of encapsulating drugs for localized therapeutics, without invoking higher dimension moment treatments. Specifically, the case of RAFT polymerization with a polymerizable double bond incorporated into the RAFT agent is modeled. This gives a very highly-branched material without the complexity of dendrimer synthesis. The model is then used to simulate three copolymerizations that illustrate the power of this model to accurately predict the copolymer properties and illustrate the polydispersity of the individual segments of the hyperbranched polymer, and the overall hyperbranched polymer. This paper models three different hyperbranched copolymer blends: acrylamide-acrylic acid, acrylonitrile-methacrylic acid, and ethylene-styrene. The first case is of specific interest in the development of hyperbranched polymers for drug delivery. The other two are included in order to explore the effects of specific kinetics on branching.

A.2 Nomenclature

A	=	Monomer of A
B	=	Monomer of B
I	=	Initiator
f	=	Efficiency of initiator
T	=	RAFT agent
R*	=	Radical from Initiator
Rˆ	=	Radical from Leaving Group
P	=	Polymer chain with terminal unit A
Q	=	Polymer chain with terminal unit B
TP	=	Polymer chain with terminal unit A bound to RAFT agent
TQ	=	Polymer chain with terminal unit B bound to RAFT agent
I	=	Initiator
M	=	Dead Chain
n	=	Specific number of monomers in polymer chain
m	=	Total number of monomers in polymer chain

A.3 Introduction

Michael Szwarcs discovery of living anionic polymerization revolutionized polymer science by allowing the production of controlled molecular architecture [249, 23]. While conventional free-radical polymerization does produce high-molecular weight polymers, the high occurence of bimolecular termination results in a minimum possible polydispersity of 1.5, and the fleeting lifetime of propagating radicals does not allow easy manipulation of molecular architecture [23]. Controlled free-radical polymerization (CRP), however, can extend the lifetime of propagating chains from seconds to

hours, which allows meaningful manipulation of molecular architecture (i.e. copolymer composition and sequence distributions) through manipulation of the ratio of various monomers during the polymerizaiton. In addition, a propagating chains lifetime during CRP is primarily spent in the dormant state, thereby reducing the occurence of bimolecular termination and producing chains with very low polydispersity.

Chiefari et al. first reported a new form of CRP that uses reversible-addition fragmentation chain transfer (RAFT) to produce polymers and copolymers with very low polydispersity indexes (typically on the order of 1.1) [144, 48, 49]. RAFT primarily uses dithio compounds as RAFT agents (also called chain transfer agents) that ensure all polymer chains grow at the same rate. These compounds consist of a leaving group (R), a di- or tri-thiocarbonate reaction core, and an activating group (Z) to drive the reversible reaction. As has been shown previously, the method of moments can be used to great success in modeling RAFT polymerization [271, 274, 309, 310]. In prior work, we have produced mathematical models illustrating the control of molecular architecture, as well as sequence determination through this method [309, 310]. Armes [267] has reported on vinyl RAFT copolymerization in which one of the monomers contains a second double bond used as the site of branching. Their work resulted in high levels of branching with unexpectedly low levels of gelation. Konkolewicz [142] has developed a kintic model of branching in RAFT polymerization. As with Armes experiments, he uses a secondary branching (divinyl) monomer. Luo [275] has developed a model based on the method of moments for the branching and ultimate crosslinking in RAFT copolymerization where on of the comonomers is a divinyl monomer. As above, they find that the presence of RAFT retards gelation. In this work, we extend our previous modeling efforts to account for hyperbranching. Highly branched nanostructures such as dendrimers and hyperbranched polymers have emerged in recent years as excellent single nanoparticle drug delivery vehicles [75]. These nanomolecular assemblies have several characteristics that make them attractive for biological and

drug delivery applications, including uniform size, water-solubility, internal cavities, and variable surface functionality [29, 51, 196]. Dendrimers in particular have been studied intensively for biological applications and are recognized as a potential breakthrough candidate as drug delivery vehicles [24, 163, 295, 45], as well as being useful in a wide variety of biomedical devices, including immunoassay tools and serodiagnostics [219, 189], magnetic resonance imaging contrast agents [279, 141] and vehicles for gene delivery [137, 51, 196, 222, 20]. Hyperbranched polymers are similar to dendrimers in the overall globular structure, and the ability to encapsulate small molecule drugs. This class of polymers is much easier to produce than its dendrimer counterpart, and by using RAFT agents that double as branching agents, hyperbranched polymers can approach the well-defined structure of dendrimers [32, 155, 268, 269]. Our work differs from that discussed above in that we do not use a secondary divinyl comonomer (brancher), but incorporate the branching double bond directly into the RAFT agent. These polymers are formed on a principle similar to that of convergent dendrimer synthesis in that they can be designed to crosslink towards a central moiety. The basic scheme for the synthesis of such a polymer consists of a one-pot condensation or polymerization in which branching moieties are present, as shown in Scheme A.1. By condensing the branching end or unit, crosslinking can be achieved for a globular three-dimensional structure not unlike that of a dendrimer. While most hyperbranched polymers have large polydispersities, under well-controlled reaction conditions, previous work has demonstrated some level of control over the polymer structure [89, 269]. In the present case, RAFT agents are used not only for control over polymer polydispersity, but also as branching agents. The special feature of these hyperbranching RAFT polymerizations is that a polymerizable double bond is incorporated into the RAFT agent. While the double bond on the RAFT agent provides a highly branching system, the RAFT mechanism itself leads to structural uniformity in the resultant polymer. As such, hyperbranched polymers have also

been shown to be good candidates for drug delivery vehicles [114, 281]. While this chemistry is commonly available, it has not been rigorously analyzed.

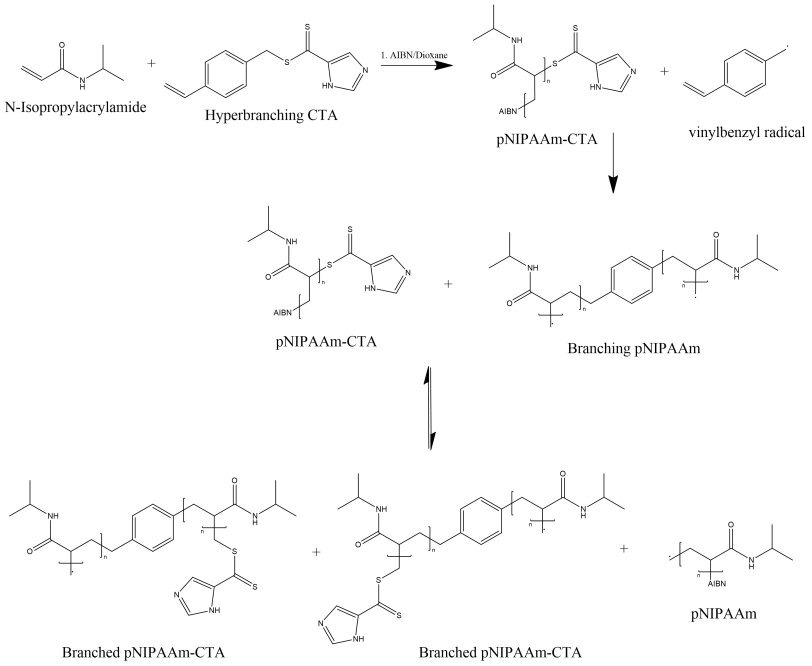

Scheme A.1: Highly branched RAFT polymerization of N-isopropylacrylamide using 4-Vinylbenzylimidazoledithioate as a chain transfer agent..

While hyperbranched polymers can provide a scaffold in which to physically encapsulate or chemically conjugate drugs, certain classes of hyperbranched polymers may provide additional benefits to drug delivery. A level of control over drug delivery can be added by designing thermally responsive hyperbranched polymers, which undergo a conformational change when the polymer warms to body temperature, releasing the drug. Polymers of N-isopropylacrylamide, or pNIPAAm, have been studied extensively for their temperature-responsive properties. It is well-established that pNIPAAm in aqueous solution exhibits a sharp phase transition at its lower critical solution temperature (LCST), at approximately 32 °C. The thermal transition of pNIPAAm causes a linear hydrodynamic radius change of almost an order of magnitude with pNIPAAm hydrogels showing an even greater difference [282, 108, 86]. LCST behavior can be varied via copolymerization with various other monomers

[72, 130]. Copolymerization schemes with acrylamide and acrylic acid in particular have received much attention as a biologically benign method of raising the LCST [108, 301, 86, 138, 226, 62, 130] and provide some measure of pH responsivity, another useful property in the design of drug delivery vehicles [25, 301, 138, 62, 130]. In this paper, we introduce the concept of a segment model to account for highly branched systems and illustrate its utility using batch copolymerizations of acrylamide-acrylic acid, acrylonitrile-methacrylic acid, and ethylene-styrene. This segment model is a simple alternative to our previous model [205] that uses complex, multi-dimensional moment formulations. Using this model, we can simulate highly branched polymerizations with a one-dimensional moment formulation. We will compare the polydispersity of polymer segments to the polydispersity of the entire polymer using statisitical arguments. We chose to model the acrylamide-acrylic acid system as a fascimile of the pNIPAAm-acrylic acid copolymerization, and thus, our model provides a foundation for the experimental synthesis of hyperbranched, thermally responsive polymers for use in therapeutic applications. The other two copolymerization schemes we chose to model, while not directly applicable to drug delivery, investigate the effects of varying reactivity ratios on the segment polydispersities, the overall polydispersity and the final molecular architecture.

A.4 Model Development

As discussed previously, our prior work has used the method of moments to model RAFT polymerization. The RAFT agent used in this work has a single double bond on the Z portion of the RAFT agent, which provides the branching capability necessary to make the desired hyperbranched structure as shown in Scheme A.1. The model for this system provides a low-dimensional analysis to account for branching, a property that has previously required multiple-dimension moments to describe [205]. The current model consists of a simplified segment model combined with branch trackers

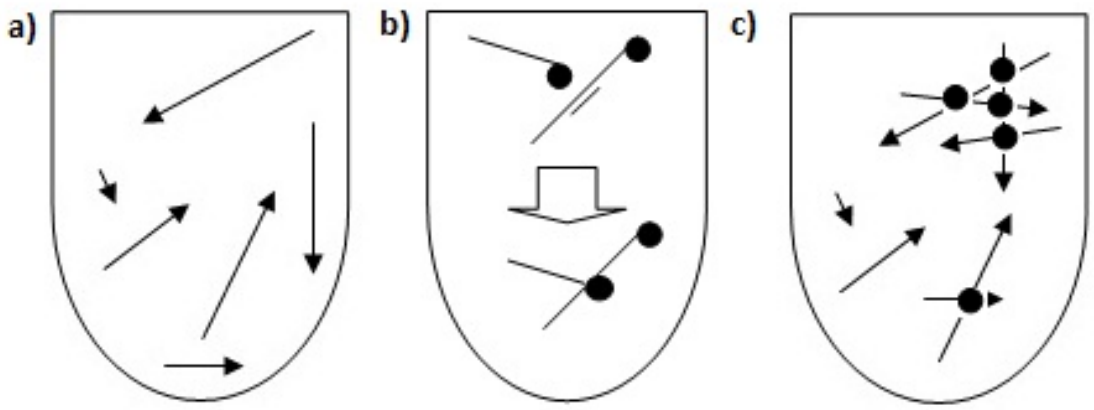

Figure A.1: a) "Segment model" treats each propagating radical separately b) "Branch trackers" account for each branching occurrence c) Combining "segment model" and "branch trackers" leads to complete analysis of polymerization

that account for branching and the generation of molecules. As illustrated in Figure A.1, each segment is modeled as an individual propagating chain with branching having no effect on the segment (original chain). Branch trackers do not affect the kinetics of the segment model, but merely track the occurrence of branching events and polymer generation. Unifying the segment model and the branching trackers provides a complete picture of the copolymerization.

Each segment is a linear polymer chain which may or may not contain multiple branch points. A segment begins when a radical initiates polymerization. The segment ends only when it is terminated; branching does not affect the kinetics of the segment. Segments may propagate through chains containing a residual double bond (on the RAFT agent). This is counted as a branching event, but does not "terminate" the segment. That is, the segment model treats the segment the same before and after branching occurs.

By using a single dimension to account for propagating chains and degree of branching, a complete analysis that includes copolymer composition, monomer conversion, molecular weight and polydispersity is produced without higher dimensional moments. Using statistical arguments, the polydispersity of overall molecules can be

related to the polydispersity of individual segments. Certain simplifying assumptions were made without detracting from the goals of accounting for higher-dimensional phenomena in a single moment dimension, and examining the hyperbranching resulting from RAFT polymerization with a hyperbranching RAFT agent. Clearly, the effect of branching on kinetic parameters has been ignored. To maintain a single dimension, the end monomer unit is assumed to control the rate constant for propagation [274]. While the degree of polymerization has been shown to affect propagation, termination, and RAFT transfer, it has also been ignored in this work [206, 173, 258]. Also, despite reports of the stability of the macro-radical intermediate, this mathematical model assumes its existence to be transitory, and it has not been modeled here [176, 202, 13, 28, 206, 46]. While kinetic parameters for the three copolymerizations have been taken from literature, the measurement of RAFT transfer has been a subject of much debate [271], therefore a value has been selected that falls in the appropriate range and produces polymers with low polydispersity. We have not considered branching due to chain transfer to polymer, since we feel that this effect will be dwarfed by the branching induced by polymerization through the RAFT double bonds.

The segment model is presented in Table A.1. The standard reactions of initiation, RAFT initiation, RAFT transfer, propagation, and termination are shown. Accordingly, propagating polymers with terminal unit A or B, that is, the radical initator terminal unit and the R group from the chain transfer agent respectively, (P_n and Q_n), dormant polymers with terminal unit A or B (TP_n and TQ_n) and terminated polymers (M_n) are shown, with the subscript n denoting the degree of polymerization. Additionally, the reactions of the branch trackers are shown. A branch point, a double bond on the RAFT agent that can be attacked by an active polymer radical and initiate a branch, is denoted by D$^{\wedge}$. When a branch point is attacked by an active (polymeric) radical, the branch point is consumed, but the active polymer is

Table A.1: Reactions of "Segment Model"

Initiation

$$I \xrightarrow{k_{df}} 2R^*$$

$$R^* + A \xrightarrow{k_{i1}} P_1$$

$$R^* + B \xrightarrow{k_{i2}} Q_1$$

$$R\hat{} + A \xrightarrow{k_{i1}} P_1$$

$$R\hat{} + B \xrightarrow{k_{i2}} Q_1$$

RAFT transfer

$$P_n + TQ_m \underset{k_{raft12}}{\overset{k_{raft11}}{\leftrightarrow}} TP_n + Q_m \qquad P_n + TP_m \underset{k_{raft32}}{\overset{k_{raft31}}{\leftrightarrow}} TP_n + P_m$$

$$Q_n + TP_m \underset{k_{raft12}}{\overset{k_{raft11}}{\leftrightarrow}} TQ_n + P_m \qquad Q_n + TQ_m \underset{k_{raft22}}{\overset{k_{raft21}}{\leftrightarrow}} TQ_n + Q_m$$

RAFT activation

$$T + P_n \underset{k_{r12}}{\overset{k_{r11}}{\leftrightarrow}} R\hat{} + TP_n \qquad T + Q_n \underset{k_{r22}}{\overset{k_{r21}}{\leftrightarrow}} R\hat{} + TQ_n$$

Propagation

$$P_n + A \xrightarrow{k_{p1}} P_{n+1} \qquad Q_n + A \xrightarrow{k_{p3}} P_{n+1} \qquad P_n + B \xrightarrow{k_{p2}} Q_{n+1} \qquad Q_n + B \xrightarrow{k_{p4}} Q_{n+1}$$

Termination

$$P_n + Q_r \xrightarrow{k_{tc1}} M_{n+r} \qquad P_n + Q_r \xrightarrow{k_{td1}} M_n + M_r$$

$$P_n + P_r \xrightarrow{k_{tc2}} M_{n+r} \qquad P_n + P_r \xrightarrow{k_{td2}} M_n + M_r$$

$$Q_n + Q_r \xrightarrow{k_{tc3}} M_{n+r} \qquad Q_n + Q_r \xrightarrow{k_{td3}} M_n + M_r$$

$$Q_n + P_r \xrightarrow{k_{tc1}} M_{n+r} \qquad Q_n + P_r \xrightarrow{k_{tc1}} M_n + M_r$$

Branch trackers

$$R\hat{} + A \xrightarrow{k_{i1}} D\hat{} \qquad R\hat{} + A \xrightarrow{k_{i1}} D\hat{}$$

$$R^* + B \xrightarrow{k_{i2}} D\hat{} \qquad R^* + B \xrightarrow{k_{i2}} D\hat{}$$

$$P_n + D\hat{} \xrightarrow{k_{b1}} P_n \qquad Q_n + D\hat{} \xrightarrow{k_{b2}} Q_n$$

considered unaltered. The branch trackers are used to produce a population balance on the highly branched polymer (HBP). The HBP balance provides an assessment of the total number of molecules at any time, and the segment model provides the number of segments at any time. The reactions of Table A.1 are used to produce the mass balances in Table A.2.

The definition of each moment is illustrated in Table A.3, and population balances are used to provide the overall model in Table A.4, which are closed with the mass balances of the minor species in Table A.3 (i.e. monomers A & B, initiator, RAFT agent, leaving agent, and free radicals).

The segment model produces the standard parameters of conversion and copolymer composition with the novel parameters of number average segment length (NASL) and polydispersity of a segment, which are measures of the size and uniformity of the segments. Additionally, the branch trackers produce the number of branch points and the number of molecules, and, when combined with the segment model, the polydispersity of the overall hyperbranched polymer. The derivations of these important parameters are illustrated in Table A.6.

Table A.2: Mass balances for the segment model

Segment Model

$$\frac{dP_1 + dP_n}{dt} = k_{i1}[R*][A] + k_{r12}[R^{\hat{}}][TP_n] - k_{r11}[T][P_n]$$
$$- k_{raft\,11}[Z_0^b][P_n] + k_{raft\,12}[Y_0^b][TP_n] - k_{raft\,31}[Z_0^a][P_n] + k_{raft\,32}[Y_0^a][TP_n]$$
$$- k_{p1}[A][P_n] - k_{p2}[B][P_n] + k_{p1}[A][P_{n-1}] + k_{p3}[A][Q_{n-1}]$$
$$- k_{tc1}[Y_0^b][P_n] - k_{tc2}[Y_0^a][P_n] - k_{td1}[Y_0^b][P_n] - k_{td2}[Y_0^a][P_n]$$

$$\frac{dQ_1 + dQ_n}{dt} = k_{i2}[R^*][B] + k_{r22}[R^{\hat{}}][TQ_n] - k_{r21}[T][Q_n]$$
$$- k_{raft\,11}[Z_0^a][Q_n] + k_{raft\,12}[Y_0^a][TQ_n] - k_{raft\,21}[Z_0^b][Q_n] + k_{raft\,22}[Y_0^b][TQ_n]$$
$$- k_{p3}[A][Q_n] - k_{p4}[B][Q_n] + k_{p2}[B][P_{n-1}] + k_{p4}[B][Q_{n-1}]$$
$$- k_{tc3}[Y_0^b][Q_n] - k_{tc1}[Y_0^a][Q_n] - k_{td3}[Y_0^b][Q_n] - k_{td1}[Y_0^a][Q_n]$$

$$\frac{dTP_n}{dt} = -k_{r12}[R^{\hat{}}][TP_n] + k_{r11}[T][P_n] + k_{raft11}[Z_0^b][P_n] - k_{raft12}[Y_0^b][TP_n] + k_{raft31}[Z_0^a][P_n] - k_{raft32}[Y_0^a][TP_n]$$

$$\frac{dM_n}{dt} = k_{tc1}\left(\sum_{a=0}^{n} P_a Q_{n-a}\right) + \tfrac{1}{2}k_{tc2}\left(\sum_{a=0}^{n} P_a P_{n-a}\right) + \tfrac{1}{2}k_{tc3}\left(\sum_{a=0}^{n} Q_a Q_{n-a}\right)$$
$$+ k_{td1}[Y_0^b][P_n] + k_{td2}[Y_0^a][P_n] + k_{td3}[Y_0^b][Q_n] + k_{td1}[Y_0^a][Q_n]$$

Small Molecules

$$\frac{dI}{dt} = -k_d[I]$$

$$\frac{dR^*}{dt} = 2^* k_d(f)[I] - k_{i1}[A][R^*] - k_{i2}[B][R^*]$$

$$\frac{dR^{\hat{}}}{dt} = -k_{i1}[A][R^{\hat{}}] - k_{i2}[B][R^{\hat{}}] - k_{r12}[Z_0^a][R^{\hat{}}] + k_{r11}[Y_0^a][T] - k_{r22}[Z_0^b][R^{\hat{}}] + k_{r21}[Y_0^b][T]$$

$$\frac{dA}{dt} = -k_{i1}[R^*][A] - k_{i1}[R^{\hat{}}][A] - k_{p1}[Y_0^a][A] - k_{p3}[Y_0^b][A]$$

$$\frac{dB}{dt} = -k_{i2}[R^*][B] - k_{i2}[R^{\hat{}}][B] - k_{p2}[Y_0^a][B] - k_{p4}[Y_0^b][B]$$

$$\frac{dT}{dt} = k_{r22}[R^{\hat{}}][Z_0^b] - k_{r21}[T][Y_0^b] + k_{r12}[R^{\hat{}}][Z_0^a] - k_{r11}[T][Y_0^a]$$

$$\frac{dD^{\hat{}}}{dt} = k_{i1}[A][R^*] + k_{i2}[B][R^*] + k_{i1}[A][R^{\hat{}}] + k_{i2}[B][R^{\hat{}}] - k_b[Y_0^a][D^{\hat{}}] - k_b[Y_0^b][D^{\hat{}}]$$

$$\frac{dHBP}{dt} = k_{i1}[A][R^*] + k_{i2}[B][R^*] + k_{i1}[A][R^{\hat{}}] + k_{i2}[B][R^{\hat{}}]$$
$$- k_{tc1}[Y_0^a][Y_0^b] - k_{tc2}[Y_0^a][Y_0^a] - k_{tc3}[Y_0^b][Y_0^b] - k_b[Y_0^a][D^{\hat{}}] - k_b[Y_0^b][D^{\hat{}}]$$

Table A.3: Definition of moments

Segment Model

Propagating chains	Dormant chains	Terminated chains
$Y_i^a = \sum_{n=0}^{\infty} n^i[P_n]$	$Z_i^a = \sum_{n=0}^{\infty} n^i[TP_n]$	$D_i^a = \sum_{n=0}^{\infty} n^i[M_n]$
$Y_i^b = \sum_{n=0}^{\infty} n^i[Q_n]$	$Z_i^b = \sum_{n=0}^{\infty} n^i[TQ_n]$	

A.5 Results and Discussion

The first simulation is a copolymerization of acrylamide and acrylic acid which acts as an analog to the copolymerization of NIPAAm and acrylic acid, a particularly important copolymer for biological applications such as drug delivery. The initial charge to the reactor is 1.28 M acrylamide and 0.14 M acrylic acid. The initiator azobis-isobutyronitrle (AIBN) is used with a molar concentration of 0.014 M with twice the molar ratio of the RAFT agent as initiator. The model parameters and kinetic rate constants are shown in Table A.7.

With a 100% conversion being reached, the copolymer composition values reach the initial composition of monomer, with 90.1% acrylamide and 9.9% acrylic acid. The NASL reaches a value of 50 monomer units before dropping slightly to 49. This drop is attributed to the slow dissociation of initiator, as the formation of polymer with a low degree of polymerization at the end of the copolymerization slightly reduces the value of NASL. Each polymer molecule contains 307 segments, so the number average chain length (NACL), the average number of monomers added to each polymerizing radical during the polymerization, is approximately 15,000 (NASL*segments per molecule). The large number of segments per molecule indicates the highly branched nature of this polymer. Using this simple model, the exact morphology of the molecular structure is not accessible, but some conclusions can be made. As expected, the polydispersity of the segments is much higher than the polydispersity of the branched

Table A.4: Moment equations of segment model

Zeroth order moments

$$\frac{dY_0^a}{dt} = k_{i1}[R^*][A] + k_{i1}[R\hat{}][A] + k_{r12}[R\hat{}][Z_0^a] - k_{r11}[Y_0^a][T]$$
$$- k_{raft11}[Y_0^a][Z_0^b] + k_{raft12}[Z_0^a][Y_0^b] - k_{raft31}[Y_0^a][Z_0^a] + k_{raft32}[Z_0^a][Y_0^a]$$
$$- k_{p1}[A][Y_0^a] - k_{p2}[B][Y_0^a] + k_{p1}[A][Y_0^a] + k_{p3}[A][Y_0^b]$$
$$- k_{tc1}[Y_0^b][Y_0^a] - k_{tc2}[Y_0^a][Y_0^a] - k_{td1}[Y_0^b][Y_0^a] - k_{td2}[Y_0^a][Y_0^a]$$

$$\frac{dY_0^b}{dt} = k_{i2}[R^*][B] + k_{i1}[R\hat{}][B] + k_{r22}[R\hat{}][Z_0^b] - k_{r21}[T][Y_0^b]$$
$$- k_{raft11}[Y_0^b][Z_0^a] + k_{raft12}[Z_0^b][Y_0^a] - k_{raft21}[Y_0^b][Z_0^a] + k_{raft22}[Z_0^b][Y_0^b]$$
$$- k_{p3}[A][Y_0^b] - k_{p4}[B][Y_0^b] + k_{p2}[B][Y_0^a] + k_{p4}[B][Y_0^b]$$
$$- k_{tc3}[Y_0^b][Y_0^b] - k_{tc1}[Y_0^a][Y_0^b] - k_{td3}[Y_0^b][Y_0^b] - k_{td1}[Y_0^a][Y_0^b]$$

$$\frac{dZ_0^a}{dt} = -k_{r12}[R\hat{}][Z_0^a] + k_{r11}[T][Y_0^a]$$
$$+ k_{raft11}[Y_0^a][Z_0^b] - k_{raft12}[Z_0^a][Y_0^b] + k_{raft31}[Y_0^a][Z_0^a] - k_{raft32}[Z_0^a][Y_0^a]$$

$$\frac{dZ_0^b}{dt} = -k_{r22}[R\hat{}][Z_0^b] + k_{r21}[T][Y_0^b]$$
$$+ k_{raft11}[Y_0^b][Z_0^a] - k_{raft12}[Z_0^b][Y_0^b] + k_{raft21}[Y_0^b][Z_0^b] - k_{raft22}[Z_0^b][Y_0^b]$$

$$\frac{dD_0}{dt} = k_{tc1}[Y_0^a][Y_0^b] + \tfrac{1}{2}k_{tc2}[Y_0^a][Y_0^a] + \tfrac{1}{2}k_{tc3}[Y_0^b][Y_0^b]$$
$$+ k_{td1}[Y_0^b][Y_0^a] + k_{td2}[Y_0^a][Y_0^a] + k_{td3}[Y_0^b][Y_0^b] + k_{td1}[Y_0^a][Y_0^b]$$

First order moments

$$\frac{dY_1^a}{dt} = k_{i1}[R^*][A] + k_{i1}[R\hat{}][A] + k_{r12}[R\hat{}][Z_1^a] - k_{r11}[T][Y_1^a]$$
$$- k_{raft11}[Y_1^a][Z_1^b] + k_{raft12}[Z_1^a][Y_1^b] - k_{raft31}[Y_1^a][Z_1^a] + k_{raft32}[Z_1^a][Y_1^a]$$
$$- k_{p1}[A][Y_1^a] - k_{p2}[B][Y_1^a] + k_{p1}[A][Y_1^a + Y_0^a] + k_{p3}[A][Y_1^b + Y_0^b]$$
$$- k_{tc1}[Y_0^b][Y_1^a] - k_{tc2}[Y_0^a][Y_1^a] - k_{td1}[Y_0^b][Y_1^a] - k_{td2}[Y_0^a][Y_1^a]$$

$$\frac{dY_1^b}{dt} = k_{i2}[R^*][B] + k_{i1}[R\hat{}][B] + k_{r22}[R\hat{}][Z_1^b] - k_{r21}[T][Y_1^b]$$
$$- k_{raft11}[Y_1^b][Z_0^a] + k_{raft12}[Z_1^b][Y_0^a] - k_{raft21}[Y_1^b][Z_0^b] + k_{raft22}[Z_1^b][Y_0^b]$$
$$- k_{p3}[A][Y_1^b] - k_{p4}[B][Y_1^b] + k_{p2}[B][Y_1^a + Y_0^a] + k_{p4}[B][Y_1^b + Y_0^b]$$
$$- k_{tc3}[Y_0^b][Y_1^b] - k_{tc1}[Y_0^a][Y_1^b] - k_{td3}[Y_0^b][Y_1^b] - k_{td1}[Y_0^a][Y_1^b]$$

$$\frac{dZ_1^a}{dt} = -k_{r12}[R\hat{}][Z_1^a] + k_{r11}[T][Y_1^a]$$
$$+ k_{raft11}[Y_1^a][Z_0^b] - k_{raft12}[Z_1^a][Y_0^b] + k_{raft31}[Y_1^a][Z_0^a] - k_{raft32}[Z_1^a][Y_0^a]$$

$$\frac{dZ_1^b}{dt} = -k_{r22}[R\hat{}][Z_1^b] + k_{r21}[T][Y_1^b]$$
$$+ k_{raft11}[Y_1^b][Z_0^a] - k_{raft12}[Z_1^b][Y_0^a] + k_{raft21}[Y_1^b][Z_0^b] - k_{raft22}[Z_1^b][Y_0^b]$$

$$\frac{dD_1}{dt} = k_{tc1}[Y_0^a Y_1^b + Y_1^a Y_0^b] + \tfrac{1}{2}k_{tc2}[Y_0^a Y_1^a + Y_1^a Y_0^a] + \tfrac{1}{2}k_{tc3}[Y_0^b Y_1^b + Y_1^b Y_0^b]$$
$$+ k_{td1}[Y_0^b][Y_1^a] + k_{td2}[Y_0^a][Y_1^a] + k_{td3}[Y_0^b][Y_1^b] + k_{td1}[Y_0^a][Y_1^b]$$

Table A.5: Moment equations of segment model continued

Second order moments

$$\frac{dY_2^a}{dt} = k_{i1}[R^*][A] + k_{i1}[R\hat{}][A] + k_{r12}[R\hat{}][Z_2^a] - k_{r11}[T][Y_2^a]$$
$$- k_{raft11}[Y_2^a][Z_0^b] + k_{raft12}[Z_2^a][Y_0^b] - k_{raft31}[Y_2^a][Z_0^a] + k_{raft32}[Z_2^a][Y_2^a]$$
$$- k_{p1}[A][Y_2^a] - k_{p2}[B][Y_2^a] + k_{p1}[A][Y_2^a + 2^*Y_1^a + Y_0^a] + k_{p3}[A][Y_2^b + 2^*Y_1^b + Y_0^b] +$$
$$- k_{tc1}[Y_0^b][Y_2^a] - k_{tc2}[Y_0^a][Y_2^a] - k_{td1}[Y_0^b][Y_2^a] - k_{td2}[Y_0^a][Y_2^a]$$

$$\frac{dY_2^b}{dt} = k_{i2}[R^*][B] + k_{i1}[R\hat{}][B] + k_{r22}[R\hat{}][Z_2^b] - k_{r21}[T][Y_2^b]$$
$$- k_{raft11}[Y_2^b][Z_0^a] + k_{raft12}[Z_2^b][Y_0^a] - k_{raft21}[Y_2^b][Z_0^b] + k_{raft22}[Z_2^b][Y_0^b]$$
$$- k_{p3}[A][Y_2^b] - k_{p4}[B][Y_2^b] + k_{p2}[B][Y_2^a + 2^*Y_1^a + Y_0^a] + k_{p4}[B][Y_2^b + 2^*Y_1^b + Y_0^b]$$
$$- k_{tc3}[Y_0^b][Y_2^b] - k_{tc1}[Y_0^a][Y_2^b] - k_{td3}[Y_0^b][Y_2^b] - k_{td1}[Y_0^a][Y_2^b]$$

$$\frac{dZ_2^a}{dt} = -k_{r12}[R\hat{}][Z_2^a] + k_{r11}[T][Y_2^a]$$
$$+ k_{raft11}[Y_2^a][Z_0^b] - k_{raft12}[Z_2^a][Y_0^b] + k_{raft31}[Y_2^a][Z_0^a] - k_{raft32}[Z_2^a][Y_2^a]$$

$$\frac{dZ_2^b}{dt} = -k_{r22}[R\hat{}][Z_2^b] + k_{r21}[T][Y_2^b]$$
$$+ k_{raft11}[Y_2^b][Z_0^a] - k_{raft12}[Z_2^b][Y_0^a] + k_{raft21}[Y_2^b][Z_0^b] - k_{raft22}[Z_2^b][Y_0^b]$$

$$\frac{dD_2}{dt} = k_{tc1}[Y_0^a Y_2^b + 2^*Y_1^a Y_1^b + Y_2^a Y_0^b] + 1/2 k_{tc2}[Y_0^a Y_2^a + 2^*Y_1^a Y_1^a + Y_2^a Y_0^a]$$
$$1/2 k_{tc3}[Y_0^b Y_2^b + 2^*Y_1^b Y_1^b + Y_2^b Y_0^b]$$
$$+ k_{td1}[Y_0^b][Y_2^a] + k_{td2}[Y_0^a][Y_2^a] + k_{td3}[Y_0^b][Y_2^b] + k_{td1}[Y_0^a][Y_2^b]$$

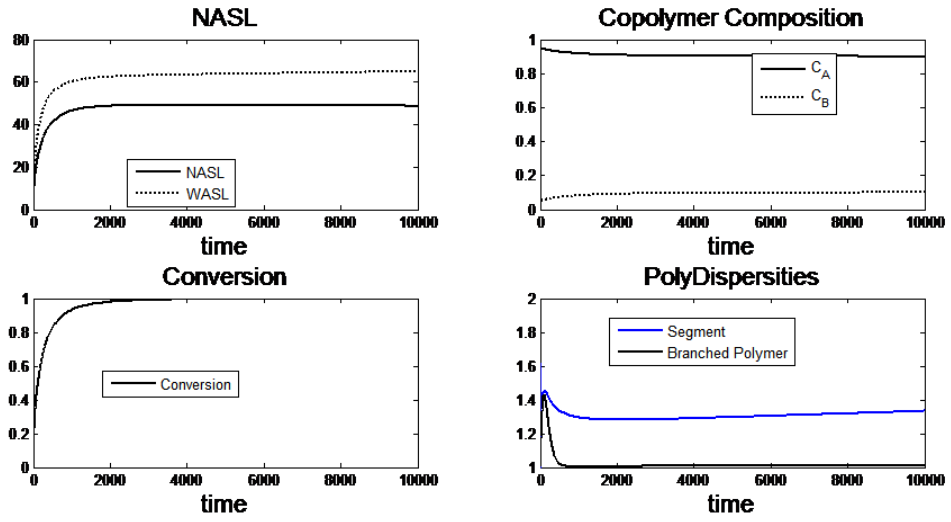

Figure A.2: Model of hyperbranched copolymerization of acrylamide and acrylic acid with time measured in seconds. A) The number averaged segment length and weight averaged segment length vs time. B) The copolymer composition with CA being the mole fraction of acrylamide and CB being the mole fraction of acrylic acid. C) Overall conversion to polymer. D) The polydispersity index of the segments and the overall polymer.

Table A.6: Important parameters of segment model

$$\text{NASL} = \mu_{\text{seg}} = \frac{Y_1^a + Y_1^b + Z_1^a + Z_1^b + D_1}{Y_0^a + Y_0^b + Z_0^a + Z_0^b + D_0}$$

$$\text{WASL} = \frac{Y_2^a + Y_2^b + Z_2^a + Z_2^b + D_2}{Y_1^a + Y_1^b + Z_1^a + Z_1^b + D_1}$$

$$\sigma_{\text{seg}}^2 = \frac{Y_2^a + Y_2^b + Z_2^a + Z_2^b + D_2}{Y_0^a + Y_0^b + Z_0^a + Z_0^b + D_0} - \left(\frac{Y_1^a + Y_1^b + Z_1^a + Z_1^b + D_1}{Y_0^a + Y_0^b + Z_0^a + Z_0^b + D_0}\right)^2$$

$$D_{\text{seg}} = 1 + \left(\frac{\sigma_{\text{seg}}}{\mu_{\text{seg}}}\right)^2 = \frac{\text{WASL}}{\text{NASL}}$$

$$D_{\text{molec}} = 1 + \left(\frac{\sigma_{\text{molec}}}{\mu_{\text{molec}}}\right)^2 \left(\frac{\sigma_{\text{molec}}}{\mu_{\text{molec}}}\right)^2 = \frac{1}{N}\left(\frac{\sigma_{\text{molec}}}{\mu_{\text{molec}}}\right)^2$$

$$N = \frac{\text{No. of segments}}{\text{molecule}}$$

$$D_{\text{molec}} = 1 + \frac{1}{N}\left(\frac{\sigma_{\text{molec}}}{\mu_{\text{molec}}}\right)^2$$

$$\text{Conversion} = \frac{Y_1^a + Y_1^b + Z_1^a + Z_1^b + D_1}{Y_1^a + Y_1^b + Z_1^a + Z_1^b + D_1 + A + B}$$

$$C_A = \frac{A_{\text{initial}} - A_{\text{final}}}{A_{\text{initial}} - A_{\text{final}} + B_{\text{initial}} - B_{\text{final}}}$$

$$C_B = \frac{B_{\text{initial}} - B_{\text{final}}}{A_{\text{initial}} - A_{\text{final}} + B_{\text{initial}} - B_{\text{final}}}$$

Table A.7: Model Parameters and Kinetic Rate Constants (acrylamide-acrylic acid) [26, 91, 184]

Parameter	Value	Parameter	Value
F	0.6	k_r	10^7
k_d	9.14×10^{-6}	k_{raft}	10^7
$k_{i,ACRYL}$	37.2×10^4	$k_{tc,ACRYL}$	1.7×10^8
$k_{i,AA}$	2620	$k_{tc,AA}$	2×10^7
$k_{p,ACRYL}$	37.2×10^4	$k_{tc,ACRYL-AA}$	9.5×10^7
$k_{p,AA}$	2620	$k_{b,ACRYL}$	1.7×10^8
r_{ACRYL}	0.48	$k_{b,AA}$	2×10^7
r_{AA}	1.73		

polymer, and the polydispersity of the polymer can be derived from the polydispersity of the segments. It follows from the central limit theorem of statistics that variance of the molecules will be much lower than that of the segments. The polydispersity index of the polymer can been calculated from that of the chains via Equation 6 where Dpolymer is the polydispersity index of the polymer, $D_{segment}$ is the polydispersity index of the segment, and N is the average number of segments per chain.

$$D_{polymer} = 1 + \frac{1}{N}(D_{segment} - 1) \tag{6}$$

As shown in Figure A.2D, the polydispersity of the segments is closer to 1.5 than 1. This may seem odd for a controlled radical polymerization where the molecular weight polydispersity index approaches one; however, termination has been included in the model, and the segments are not truly living. Contrary to the segments, the polydispersity of the overall hyperbranched polymer is close to 1, as would be expected for a controlled radical polymerization. The polymer chain is almost always living, even when many of its chains may have terminated. The polydispersity of the hyperbranched polymer begins near 1.3 due to the highest occurrence of bimolecular termination occurring at the beginning of the copolymerization and quickly drops, approaching one, as is common for controlled radical systemsBimolecular termination does not reduce the likelihood of branching, as the branch points on the RAFT agent are not eliminated due to termination. This also explains the drop in polydispersity of the segment as a dead polymer is reactivated due to an active segment polymerizing through a branch point of a dead polymer. The low polydispersity of the hyperbranched polymers caused by the use of the RAFT chemistry confirms the well-defined nature of such hyperbranched polymers and further promotes such systems as a platform for thermally responsive drug delivery. Indeed, our comparable experimental data for hyperbranched pNIPAAm-co-acrylic acid shows a number average molecular weight of 1723 and a polydispersity of 1.13. In this case, the model

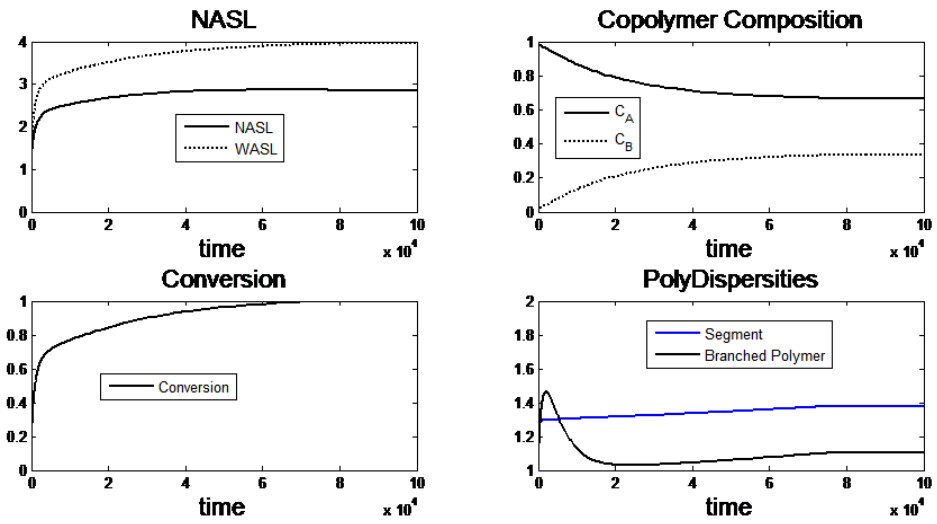

Figure A.3: Model of hyperbranched copolymerization of acrylonitrile and methacrylic acid with time measured in seconds. A) The number averaged segment length and weight averaged segment length vs time. B) The copolymer composition with C_A being the mole fraction of acrylonitrile and C_B being the mole fraction of methacrylic acid. C) Overall conversion to polymer. D) The polydispersity index of the segments and the overall polymer.

slightly overestimates the control achieved; however, it still provides a wealth of information about the synthesis. The second copolymerization modeled is acrylonitrile-methacrylic acid. The initial conditions are 1 M acrylonitrile and 0.5 M methacrylic acid with 0.2 M AIBN as initiator. The RAFT agent is 2.5 times the molar concentration of initiator. The model parameters and kinetic rate constants are shown in Table 7.

With full monomer conversion, and a very low ratio of kp/kt (the propagation rate/the termination rate), the NASL reaches only 3.95. With only 16 segments per molecule, the NACL for the polymer molecules is approximately 63. The polydispersity of the segment reaches a value of 1.38, which indicates that more segments have terminated than are active. This simulation had to strike a balance between uniformity and high conversion. A higher charge of RAFT agent would reduce the NASL, while a lower charge would result in even higher proportion of terminated segments and therefore increase the value of segment and branch polydispersity. The branch

Table A.8: Model Parameters and Kinetic Rate Constants (Ethylene-Styrene) [22]

Parameter	Value	Parameter	Value
F	0.6	k_r	10^7
k_d	9.14×10^{-6}	k_{raft}	10^7
$k_{i,ETHYL}$	470	$k_{tc,ETHYL}$	10.5×10^8
$k_{i,STY}$	187	$k_{tc,STY}$	63×10^6
$k_{p,ETHYL}$	470	$k_{tc,ETHYL-STY}$	5.56×10^7
$k_{p,STY}$	187	$k_{b,ETHYL}$	10.5×10^8
r_{ETHYL}	0.05	$k_{b,STY}$	63×10^6
r_{STY}	14.88		

polydispersity rises quickly to 1.45 then drops to 1.05 before steadily settling at a value of 1.11. This fluctuation can be accounted for by the slow initiation allowing greater polymer death to occur at the beginning of the polymerization, followed by a drop precipitated by the prevalence of branching, and a small rise again due to the lack of further RAFT agents. The low final polydispersity indicates that although most segments are inactive, almost all hyperbranched polymers have a living segment. The third copolymerization modeled is that of ethylene and styrene. The initial conditions are 1 M ethylene and 0.5 M styrene with 0.2 M AIBN as initiator. The RAFT agent is 2.5 times the molar concentration of initiator. The model parameters and kinetic rate constants are shown in Table 8. The ethylene-styrene system, while not relevant in biotechnology applications, is included here to demonstrate the effect of widely differing reactivity ratios.

With a conversion of 94.8%, the copolymer composition is 70.3% ethylene and 29.7% styrene. With a very low ratio of k_p/k_t, the NASL reaches only 2.45. There are 33 segments per polymer molecule for a NACL of approximately 80. Ethylene and styrene have vastly different reactivity ratios (14.88 and 0.05), which contributes to the difference in copolymer composition of ethylene in the polymer to the initial charge. The polydispersity of the segment reaches a value of 1.38, indicating that there are more terminated segments than active ones. This simulation also strikes a balance

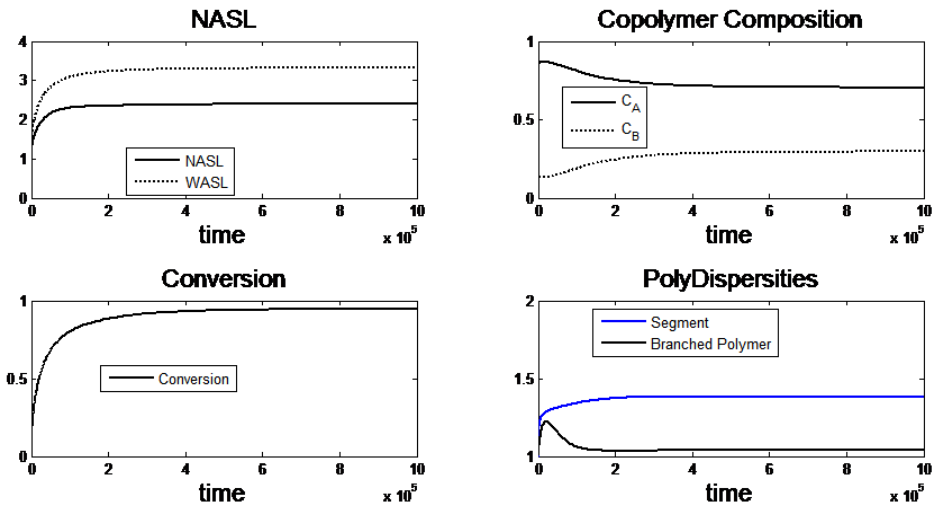

Figure A.4: Model of hyperbranched copolymerization of ethylene and styrene with time measured in seconds. A) The number averaged segment length and weight averaged segment length vs time. B) The copolymer composition with C_A being the mole fraction of ethylene and C_B being the mole fraction of styrene. C) Overall conversion to polymer. D) The polydispersity index of the segments and the overall polymer.

between uniformity and conversion rate. A higher charge of RAFT agent would reduce the segment polymerization, but the NASL and rate of conversion would drop even further. A lower charge would result in even higher proportion of dead segments and would therefore increase the value of segment and branch polydispersity. The branch polydispersity begins at 1.2 and drops steadily to a value of 1.02, indicating that although most segments are inactive, almost all hyperbranched polymers have a living segment. These three examples indicate that it is possible to produce a hyperbranched material out of certain copolymers such as acrylamide-acrylic acid with this chemistry; however, under other conditions with different kinetic rate constants such as the copolymerizations of acrylonitrile-methacrylic acid and ethylene-styrene, the desired hyperbranched structure is not obtained. Using this simple model, we can now predict the success of hyperbranching using RAFT agents on various copolymerizations. Such simulations can prove to be a valuable tool in the development of novel hyperbranching materials for drug delivery or other applications.

A.6 Conclusion

It has been shown that the method of moments can be used to produce a reasonably simple and mathematically efficient accounting of a system that approaches dendritic complexity. By combining an independent segment model that accounts for the lifetime events of segments with branching trackers that account for the occurence of branching and the number of molecules, a set of one-dimensional moment equations provides an accurate description of a hyperbranched copolymerization. Hyperbranched polymers have been shown to be useful in many applications, notably in the design of drug delivery systems, and as such, copolymerizations of different comonomers have been simulated to illustrate the power of this model to manipulate structure. The chemistry modeled here (RAFT polymerization with a single double bond on each molecule of the RAFT agent) is an effective way of producing a highly-branched, very uniform, non-crosslinked polymer structure for certain copolymers. Using this model, we can easily predict the success of hyperbranched polymer synthesis via RAFT polymerization for any given set of copolymers.

APPENDIX B

SUPPLEMENTARY MATERIALS

As shown in Figure B.1, **1** was successfully synthesized with a high degree of purity. The peak at 242 corresponds to the catalyst (tetrabutylammonium hydrogen sulfate) in the reaction. All other peaks correspond to the product, **1**. With positive electrospray mass spectroscopy a proton in added to the molecule yielding an m/z value of 283 as seen in the spectrum. In this spectrum, most of the positive ions were a result of ionization with NH3 which results in a peak at m/z of 300. Sodium adducts also make up a major portion of this spectrum yielding peaks at 305. The addition of two sodium adducts yields an m/z value of 163. The peak at 582 corresponds to a conglomeration of two molecules of **1** with one ammonia while 587 corresponds to two molecules of **1** with one sodium ion. The peaks at 864 and 867 again correspond to conglomerates of **1**, this case with three molecules of **1** with ammonia and sodium adducts respectively. 1146 similarly corresponds to four molecules of **1** with ammonia.

As shown in Figure B.2, high temperature polymerized pNIPAAm-**1** and pNIPAAm-**1**s both show lower racemo content when compared with pNIPAAm-1 and pNIPAAm-**1**s polymerized with a temperature shock for 1 hr and a long room temperature polymerization. The difference is slight (on the order of 1-6.5%) but does contribute to the difference seen in the LCST ranges.

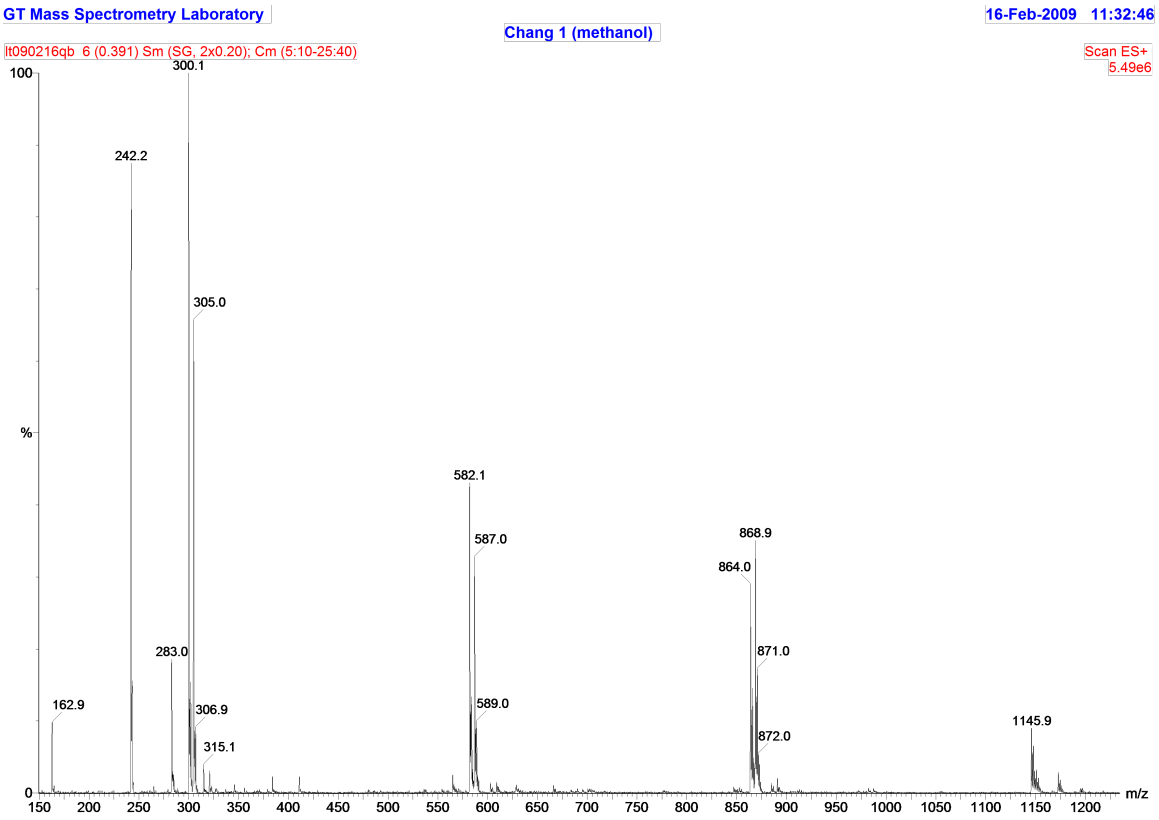

Figure B.1: Electrospray mass spectrum of **1**. Molecular weight of **1** is calculated to be 282.

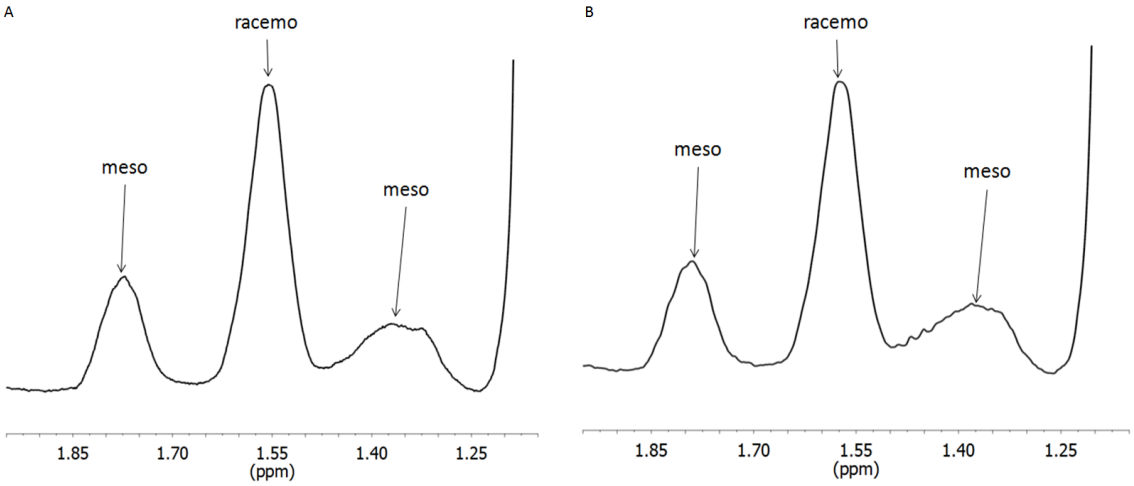

Figure B.2: Expanded ^{1}H NMR spectra of A) pNIPAAm-**1**-HT polymerized at 65 °C for 48 hrs and B) comparable polymer pNIPAAm-**1**s-HT polymerized at 65 °C for 48 hrs. Atactic pNIPAAm shows a racemo diad content of 51.8% while syndiotactic pNIPAAm shows a racemo diad content of 60%.

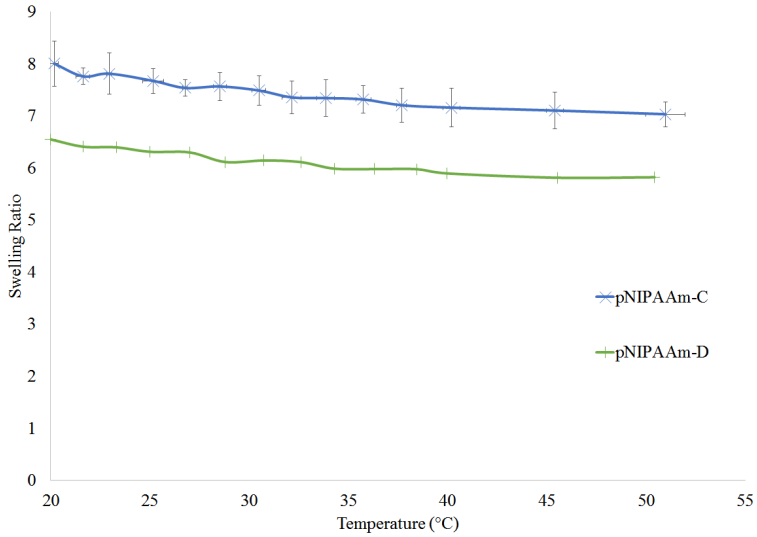

Figure B.3: Temperature dependence of pNIPAAm-C and pNIPAAm-D hydrogels. As shown, no LCST is seen in these hydrogels.

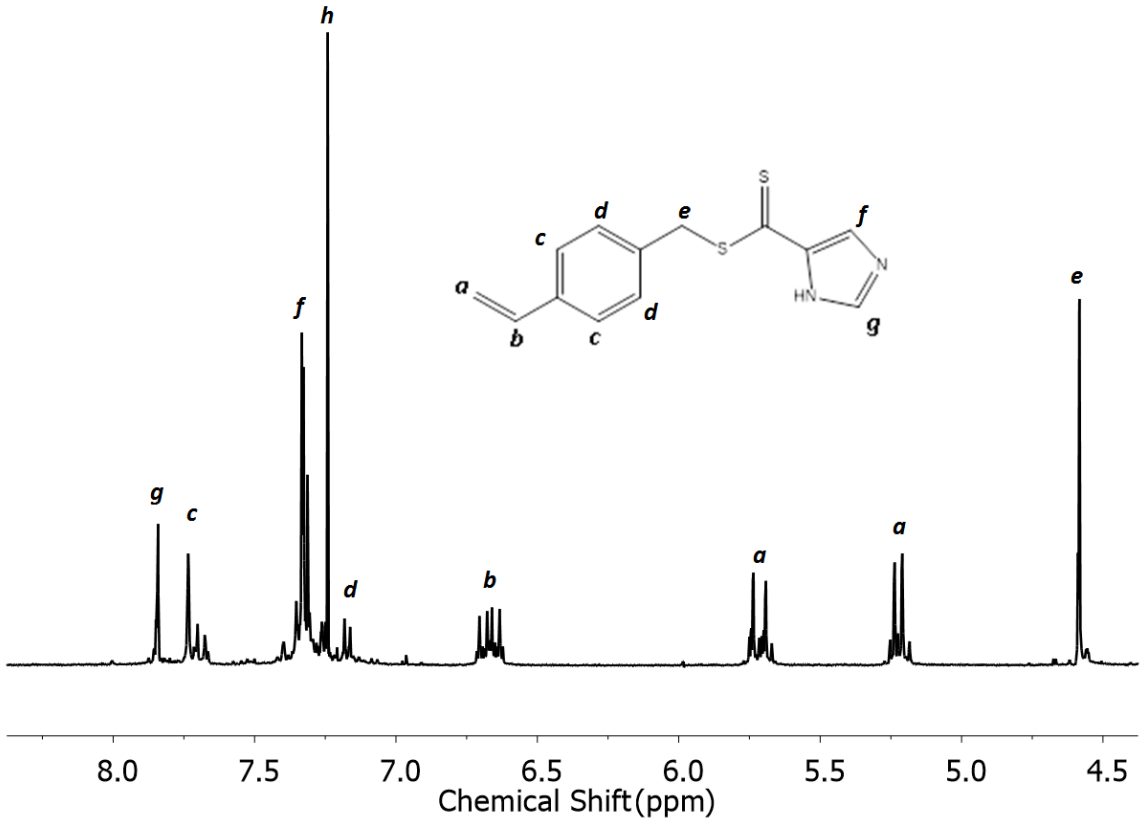

Figure B.4: NMR Spectrum of **2** scanned using a Varian Mercury Vx 400 spectrometer. Peak *h* corresponds to the $CDCl_3$ solvent peak. All other peaks are labeled as per the structure.

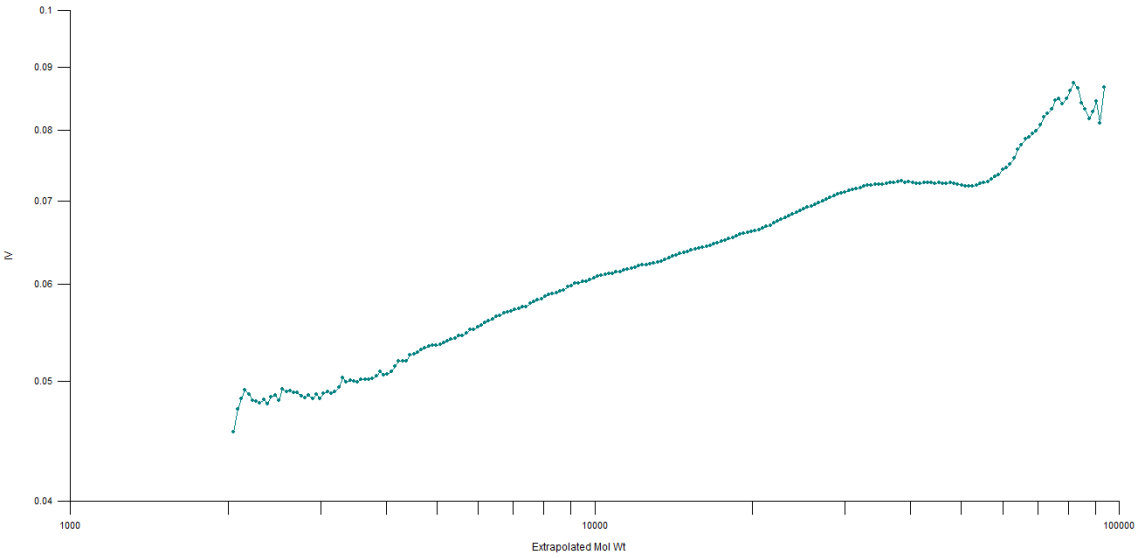

Figure B.5: Mark-Houwink plot of highly branched pNIPAAm on a typical sample with Mn=12967, Mw=23386, PDI=1.8. The α value was 0.13, far below that of linear polymers which have α values on the order of 0.6.

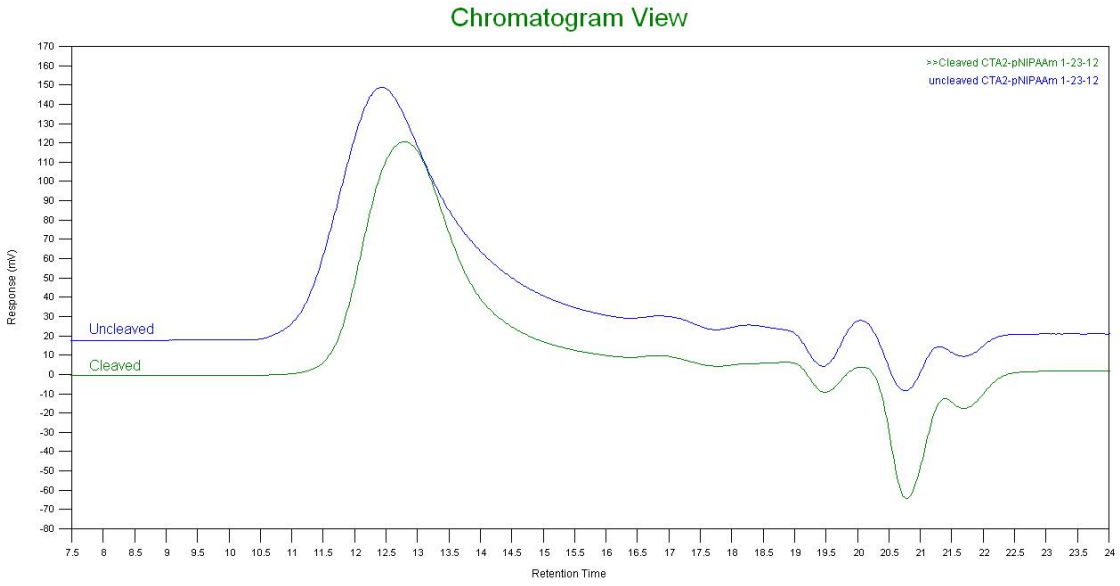

Figure B.6: GPC traces of uncleaved and cleaved hyperbranched pNIPAAm. As shown here, the cleaved pNIPAAm displays a longer retention time compared to the uncleaved pNIPAAm, corresponding to lower molecular weight.

Table B.1: Molecular weights and PDIs of copolymers. M_n, M_w, and PDI were calculated using GPC with polystyrene standards. High percentages of AAm made the copolymers insoluble in THF.

	M_n	M_w	PDI
pNIPAAm	17,600	30,200	1.7
5% AAc	14,500	26,000	1.8
10% AAc	13,400	24,700	1.8
15% AAc	9,500	20,300	2.1
20% AAm	13,300	30,400	2.3
30% AAm			
40% AAm			
60% AAm			
20% DMA	7,600	16,334	2.1
35% DMA	14,100	28,400	2.0
50% DMA	6,500	10,200	1.6
100% DMA	19,900	25,000	1.3
pNIPAAm-linear	5,900	8,600	1.4
5% AAc-linear	6,200	8,100	1.3
10% AAc-linear	6,000	7,600	1.3
20% DMA-linear	4,500	6,200	1.4
35% DMA-linear	3,700	5,000	1.4
50% DMA-linear	3,000	3,700	1.2

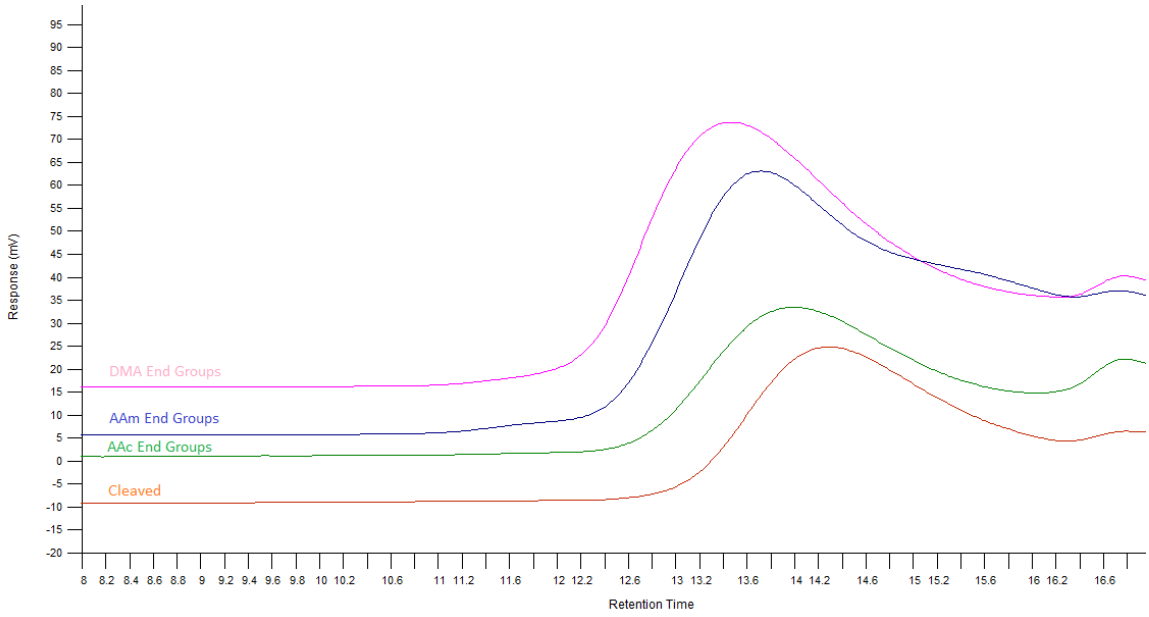

Figure B.7: GPC trace of hyperbranched pNIPAAm with various end groups. The polymers with end groups clicked on clearly show lower retention times compared to that of hyperbranched pNIPAAm without the end groups, indicating larger molecular weight and successful end group incorporation into the polymer.

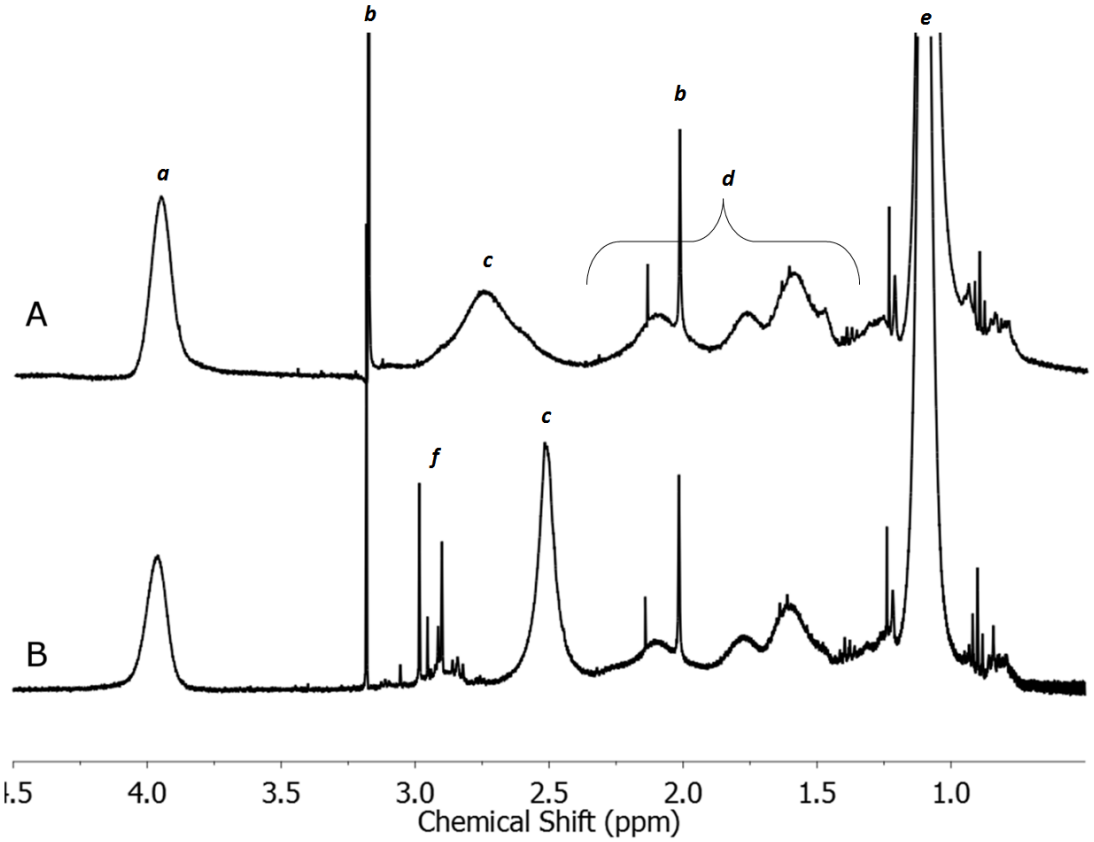

Figure B.8: ^{1}H NMR spectra of highly branched pNIPAAm with A) AAc end-groups, and B) DMA end-groups. The labeled peaks are the lone proton from the *n*-isopropyl group (*a*), the THF solvent peak (*b*), the methylene protons from the branching group (*c*), the methylene and methyne protons from the polymer backbone (*d*), the methyl protons of the N-isopropyl group (*e*), and the methyl protons from the DMA group (*f*). AAc end-group composition was determined via 1-($4a/(c+d)$). DMA end-group composition was determined via $f/(a+f)$.

REFERENCES

[1] Amjad, M. W., Amin, M., Katas, H., and Butt, A. M., "Doxorubicin-loaded cholic acid-polyethyleneimine micelles for targeted delivery of antitumor drugs: synthesis, characterization, and evaluation of their in vitro cytotoxicity," *Nanoscale Research Letters*, vol. 7, 2012.

[2] Andersson, A., Isaksson, A., Brattstrom, L., and Hultberg, B., "Homocysteine and other thiols determined in plasma by hplc and thiol-specific postcolumn derivatization," *Clinical Chemistry*, vol. 39, no. 8, pp. 1590–1597, 1993.

[3] Andersson, A., Lindgren, A., Arnadottir, M., Prytz, H., and Hultberg, B., "Thiols as a measure of plasma redox status in healthy subjects and in patients with renal or liver failure," *Clinical Chemistry*, vol. 45, no. 7, pp. 1084–1087, 1999.

[4] Ankareddi, I. and Brazel, C. S., "Development of a thermosensitive grafted drug delivery system-synthesis and characterization of NIPAAm-based grafts and hydrogel structure," *Journal of Applied Polymer Science*, vol. 120, no. 3, pp. 1597–1696, 2011.

[5] Antoni, P., Robb, M. J., Campos, L., Mopntanez, M., Hult, A., Malmstrom, E., Malkoch, M., and Hawker, C. J., "Pushing the limits for thiol-ene and CuAAC reactions: Synthesis of a 6th generation dendrimer in a single day," *Macromolecules*, vol. 43, no. 16, pp. 6625–6631, 2010.

[6] Antonietti, M., Caruso, R. A., Goltner, C. G., and Weissenberger, M. C., "Morphology variation of porous polymer gels by polymerization in

lyotropic surfactant phases," *Macromolecules*, vol. 32, no. 5, pp. 1383–1389, 1999.

[7] Aries, L. J., "Experimental studies with synthetic fiber (nylon) as a buried suture," *Surgery*, vol. 9, pp. 51–60, 1941.

[8] Aseyev, V. O., Tenhu, H., and Klenin, S. I., "Collapse of poly(methacryloylethyl trimethylammonium methylsulfate) on addition of acetone into an aqueous solution," *Polymer*, vol. 40, no. 5, pp. 1173–1180, 1999.

[9] Bahadur, R. K. C., Thapa, B., and Xu, P., "ph and redox dual responsive nanoparticle for nuclear targeted drug delivery," *Molecular Pharmaceutics*, vol. 9, no. 9, pp. 2719–2729, 2012.

[10] Bailly, N., Thomas, M., and Klumperman, B., "Poly(n-vinylpyrrolidone)-block-poly(vinyl acetate) as a drug delivery vehicle for hydrophobic drugs," *Biomacromolecules*, vol. 13, no. 12, pp. 4109–4117, 2012.

[11] Ballico, M., Drioli, S., and Bonora, G. M., "MultiPEGs: High molecular weight multifunctional poly(ethylene glycol)s assembled by a dendrimer-like approach," *European Journal of Organic Chemistry*, vol. 2005, no. 10, pp. 2064–2073, 2005.

[12] Barner, L., Davis, T. P., Stenzel, M. H., and Barner-Kowollik, C., "Complex macromolecular architectures by reversible addition fragmentation chain transfer chemistry: Theory and practice," *Macromolecular Rapid Communications*, vol. 28, pp. 539–559, 2007.

[13] Barner-Kowollik, C., Coote, M. L., Davis, T. P., Radom, L., and Vana, P., "The reversible addition-fragmentation chain transfer process and the strength and limitations of modeling: Comment on "the magnitude of the

fragmentation rate coefficient"," *Journal of Polymer Science Part a-Polymer Chemistry*, vol. 41, no. 18, pp. 2828–2832, 2003.

[14] Baum, M. and Brittain, W. J., "Synthesis of polymer brushes on silicate substrates via reversible addition fragmentation chain transfer technique," *Macromolecules*, vol. 35, no. 3, pp. 610–615, 2002.

[15] Bearat, H. H., Lee, B. H., and Vernon, B. L., "Comparison of properties between nipaam-based simultaneously physically and chemically gelling polymer systems for use in vivo," *Acta Biomaterialia*, vol. 8, no. 10, pp. 3629–3642, 2012.

[16] Beebe, D. J., Moore, J. S., Bauer, J. M., Yu, Q., Liu, R. H., Devadoss, C., and Jo, B. H., "Functional hydrogel structures for autonomous flow control inside microfluidic channels," *Nature*, vol. 404, no. 6778, p. 588, 2000.

[17] Bhattarai, N., Ramay, H. R., Gunn, J., Matsen, F. A., and Zhang, M. Q., "Peg-grafted chitosan as an injectable thermosensitive hydrogel for sustained protein release," *Journal of Controlled Release*, vol. 103, no. 3, pp. 609–624, 2005.

[18] Bikram, M., Gobin, A. M., Whitmire, R. E., and West, J. L., "Temperature-sensitive hydrogels with SiO2-Au nanoshells for controlled drug delivery," *Journal of Controlled Release*, vol. 123, pp. 219–227, 2007.

[19] Blakemore, A. H. and Voorhees, A. B., "The use of tubes constructed from vinyon n-cloth in bridging arterial defects - experimental and clinical," *Annals of Surgery*, vol. 140, no. 3, pp. 324–334, 1954.

[20] Boas, U. and Heegaard, P. M. H., "Dendrimers in drug research," *Chemical Society Reviews*, vol. 33, pp. 43–63, 2004.

[21] Boutris, C., Chatzi, E. G., and Kiparissides, C., "Characterization of the LCST behaviour of aqueous poly(N-isopropylacrylamide) solutions by thermal and cloud point techniques," *Polymer*, vol. 38, no. 10, pp. 2567–2570, 1997.

[22] Brandrup, J., Immergut, E. H., Grulke, E. A., Abe, A., and Bloch, D. R., *Polymer Handbook*. John Wiley & Sons, 4 ed., 2005.

[23] Braunecker, W. A. and Matyjaszewski, K., "Controlled/living radical polymerization: Features, developments, and perspectives," *Progress in Polymer Science*, vol. 32, no. 1, pp. 93–146, 2007.

[24] Brigger, I., Dubernet, C., and Couvreur, P., "Nanoparticles in cancer therapy and diagnosis," *Advanced Drug Delivery Reviews*, vol. 54, no. 5, pp. 631–651, 2002.

[25] Burmistrova, A. and Kiltzing, R. v., "Control of number density and swelling/shrinking behavior of P(NIPAM-AAc) particles at solid surfaces," *Journal of Materials Chemistry*, vol. 20, no. 3502-3507, 2010.

[26] Cabaness, W. R., Lin, T. Y. C., and Parkanyi, C., "Effect of ph on reactivity ratios in copolymerization of acrylic acid and acrylamide," *Journal of Polymer Science Part a-1-Polymer Chemistry*, vol. 9, no. 8, p. 2155, 1971. Times Cited: 57.

[27] Cai, S., Liu, Y., Shu, X. Z., and Prestwich, G. D., "Injectable glycosaminoglycan hydrogels for controlled release of human basic fibroblast growth factor," *Biomaterials*, vol. 26, no. 31, pp. 6054–6067, 2005.

[28] Calitz, F. M., McLeary, J. B., McKenzie, J. M., Tonge, M. P., Klumperman, B., and Sanderson, R. D., "Evidence for termination of intermediate radical species in raft-mediated polymerization," *Macromolecules*, vol. 36, no. 26, pp. 9687–9690, 2003.

[29] Carnahan, M. A. and Grinstaff, M. W., "Synthesis and characterization of polyether-ester dendrimers from glycerol and lactic acid," *Journal of the American Chemical Society*, vol. 123, no. 12, pp. 2905–2906, 2001.

[30] Carter, S., Hunt, B., and Rimmer, S., "Highly branched poly(N-isopropylacrylamide)s with imidazole end groups prepared by radical polymerization in the presence of styryl monomer containing a dithioester group," *Macromolecules*, vol. 38, no. 11, pp. 4595–4603, 2005.

[31] Carter, S., Rimmer, S., Rutkaite, R., Swanson, L., Fairclough, J. P. A., Sturdy, A., and Webb, M., "Highly branched poly(N-isopropylacrylamide) for use in protein purification," *Biomacromolecules*, vol. 7, no. 4, pp. 1124–1130, 2006.

[32] Carter, S., Rimmer, S., Sturdy, A., and Webb, M., "Highly branched stimuli responsive poly[(N-isopropyl acrylamide)-co-(1,2-propandiol-3-methacrylate)]s with protein binding functionality," *Macromolecular Bioscience*, vol. 5, pp. 373–378, 2005.

[33] Chae, S. Y., Kim, S. W., and Bae, Y. H., "Bioactive polymers for biohybrid artificial pancreas," *Journal of Drug Targeting*, vol. 9, no. 6, pp. 473–484, 2001.

[34] Chakrabarty, S. and Bagchi, B., "Self-organization of n-alkane chains in water: Length dependent crossover from helix and toroid to molten globule," *Journal of Physical Chemistry B*, vol. 113, no. 25, pp. 8446–8448, 2009.

[35] Chang, K., Dicke, Z. T., and Taite, L. J., "Engineering a sharp physiological transition state for poly(n-isopropylacrylamide) through structural control," *Journal of Polymer Science Part A: Polymer Chemistry*, vol. 50, no. 5, pp. 976–985, 2012.

[36] Chang, K., Rubright, N. C., Lowery, P. D., and Taite, L. J., "Structural optimization of highly branched thermally responsive polymers as a means of controlling transition temperature," *Journal of Polymer Science Part A: Polymer Chemistry*, vol. 51, no. 9, pp. 2068–2078, 2013.

[37] Charnley, J., "Arthroplasty of hip - a new operation," *Lancet*, vol. 1, no. 718, p. 1129, 1961.

[38] Charnley, J., McKee, G. K., Coltart, W. D., and Scales, J. T., "Arthroplasty of the hip by the low-friction technique," *Journal of Bone and Joint Surgery-British Volume*, vol. 43, no. 3, pp. 601–601, 1961.

[39] Chauhan, A. S., Svenson, S., Reyna, L., and Tomalia, D., "Solubility enhancement of poorly water soluble molecules using dendrimers," *Material Matters*, vol. 2, no. 1, p. 24, 2007.

[40] Chen, J. Y., Wiley, B., Li, Z. Y., Campbell, D., Saeki, F., Cang, H., Au, L., Lee, J., Li, X. D., and Xia, Y. N., "Gold nanocages: Engineering their structure for biomedical applications," *Advanced Materials*, vol. 17, no. 18, pp. 2255–2261, 2005.

[41] Chen, J., Wang, D., Xi, J., Au, L., Siekkinen, A., Warsen, A., Li, Z.-Y., Zhang, H., Xia, Y., and Li, X., "Immuno gold nanocages with tailored optical properties for targeted photothermal destruction of cancer cells," *Nano Letters*, vol. 7, no. 5, pp. 1318–1322, 2007.

[42] Chen, S. B., Zhong, H., Gu, B., Wang, Y. Z., Li, X. M., Cheng, Z. P., Zhang, L. L., and Yao, C., "Thermosensitive phase behavior and drug release of in situ n-isopropylacrylamide copolymer," *Materials Science and Engineering C-Materials for Biological Applications*, vol. 32, no. 8, pp. 2199–2204, 2012.

[43] Chen, S. C., Wu, Y. C., Mi, F. L., Lin, Y. H., Yu, L. C., and Sung, H. W., "A novel ph-sensitive hydrogel composed of n,o-carboxymethyl chitosan and alginate cross-linked by genipin for protein drug delivery," *Journal of Controlled Release*, vol. 96, no. 2, pp. 285–300, 2004.

[44] Cheng, S. X., Zhang, J. T., and Zhuo, R. X., "Macroporous poly(n-isopropylacrylamide) hydrogels with fast response rates and improved protein release properties," *Journal of Biomedical Materials Research Part A*, vol. 67A, no. 1, pp. 96–103, 2003.

[45] Cheng, Y. and Xu, T., "The effect of dendrimers on the pharmacodynamic and pharmacokinetic behaviors of non-covalently or covalently attached drugs," *European Journal of Medicinal Chemistry*, vol. 43, pp. 2291–2297, 2008.

[46] Chernikova, E., Morozov, A., Leonova, E., Garina, E., Golubev, V., Bui, C. O., and Charleux, B., "Controlled free-radical polymerization of n-butyl acrylate by reversible addition-fragmentation chain transfer in the presence of tert-butyl dithiobenzoate. a kinetic study," *Macromolecules*, vol. 37, no. 17, pp. 6329–6339, 2004.

[47] Chiantore, O., Guaita, M., and Trossarelli, L., "Solution properties of poly(n-isopropylacrylamide)," *Makromolekulare Chemie-Macromolecular Chemistry and Physics*, vol. 180, no. 4, pp. 969–973, 1979.

[48] Chiefari, J., Chong, Y. K., Ercole, F., Krstina, J., Jeffery, J., Le, T. P. T., Mayadunne, R. T. A., and Meijs, G. F., "Living free-radical polymerization by reversible addition-fragmentation chain transfer: The RAFT process," *Macromolecules*, vol. 31, no. 16, pp. 5559–5562, 1998.

[49] Chong, Y. K., Le, T. P. T., Moad, G., Rizzardo, E., and Thang, S. H., "A more versatile route to block copolymers and other polymers of complex architecture by living radical polymerization: The raft process," *Macromolecules*, vol. 32, no. 6, pp. 2071–2074, 1999.

[50] Chong, Y. K., Moad, G., Rizzardo, E., and Thang, S. H., "Thiocarbonylthio end group removal from RAFT-synthesized polymers by radical-induced reduction," *Macromolecules*, vol. 40, no. 13, pp. 4446–4455, 2007.

[51] Cloninger, M. J., "Biological applications of dendrimers," *Current Opinion in Chemical Biology*, vol. 6, no. 6, pp. 742–748, 2002.

[52] Convertine, A. J., Lokitz, B. S., Vasileva, Y., Myrick, L. J., Scales, C. W., Lowe, A. B., and McCormick, C. L., "Direct synthesis of thermally responsive DMA/NIPAM diblock and DMA/NIPAM/DMA triblock copolymers via aqueous, room temperature RAFT polymerization," *Macromolecules*, vol. 39, no. 5, pp. 1724–1730, 2006.

[53] Coughlan, D. C., Quilty, F. P., and Corrigan, O. I., "Effect of drug physicochemical properties on swelling/deswelling kinetics and pulsatile drug release from thermoresponsive poly(n-isopropylacrylamide) hydrogels," *Journal of Controlled Release*, vol. 98, no. 1, pp. 97–114, 2004.

[54] Dadsetan, M., Liu, Z., Pumberger, M., Giraldo, C. V., Ruesink, T., Lu, L. C., and Yaszemski, M. J., "A stimuli-responsive hydrogel for doxorubicin delivery," *Biomaterials*, vol. 31, no. 31, pp. 8051–8062, 2010.

[55] Dahan, A., Dimant, H., and Portnoy, M., "Synthesis of tetrafurcated dendritic units on solid support," *Journal of Combinatorial Chemistry*, vol. 6, no. 305-307, 2004.

[56] Dahan, A. and Portnoy, M., "Synthesis of poly(aryl benzyl ether) dendrimers on solid support," *Macromolecules*, vol. 36, pp. 1034–1038, 2003.

[57] Das, B., Kumar, A. S., Ravikanth, B., Damodar, K., and Krishnaiah, M., "Rapid, efficient and selective conjugate addition of thiols to , -unsaturated carbonyl compounds using silica supported sodium hydrogen sulfate under solvent-free conditions," *Journal of Sulfur Chemistry*, vol. 29, no. 5, pp. 489–494, 2008.

[58] de Brouwer, H., Schellekens, M. A. J., Klumperman, B., Monteiro, M. J., and German, A. L., "Controlled radical copolymerization of styrene and maleic anhydride and the synthesis of novel polyolefin-based block copolymers by reversible addition-fragmentation chain-transfer (RAFT) polymerization," *Journal of Polymer Science Part A: Polymer Chemistry*, vol. 38, no. 19, pp. 3596–3603, 2000.

[59] de Graaf, A. J., dos Santos, I., Pieters, E. H. E., Rijkers, D. T. S., van Nostrum, C. F., Vermonden, T., Kok, R. J., Hennink, W. E., and Mastrobattista, E., "A micelle-shedding thermosensitive hydrogel as sustained release formulation," *Journal of Controlled Release*, vol. 162, no. 3, pp. 582–590, 2012.

[60] Deka, S. R., Quarta, A., Di Corato, R., Riedinger, A., Cingolani, R., and Pellegrino, T., "Magnetic nanobeads decorated by thermoresponsive pnipam shell as medical platforms for the efficient delivery of doxorubicin to tumour cells," *Nanoscale*, vol. 3, no. 2, pp. 619–629, 2011.

[61] Dickerson, E. B., Dreaden, E. C., Huang, X., El-Sayed, I. H., Chu, H., Pushpanketh, S., McDonald, J. F., and El-Sayed, M. A., "Gold

nanorod assisted near-infrared plasmonic photothermal therapy (pptt) of squamous cell carcinoma in mice," *Cancer Letters*, vol. 269, no. 1, pp. 57–66, 2008.

[62] Don, T.-M., Huang, M.-L., Chiu, A.-C., Kuo, K.-H., Chiu, W.-Y., and Chiu, L.-H., "Preparation of thermo-responsive acrylic hydrogels useful for the application in transdermal drug delivery systems," *Materials Chemistry and Physics*, vol. 107, no. 2-3, pp. 266–273, 2008.

[63] Dondoni, A., "The emergence of thiol-ene coupling as a click process for materials and bioorganic chemistry," *Angewandte Chemie International Edition*, vol. 47, no. 47, pp. 8995–8997, 2008.

[64] Dong, L. C. and Hoffman, A. S., "Synthesis and application of thermally reversible heterogels for drug delivery," *Journal of Controlled Release*, vol. 13, no. 1, pp. 21–31, 1990.

[65] Ebara, M., Yamato, M., Nagai, S., Aoyagi, T., Kikuchi, A., Sakai, K., and Okano, T., "Incorporation of new carboxylate functionalized comonomers to temperature-responsive polymer-grafted cell culture surfaces," *Surface Science*, vol. 570, pp. 134–141, 2004.

[66] Egdahl, R. H., "Silicone rubber as aortic grafting material," *Archives of Surgery*, vol. 71, no. 5, pp. 694–696, 1955.

[67] El-Sherbiny, I. M. and Smyth, H. D. C., "Smart magnetically responsive hydrogel nanoparticles prepared by a novel aerosol-assisted method for biomedical and drug delivery applications," *Journal of Nanomaterials*, 2011.

[68] Elbert, D. L. and Hubbell, J. A., "Surface treatments of polymers for biocompatibility," *Annual Review of Materials Science*, vol. 26, pp. 365–394, 1996.

[69] Eliassaf, J., "Aqueous-solutions of poly(n-isopropylacrylamide)," *Journal of Applied Polymer Science*, vol. 22, no. 3, pp. 873–874, 1978.

[70] Ellman, G. L., "Tissue sulfhydryl groups," *Archives of Biochemistry and Biophysics*, vol. 82, no. 1, pp. 70–77, 1959.

[71] England, R. M. and Rimmer, S., "Hyper/highly-branched polymers by radical polymerisations," *Polymer Chemistry*, vol. 1, no. 10, pp. 1533–1544, 2010.

[72] Erbil, C. and Sarac, A. S., "Description of the turbidity measurements near the phase transition temperature of poly(N-isopropyl acrylamide) copolymers: the effect of pH, concentration, hydrophilic and hydrophobic content on the turbidity," *European Polymer Journal*, vol. 38, no. 7, pp. 1305–1310, 2002.

[73] Feil, H., Bae, Y. H., Feijen, J., and Kim, S. W., "Mutual influence of ph and temperature on the swelling of ionizable and thermosensitive hydrogels," *Macromolecules*, vol. 25, no. 20, pp. 5528–5530, 1992.

[74] Feil, H., Bae, Y. H., Feijen, J., and Kim, S. W., "Effect of comonomer hydrophilicity and ionization on the lower critical solution temperature of n-isopropylacrylamide copolymers," *Macromolecules*, vol. 26, pp. 2496–2500, 1993.

[75] Fréchet, J. M. J., "Dendrimers and supramolecular chemistry," *Proceedings of the National Academy of Sciences of the United States of America*, vol. 99, no. 8, pp. 4782–4787, 2002.

[76] Fréchet, J. M. J., Henmi, M., Gitsov, I., Aoshima, S., Leduc, M. R., and Grubbs, R. B., "Self-condensing vinyl polymerization: An approach to dendritic materials," *Science*, vol. 269, pp. 1080–1083, 1995.

[77] Friis, N. and Hamielec, A. E., "Gel-effect in emulsion polymerization of vinyl monomers," *ACS Symposium Series*, no. 24, pp. 82–91, 1976.

[78] Fujishige, S., "Intrinsic viscosity-molecular weight relationships for poly(n-isopropylacrylamide) solutions," *Polymer Journal*, vol. 19, no. 3, pp. 297–300, 1987.

[79] Fujishige, S., Kubota, K., and Ando, I., "Phase-transition of aqueous-solutions of poly(n-isopropylacrylamide) and poly(n-isopropylmethacrylamide)," *Journal of Physical Chemistry*, vol. 93, no. 8, pp. 3311–3313, 1989.

[80] Fukunda, T., Goto, A., and Ohno, K., "Mechanisms and kinetics of living radical polymerization," *Macromolecular Rapid Communications*, vol. 21, pp. 151–165, 2000.

[81] Ganachaud, F., Monteiro, M. J., Gilbert, R. G., Dourges, M. A., Thang, S. H., and Rizzardo, E., "Molecular weight characterization of poly(n-isopropylacrylamide) prepared by living free-radical polymerization," *Macromolecules*, vol. 33, no. 18, pp. 6738–6745, 2000.

[82] Garbern, J. C., Minami, E., Stayton, P. S., and Murry, C. E., "Delivery of basic fibroblast growth factor with a ph-responsive, injectable hydrogel to improve angiogenesis in infarcted myocardium," *Biomaterials*, vol. 32, no. 9, pp. 2407–2416, 2011.

[83] Gaynor, S. G., Edelman, S., and Matyjaszewski, K., "Synthesis of branched and hyperbranched polystyrenes," *Macromolecules*, vol. 29, no. 3, pp. 1079–1081, 1996.

[84] Gehrke, S. H., Palasis, M., and Akhtar, M. K., "Effect of synthesis conditions on properties of poly(n-isopropylacrylamide) gels," *Polymer International*, vol. 29, no. 1, pp. 29–36, 1992.

[85] Ghosh, S., Yang, C., Cai, T., Hu, Z., and Neogi, A., "Oscillating magnetic field-actuated microvalves for micro- and nanofluidics," *Journal of Physics D-Applied Physics*, vol. 42, no. 13, 2009.

[86] Gil, E. S. and Hudson, S. M., "Stimuli-responsive polymers and their bioconjugates," *Progress in Polymer Science*, vol. 29, no. 12, pp. 1173–1222, 2004.

[87] Gil, E. S. and Hudson, S. M., "Effect of silk fibroin interpenetrating networks on swelling/deswelling kinetics and rheological properties of poly(n-isopropylacrylamide) hydrogels," *Biomacromolecules*, vol. 8, no. 1, pp. 258–264, 2007.

[88] Gobin, A. M., Watkins, E. M., Quevedo, E., Colvin, V. L., and West, J. L., "Near-infrared-resonant gold/gold sulfide nanoparticles as a photothermal cancer therapeutic agent," *Small*, vol. 6, no. 6, pp. 745–752, 2010.

[89] Gondi, S. R., Vogt, A. P., and Sumerlin, B. S., "Versatile pathway to funcitonal telechelics via RAFT polymerization and click chemistry," *Macromolecules*, vol. 40, pp. 474–481, 2007.

[90] Gong, C., Qi, T., Wei, X., Qu, Y., Wu, Q., Luo, F., and Qian, Z., "Thermosensitive polymeric hydrogels as drug delivery systems," *Current Medicinal Chemistry*, vol. 20, no. 1, pp. 79–94, 2013.

[91] Gromov, V. F., Galperina, N. I., Osmanov, T. O., Khomikovskii, P. M., and Abkin, A. D., "Effect of solvent on chain propagation and termination reaction-rates in radical polymerization," *European Polymer Journal*, vol. 16, no. 6, pp. 529–535, 1980.

[92] Guan, Z., Cotts, P. M., McCord, E. F., and McLain, S. J., "Chain walking: A new strategy to control polymer topology," *Science*, vol. 283, no. 5410, pp. 2059–2062, 1999.

[93] Hahn, M. S., Taite, L. J., Moon, J. J., Rowland, M. C., Ruffino, K. A., and West, J. L., "Photolithographic patterning of polyethylene glycol hydrogels," *Biomaterials*, vol. 27, no. 12, pp. 2519–2524, 2006.

[94] Han, C. K. and Bae, Y. H., "Inverse thermally-reversible gelation of aqueous n-isopropylacrylamide copolymer solutions," *Polymer*, vol. 39, no. 13, pp. 2809–2814, 1998.

[95] Hawker, C., Lee, R., and Frchet, J., "One-step synthesis of hyperbranched dendritic polyesters," *Journal of the American Chemical Society*, vol. 113, pp. 4583–4588, 1991.

[96] Hawker, C. J., Bosman, A. W., and Harth, E., "New polymer synthesis by nitroxide mediated living radical polymerizations," *Chemical Reviews*, vol. 101, no. 12, pp. 3661–3688, 2001.

[97] Hawker, C. J. and Frechet, J. M. J., "Preparation of polymers with controlled molecular architecture. a new convergent approach to dendritic macromolecules," *Journal of the American Chemical Society*, vol. 112, no. 12, pp. 7638–7647, 1990.

[98] Hendrickson, G. R., Smith, M. H., South, A. B., and Lyon, L. A., "Design of multiresponsive hydrogel particles and assemblies," *Advanced Functional Materials*, vol. 20, no. 11, pp. 1697–1712, 2010.

[99] Higashihara, T., Segawa, Y., Sinananwanich, W., and Ueda, M., "Synthesis of hyperbranched polymers with controlled degree of branching," *Polymer Journal*, vol. 44, no. 1, pp. 14–29, 2012.

[100] Hirano, T., Ishizu, H., and Sato, T., "Metal-free isotactic-specific radical polymerization of N-isopropylacrylamide with pyridine N-oxide derivatives: The effect of methyl substitutents of pyridine N-oxide on the isotactic specificity and the proposed mechanism for the isotactic-specific radical polymerization," *Polymer*, vol. 49, pp. 438–445, 2008.

[101] Hirano, T., Ishizu, H., Seno, M., and Sato, T., "Hydrogen-bond-assisted isotactic-specific radical polymerization of N-isopropylacrylamide with pyridine N-oxide," *Polymer*, vol. 46, no. 24, pp. 10607–10610, 2005.

[102] Hirano, T., Kamikubo, T., Fujioka, Y., and Sato, T., "Hydrogen-bond-assisted syndiotactic-specific radical polymerization of N-isopropylacrylamide: The solvent effect on the stereospecificity," *European Polymer Journal*, vol. 44, no. 4, pp. 1053–1059, 2008.

[103] Hirano, T., Kamikubo, T., Okumura, Y., and Sato, T., "Heterotactic poly(N-isopropylacrylamide) prepared via radical polymerization in the presence of flourinated alcohols," *Polymer*, vol. 48, no. 17, pp. 4921–4925, 2007.

[104] Hirano, T., Kitajima, H., Seno, M., and Sato, T., "Hydrogen-bond-assisted stereocontrol in the radical polymerization of N-isopropylacrylamide with bidentate Lewis base," *Polymer*, vol. 47, pp. 539–546, 2006.

[105] Hirano, T., Miki, H., Seno, M., and Sato, T., "Direct synthesis of syndiotactic-rich poly(N-isopropylacrylamide) via radical polymerization of hydrogen-bond-complexed monomer," *Polymer*, vol. 46, no. 11, pp. 3693–3699, 2005.

[106] Hirano, T., Miki, H., Seno, M., and Sato, T., "Effect of polymerization conditions on the syndiotactic-specificity in radical polymerization of N-isopropylacrylamide and fractionation of the obtained polymer according to stereoregularity," *Polymer*, vol. 46, no. 15, pp. 5501–5505, 2005.

[107] Hirano, T., Okumura, Y., Kitajima, H., Seno, M., and Sato, T., "Dual roles of alkyl alcohols as syndiotactic-specificity inducers and accelerators in the radical polymerization of N-isopropylacrylamide and some properties of syndiotactic poly(N-isopropylacrylamide)," *Journal of Polymer Science: Part A: Polymer Chemistry*, vol. 44, no. 15, pp. 4450–4460, 2006.

[108] Hirose, H. and Shibayama, M., "Kinetics of volume phase transition in poly(n-isopropylacrylamide-co-acrylic acid) gels," *Macromolecules*, vol. 31, no. 16, pp. 5336–5342, 1998.

[109] Hirsch, L. R., Stafford, R. J., Bankson, J. A., Sershen, S. R., Rivera, B., Price, R. E., Hazle, J. D., Halas, N. J., and West, J. L., "Nanoshell-mediated near-infrared thermal therapy of tumors under magnetic resonance guidance," *Proceedings of the National Academy of Sciences of the United States of America*, vol. 100, no. 23, pp. 13549–13554, 2003.

[110] Hlter, D., Burgath, A., and Frey, H., "Degree of branching in hyperbranched polymers," *Acta Polymerica*, vol. 48, pp. 30–35, 1997.

[111] Ho, C.-H., Chen, S.-A., Amiridis, M. D., and Zee, J. W. V., "Dispersion polymerization of styrene in alcohol media: Effect of initiator concentration, solvent polarity, and temperature on the rate of polymerization," *Journal of Polymer Science Part A: Polymer Chemistry*, vol. 35, no. 14, pp. 2907–2915, 1997.

[112] Holden, C. A., Tyagi, P., Thakur, A., Kadam, R., Jadhav, G., Kompella, U. B., and Yang, H., "Polyamidoamine dendrimer hydrogel for enhanced delivery of antiglaucoma drugs," *Nanomedicine-Nanotechnology Biology and Medicine*, vol. 8, no. 5, pp. 776–783, 2012.

[113] Honda, M., Saito, Y., Smith, N. I., Fujita, K., and Kawata, S., "Nanoscale heating of laser irradiated single gold nanoparticles in liquid," *Optics Express*, vol. 19, no. 13, pp. 12375–12383, 2011.

[114] Hopkins, S., Carter, S., Swanson, L., MacNeil, S., and Rimmer, S., "Temperature-dependent phagocytosis of highly branches poly(N-isopropyl acrylamide-co-1,2 propandiol-3-methacrylate)s prepared by RAFT polymerization," *Journal of Materials Chemistry*, vol. 17, pp. 4022–4027, 2007.

[115] Horiguchi, Y., Honda, K., Kato, Y., Nakashima, N., and Niidome, Y., "Photothermal reshaping of gold nanorods depends on the passivating layers of the nanorod surfaces," *Langmuir*, vol. 24, pp. 12026–12031, 2008.

[116] Hoyle, C. E. and Bowman, C. N., "Thiol-ene click chemistry," *Angewandte Chemie International Edition*, vol. 49, no. 9, pp. 1540–1573, 2010.

[117] Hoyle, C. E., Lee, T. Y., and Roper, T., "Thiol-enes: Chemistry of the past with promise for the future," *Journal of Polymer Science Part A: Polymer Chemistry*, vol. 42, pp. 5301–5337, 2004.

[118] Hoyle, C. E., Lowe, A. B., and Bowman, C. N., "Thiol-click chemistry: a multifaceted toolbox for small molecules and polymer synthesis," *Chemical Society Reviews*, vol. 39, no. 4, pp. 1355–1387, 2010.

[119] Huang, Y. J., Liu, M. Z., Chen, J. C., Gao, C. M., and Gong, Q. Y., "A novel magnetic triple-responsive composite semi-ipn hydrogels for targeted and

controlled drug delivery," *European Polymer Journal*, vol. 48, no. 10, pp. 1734–1744, 2012.

[120] Huebsch, N. and Mooney, D. J., "Inspiration and application in the evolution of biomaterials," *Nature*, vol. 462, no. 7272, pp. 426–432, 2009.

[121] Hurd, C. D. and Gershbein, L. L., "Reactions of mercaptans with acrylic and methacrylic derivatives," *Journal of the American Chemical Society*, vol. 69, no. 10, pp. 2328–2335, 1947.

[122] Ingraham, F. D., Alexander, E., and Matson, D. D., "Polyethylene, a new synthetic plastic for use in surgery - experimental applications in neurosurgery," *Jama-Journal of the American Medical Association*, vol. 135, no. 2, pp. 82–87, 1947.

[123] Ingraham, F. D., Alexander, E., and Matson, D. D., "Synthetic plastic materials in surgery," *New England Journal of Medicine*, vol. 236, no. 10, pp. 362–368, 1947.

[124] Ingraham, F. D., Alexander, E., and Matson, D. D., "Synthetic plastic materials in surgery (concluded)," *New England Journal of Medicine*, vol. 236, no. 11, pp. 402–407, 1947.

[125] Isobe, Y., Fujioka, D., Habaue, S., and Okamoto, Y., "Efficient lewis acid-catalyzed stereocontrolled radical polymerization of acrylamides," *Journal of the American Chemical Society*, vol. 123, pp. 7180–7181, 2001.

[126] Ispasoiu, R. G., Balogh, L., Varnavski, O. P., Tomalia, D. A., and Theodore Goodson, I., "Large optical limiting from novel metal-dendrimer nanocomposite materials," *Journal of the American Chemical Society*, vol. 122, pp. 11005–11006, 2000.

[127] Ito, S., Ogawa, K., Suzuki, H., Wang, B., Yoshida, R., and Kokufuta, E., "Preparation of thermosensitive submicrometer gel particles with anionic and cationic charges," *Langmuir*, vol. 15, no. 12, pp. 4289–4294, 1999.

[128] Jain, P. K. and El-Sayed, M. A., "Universal scaling of plasmon coupling in metal nanostructures: Extension from particle pairs to nanoshells," *Nano Letters*, vol. 7, no. 9, pp. 2854–2858, 2007.

[129] Jain, P. K., Lee, K. S., El-Sayed, I. H., and El-Sayed, M. A., "Calculated absorption and scattering properties of gold nanoparticles of different size, shape, and composition: Applications in biological imaging and biomedicine," *Journal of Physical Chemistry B*, vol. 110, pp. 7238–7248, 2006.

[130] Janovak, L., Varga, J., Kemeny, L., and Dekany, I., "Investigation of the structure and swelling of poly(N-isopropyl-acrylamide-acrylamide) and poly(N-isopropyl-acrylamide-acrylic acid) based copolymer and composite hydrogels," *Colloid and Polymer Science*, vol. 286, no. 14-15, pp. 1575–1585, 2008.

[131] Jeong, B., Bae, Y. H., Lee, D. S., and Kim, S. W., "Biodegradable block copolymers as injectable drug-delivery systems," *Nature*, vol. 388, no. 6645, pp. 860–862, 1997.

[132] Jeong, B., Kim, S. W., and Bae, Y. H., "Thermosensitive sol-gel reversible hydrogels," *Advanced Drug Delivery Reviews*, vol. 54, no. 1, pp. 37–51, 2002.

[133] Kabra, B. G. and Gehrke, S. H., "Synthesis of fast response, temperature-sensitive poly(n-isopropylacrylamide) gel," *Polymer Communications*, vol. 32, no. 11, pp. 322–323, 1991.

[134] Katsumoto, Y. and Kubosaki, N., "Tacticity effects on the phase diagram for poly(n-isopropylacrylamide) in water," *Macromolecules*, vol. 41, pp. 5955–5956, 2008.

[135] Kawano, T., Niidome, Y., Mori, T., Katayama, Y., and Niidome, T., "Pnipam gel-coated gold nanorods for targeted delivery responding to a near-infrared laser," *Bioconjugate Chemistry*, vol. 20, pp. 209–212, 2009.

[136] Kim, J.-H. and Lee, T. R., "Thermo- and ph- responsive hydrogel-coated gold nanoparticles," *Chemistry of Materials*, vol. 16, no. 19, pp. 3647–3651, 2004.

[137] Kim, Y. and Zimmerman, S. C., "Applications of dendrimers in bio-organic chemistry," *Current Opinion in Chemical Biology*, vol. 2, no. 6, pp. 733–742, 1998.

[138] Kishi, R., Kihara, H., and Miura, T., "Structural observation of heterogenous poly(n-isopropyl acrylamide-co-acrylic acid) hydrogels in highly hydrated states," *Colloid Polymer Science*, vol. 283, pp. 113–138, 2004.

[139] Kizhakkedathu, J. N., Norris-Jones, R., and Brooks, D. E., "Synthesis of well-defined environmentally responsive polymer brushes by aqueous atrp," *Macromolecules*, vol. 37, no. 3, pp. 734–743, 2004.

[140] Kolb, H. C., Finn, M. G., and Sharpless, K. B., "Click chemistry: Diverse chemical function from a few good reactions," *Angewandte Chemie International Edition*, vol. 40, no. 11, pp. 2004–2021, 2001.

[141] Konda, S. D., Aref, M., Wang, S., Brechbiel, M., and Wiener, E. C., "Specific targeting of folate-dendrimer mri contrast agents to the high affinity fo late receptor expressed in ovarian tumor xenografts," *Magnetic Resonance Materials in Physics Biology and Medicine*, vol. 12, no. 2-3, pp. 104–113, 2001.

[142] Konkolewicz, D., Gray-Weale, A., and Perrier, S., "The structure of randomly branched polymers synthesized by living radical methods," *Polymer Chemistry*, vol. 1, no. 7, pp. 1067–1077, 2010.

[143] Kratz, K., Hellweg, T., and Eimer, W., "Influence of charge density on the swelling of colloidal poly(n-isopropylacrylamide-co-acrylic acid) microgels," *Colloids and Surfaces a-Physicochemical and Engineering Aspects*, vol. 170, no. 2-3, pp. 137–149, 2000.

[144] Krstina, J., Moad, G., Rizzardo, E., Winzor, C. L., Berge, C. T., and Fryd, M., "Narrow polydispersity block-copolymers by free-radical polymerization in the presence of macromonomers," *Macromolecules*, vol. 28, no. 15, pp. 5381–5385, 1995.

[145] Kubota, K., Fujishige, S., and Ando, I., "Solution properties of poly(n-isopropylacrylamide) in water," *Polymer Journal*, vol. 22, no. 1, pp. 15–20, 1990.

[146] Lai, J. T., Filla, D., and Shea, R., "Functional polymers from novel carboxyl-terminated trithiocarbonates as highly efficient RAFT agents," *Macromolecules*, vol. 35, no. 18, pp. 6754–6756, 2002.

[147] Lee, C. C., MacKay, J. A., Frechet, J. M. J., and Szoka, F. C., "Designing dendrimers for biological applications," *Nature Biotechnology*, vol. 23, no. 12, pp. 1517–1526, 2005.

[148] Lemke, T. L. and Williams, D. A., *Foye's Principles of Medicinal Chemistry*. Lippincott Williams & Wilkins, 7 ed., 2012.

[149] Levental, I., Georges, P. C., and Janmey, P. A., "Soft biological materials and their impact on cell function," *Soft Matter*, vol. 3, no. 3, pp. 299–306, 2007.

[150] Li, G.-Z., Randev, R. K., Soeriyadi, A. H., Rees, G., Boyer, C., Tong, Z., Davis, T. P., Becer, R., and Haddleton, D. M., "Investigation

into thiol-(meth)acrylate michael addition reactions using amine and phosphine catalysts," *Polymer Chemistry*, vol. 1, no. 8, pp. 1196 –1204, 2010.

[151] Li, H., Yu, B., Matsushima, H., Hoyle, C. E., and Lowe, A. B., "The thiol-isocyanate click reaction: Facile and quantitative access to ω-end-functional poly(N,N-diethylacrylamide) synthesized by RAFT radical polymerization," *Macromolecules*, vol. 42, no. 17, pp. 6537–6542, 2009.

[152] Li, M. Q., Tang, Z. H., Sun, H., Ding, J. X., Song, W. T., and Chen, X. S., "ph and reduction dual-responsive nanogel cross-linked by quaternization reaction for enhanced cellular internalization and intracellular drug delivery," *Polymer Chemistry*, vol. 4, no. 4, pp. 1199–1207, 2013.

[153] Li, Z., Kim, Y.-H., Min, H. S., Han, C.-K., and Huh, K. M., "Molecular weight and end group effects on the thermo-responsive property of oligomeric n-isopropylacrylamide," *Macromolecular Research*, vol. 18, no. 6, pp. 618–621, 2010.

[154] Link, S. and El-Sayed, M. A., "Spectral properties and relaxation dynamics of surface plasmon electronic oscillations in gold and silver nanodots and nanorods," *Journal of Physical Chemistry B*, vol. 103, pp. 8410–8426, 1999.

[155] Liu, B., Kazlauciunas, A., Guthrie, J. T., and Perrier, S., "One-pot hyperbranched polymer synthesis mediated by reversible addition fragmentation chain transfer (RAFT) polymerization," *Macromolecules*, vol. 38, pp. 2131–2136, 2005.

[156] Liu, D., Wang, T., Liu, X., and Tong, Z., "Accelerated cell sheet detachment by copolymerizing hydrophilic peg side chains into pnipam nanocomposite hydrogels," *Biomedical Materials*, vol. 7, no. 5, 2012.

[157] Liu, Q. F., Zhang, P., and Lu, M. G., "Synthesis and swelling behavior of comb-type grafted hydrogels by reversible addition-fragmentation chain transfer polymerization," *Journal of Polymer Science Part a-Polymer Chemistry*, vol. 43, no. 12, pp. 2615–2624, 2005.

[158] Liu, Q., Zhang, P., Qing, A., Lan, Y., and Lu, M., "Poly(n-isopropylacrylamide) hydrogels with improved shrinking kinetics by raft polymerization," *Polymer*, vol. 47, no. 7, pp. 2330–2336, 2006.

[159] Liu, Y. Y., Shao, Y. H., and Lu, J., "Preparation, properties and controlled release behaviors of ph-induced thermosensitive amphiphilic gels," *Biomaterials*, vol. 27, no. 21, pp. 4016–4024, 2006.

[160] Liu, Y., Li, K., Liu, B., and Feng, S.-S., "A strategy for precision engineering of nanoparticles of biodegradable copolymers for quantitative control of targeted drug delivery," *Biomaterials*, vol. 31, no. 35, pp. 9145–9155, 2010.

[161] Loo, C., Hirsch, L., Lee, M.-H., Chang, E., West, J., Halas, N., and Drezek, R., "Gold nanoshell bioconjugates for molecular imaging in living cells," *Optics letters*, vol. 30, no. 9, pp. 1012–1014, 2005.

[162] Loo, C., Lowery, A., Halas, N., West, J., and Drezek, R., "Immunotargeted nanoshells for integrated cancer imaging and therapy," *Nano Letters*, vol. 5, no. 4, pp. 709–711, 2005.

[163] Luman, N. R., Kim, T., and Grinstaff, M. W., "Dendritic polymers composed of glycerol and succinic acid: Synthetic methodologies and medical applications," *Pure and Applied Chemistry*, vol. 76, no. 7-8, pp. 1375–1385, 2004.

[164] Malonne, H., Eekman, F., Fontaine, D., Otto, A., Vos, L. D., Moes, A., Fontaine, J., and Amighi, K., "Preparation of poly(N-isopropylacrylamide) copolymers and preliminary assessment of their acute and

subacute toxicity in mice," *European Journal of Pharmaceutics and Biopharmaceutics*, vol. 61, pp. 188–194, 2005.

[165] Mano, J. F., "Stimuli-responsive polymeric systems for biomedical applications," *Advanced Engineering Materials*, vol. 10, no. 6, pp. 515–527, 2008.

[166] Masci, G., Giacomelli, L., and Crescenzi, V., "Atom transfer radical polymerization of n-isopropylacrylamide," *Macromolecular Rapid Communications*, vol. 25, no. 4, pp. 559–564, 2004.

[167] Masunaga, H., Sasaki, K., and Akiba, I., "Reversible gelation and phase transition of aqueous solution of hydrophobically modified poly(n-isopropylacrylamide)," *Journal of Macromolecular Science-Physics*, vol. B43, no. 5, pp. 1063–1073, 2004.

[168] Matyjaszewski, K., Gaynor, S. G., Kulfan, A., and Podwika, M., "Preparation of hyperbranched polyacrylates by atom transfer radical polymerization. 1. acrylic AB* monomers in "living" radical polymerizations," *Macromolecules*, vol. 30, no. 17, pp. 5192–5194, 1997.

[169] Matyjaszewski, K., Patten, T. E., and Xia, J., "Controlled/"living" radical polymerization. kinetics of the homogeneous atom transfer radical polymerization of styrene," *Journal of the American Chemical Society*, vol. 119, no. 4, pp. 674–680, 1997.

[170] Matyjaszewski, K. and Xia, J., "Atom transfer radical polymerization," *Chemical Reviews*, vol. 2001, no. 101, pp. 2921–2990, 2001.

[171] Mayadunne, R. T. A., Jeffery, J., Moad, G., and Rizzardo, E., "Living free radical polymerization with reversible addition-fragmentation chain transfer (RAFT polymerization): Approaches to star polymers," *Macromolecules*, vol. 36, pp. 1505–1513, 2003.

[172] Mazzolini, J., Boyron, O., Monteil, V., D'Agosto, F., Boisson, C., Sanders, G. C., Heuts, J. P. A., Duchateau, R., Gigmes, D., and Bertin, D., "Polyethylene end functionalization using thia-michael addition chemistry," *Polymer Chemistry*, vol. 3, no. 9, pp. 2383–2392, 2012.

[173] McLeary, J. B., Calitz, F. M., McKenzie, J. M., Tonge, M. P., Sanderson, R. D., and Klumperman, B., "Beyond inhibition: A h-1 nmr investigation of the early kinetics of raft-mediated polymerization with the same initiating and leaving groups," *Macromolecules*, vol. 37, no. 7, pp. 2383–2394, 2004.

[174] Mita, I. and Horie, K., "Diffusion-controlled reactions in polymer systems," *Journal of Macromolecular Science - Reviews in Macromolecular Chemistry and Physics*, vol. C27, no. 1, pp. 91–169, 1987.

[175] Moad, G., Chong, Y. K., Postma, A., Rizzardo, E., and Thang, S. H., "Advances in RAFT polymerization: the synthesis of ppolymers with defined end-groups," *Polymer*, vol. 46, pp. 8458–8468, 2005.

[176] Monteiro, M. J. and de Brouwer, H., "Intermediate radical termination as the mechanism for retardation in reversible addition-fragmentation chain transfer polymerization," *Macromolecules*, vol. 34, no. 3, pp. 349–352, 2001.

[177] Mori, H., Seng, D. C., Lechner, H., Zhang, M., and Mller, A. H. E., "Synthesis and characterization of branched polyelectrolytes. 1. preparation of hyperbranched poly(acrylic acid) via self-condensing atom transfer radical copolymerization," *Macromolecules*, vol. 35, pp. 9270–9281, 2002.

[178] Morimoto, N., Hirano, S., Takahashi, H., Loethen, S., Thompson, D. H., and Akiyoshi, K., "Self-assembled ph-sensitive cholesteryl pullulan

nanogel as a protein delivery vehicle," *Biomacromolecules*, vol. 14, no. 1, pp. 56–63, 2013.

[179] Nakayama, M., Okano, T., Miyazaki, T., Kohori, F., Sakai, K., and Yokoyama, M., "Molecular design of biodegradable polymeric micelles for temperature-responsive drug release," *Journal of Controlled Release*, vol. 115, no. 1, pp. 46–56, 2006.

[180] Narain, R., Gonzales, M., Hoffman, A. S., Stayton, P. S., and Krishnan, K. M., "Synthesis of monodisperse biotinylated p(NIIPAAm)-coated iron oxide magnetic nanoparticles and their bioconjugation to streptavidin," *Langmuir*, vol. 23, no. 11, pp. 6299–6304, 2007.

[181] Nash, M. E., Carroll, W. M., Foley, P. J., Maguire, G., Connell, C. O., Gorelov, A. V., Beloshapkin, S., and Rochev, Y. A., "Ultra-thin spin coated crosslinkable hydrogels for use in cell sheet recovery-synthesis, characterisation to application," *Soft Matter*, vol. 8, no. 14, pp. 3889–3899, 2012.

[182] Newkome, G. R., Moorefield, C. N., and Vogtle, F., *Dendrimers and Dendrons: Concepts, Syntheses, Applications*. Wiley-VCH, 2001.

[183] Newkome, G., Yao, Z., Baker, G., and Gupta, V., "Micelles .1. cascade molecules - a new approach to micelles - a [27]-arborol," *Journal of Organic Chemistry*, vol. 50, no. 11, pp. 2003–2004, 1985.

[184] Ng, S. C. and Chee, K. K., "Determination of rate constants of benzoyl peroxide and azobisisobutyronitrile dissociation via polymerization kinetics," *Journal of Polymer Science Part a-Polymer Chemistry*, vol. 20, no. 2, pp. 409–415, 1982.

[185] Noguchi, Y., Okeyoshi, K., and Yoshida, R., "Design of surfactant-grafted hydrogels with fast response to temperature," *Macromolecular Rapid Communications*, vol. 26, no. 24, pp. 1913–1917, 2005.

[186] Nuopponen, M., Kalliomaki, K., Laukkanen, A., Hietala, S., and Tenhu, H., "A-B-A stereoblock copolymers of N-isopropylacrylamide," *Journal of Polymer Science: Part A: Polymer Chemistry*, vol. 46, no. 1, pp. 38–46, 2008.

[187] Odian, G. G., *Principles of polymerization*. John Wiley and Sons, fourth edition ed., 2004.

[188] O'Neal, D. P., Hirsch, L. R., Halas, N. J., Payne, J. D., and West, J. L., "Photo-thermal tumor ablation in mice using near infrared-absorbing nanoparticles," *Cancer Letters*, vol. 209, pp. 171–176, 2004.

[189] Ong, K. K., Jenkins, A. L., Cheng, R., Tomalia, D. A., Durst, H. D., Jensen, J. L., Emanuel, P. A., Swim, C. R., and Yin, R., "Dendrimer enhanced immunosensors for biological detection," *Analytica Chimica Acta*, vol. 444, no. 1, pp. 143–148, 2001.

[190] Ono, Y. and Shikata, T., "Hydration and dynamic behavior of poly(n-isopropylacrilamide)s in aqueous solution: A sharp phase transition at the lower critical solution temperature," *Journal of the American Chemical Society*, vol. 128, pp. 10030–10031, 2006.

[191] Ono, Y. and Shikata, T., "Contrary hydration behavior of n-isopropylacrylamide to its polymer, p(NIPAm), with a lower critical solution temperature," *Journal of Physical Chemistry B*, vol. 111, no. 7, pp. 1511–1513, 2007.

[192] Orlicki, J. A., Viernes, N. O., and Moore, J. S., "Roles of molecular architecture and end-group functionality on the surface properties of branched polymers," *Langmuir*, vol. 18, pp. 9990–9995, 2002.

[193] Oxley, H. R., Corkhill, P. H., Fitton, J. H., and Tighe, B. J., "Macroporous hydrogels for biomedical applications - methodology and morphology," *Biomaterials*, vol. 14, no. 14, pp. 1064–1072, 1993.

[194] Patel, D., Vandromme, S. E., Reid, M. E., and Taite, L. J., "Synergistic activity of alpha(v)beta(3) integrins and the elastin binding protein enhance cell-matrix interactions on bioactive hydrogel surfaces," *Biomacromolecules*, vol. 13, no. 5, pp. 1420–1428, 2012.

[195] Patel, N. G., Cavicchia, J. P., Zhang, G., and Newby, B.-m. Z., "Rapid cell sheet detachment using spin-coated pnipaam films retained on surfaces by an aminopropyltriethoxysilane network," *Acta Biomaterialia*, vol. 8, no. 7, pp. 2559–2567, 2012.

[196] Patri, A. K., Majoros, I. J., and Baker, J. R., "Dendritic polymer macromolecular carriers for drug delivery," *Current Opinion in Chemical Biology*, vol. 6, no. 4, pp. 466–471, 2002.

[197] Pei, Y., Chen, J., Yang, L., Shi, L., Tao, Q., Hui, B., and Li, J., "The effect of pH on the LCST of poly(N-isopropylacrylamide) and poly(N-isopropylacrylamide-co-acrylic acid)," *Journal of Biomaterials Science Polymer Edition*, vol. 15, no. 5, pp. 585–594, 2004.

[198] Peppas, N. A., "Hydrogels and drug delivery," *Current Opinion in Colloid & Interface Science*, vol. 2, no. 5, pp. 531–537, 1997.

[199] Peppas, N. A., Bures, P., Leobandung, W., and Ichikawa, H., "Hydrogels in pharmaceutical formulations," *European Journal of Pharmaceutics and Biopharmaceutics*, vol. 50, no. 1, pp. 27–46, 2000.

[200] Peppas, N. A., Hilt, J. Z., Khademhosseini, A., and Langer, R., "Hydrogels in biology and medicine: From molecular principles to bionanotechnology," *Advanced Materials*, vol. 18, no. 11, pp. 1345–1360, 2006.

[201] Peppas, N. A., Wood, K. M., and Blanchette, J. O., "Hydrogels for oral delivery of therapeutic proteins," *Expert Opinion on Biological Therapy*, vol. 4, no. 6, pp. 881–887, 2004.

[202] Perrier, S., Barner-Kowollik, C., Quinn, J. F., Vana, P., and Davis, T. P., "Origin of inhibition effects in the reversible addition fragmentation chain transfer (raft) polymerization of methyl acrylate," *Macromolecules*, vol. 35, no. 22, pp. 8300–8306, 2002.

[203] Petrusic, S., Jovancic, P., Lewandowski, M., Giraud, S., Bugarski, B., Djonlagic, J., and Koncar, V., "Synthesis, characterization and drug release properties of thermosensitive poly(n-isopropylacrylamide) microgels," *Journal of Polymer Research*, vol. 19, no. 10, 2012.

[204] Pinchuk, L., "A review of the biostability and carcinogenicity of polyurethanes in medicine and the new-generation of biostable polyurethanes," *Journal of Biomaterials Science-Polymer Edition*, vol. 6, no. 3, pp. 225–267, 1994.

[205] Pinto, M. A., Li, R., Immanuel, C. D., Lovell, P. A., and Schork, F. J., "Effects of reversible addition fragmentation transfer (raft) on branching in vinyl acetate bulk polymerization," *Industrial & Engineering Chemistry Research*, vol. 47, no. 3, pp. 509–523, 2008.

[206] Prescott, S. W., "Chain-length dependence in living/controlled free-radical polymerizations: Physical manifestation and monte carlo simulation of reversible transfer agents," *Macromolecules*, vol. 36, no. 25, pp. 9608–9621, 2003.

[207] Price, A. D. and Huber, D. L., "Controlled polymer monolayer synthesis by radical transfer to surface immobilized transfer agents," *Polymer Chemistry*, vol. 4, p. 15651574, 2013.

[208] Qiu, X.-P. and Winnik, F. M., "Facile and efficient one-pot transformation of RAFT polymer end groups via a mild aminolysis/michael addition sequence," *Macromolecular Rapid Communications*, vol. 27, no. 19, pp. 1648–1653, 2006.

[209] Rasch, M. R., Sokolov, K. V., and Korgel, B. A., "Limitations on the optical tunability of small diameter gold nanoshells," *Langmuir*, vol. 25, no. 19, pp. 11777–11785, 2009.

[210] Ratner, B. D. and Bryant, S. J., "Biomaterials: Where we have been and where we are going," *Annual Review of Biomedical Engineering*, vol. 6, pp. 41–75, 2004.

[211] Ratner, B. D., Hoffman, A. S., Schoen, F. J., and Lemons, J. E., *Biomaterials Science: An Introduction to Materials in Medicine*. Elsevier Academic Press, 2 ed., 2004.

[212] Raula, J., Shan, J., Nuopponen, M., Niskanen, A., Jiang, H., Kauppinen, E. I., and Tenhu, H., "Synthesis of gold nanoparticles grafted with a thermoresponsive polymer by surface-induced reversible-addition-fragmentation chain-transfer polymerization," *Langmuir*, vol. 19, no. 8, pp. 3499–3504, 2003.

[213] Ravaine, V., Ancla, C., and Catargi, B., "Chemically controlled closed-loop insulin delivery," *Journal of Controlled Release*, vol. 132, no. 1, pp. 2–11, 2008.

[214] Raveendran, P., Fu, J., and Wallen, S. L., "Completely "green" synthesis and stabilization of metal nanoparticles," *Journal of the American Chemical Society*, vol. 125, no. 46, pp. 13940–13941, 2003.

[215] Ray, B., Isobe, Y., Matsumoto, K., Habaue, S., Okamoto, Y., Kamigaito, M., and Sawamoto, M., "RAFT polymerization of N-isopropylacrylamide in the absence and presence of Y(OTf)3: Simultaneous control of molecular weight and tacticity," *Macromolecules*, vol. 37, no. 5, pp. 1702–1710, 2004.

[216] Ray, B., Isobe, Y., Morioka, K., Habaue, S., Okamoto, Y., Kamigaito, M., and Sawamoto, M., "Synthesis of isotactic poly(N-isopropylacrylamide) by RAFT polymerization in the presence of lewis acid," *Macromolecules*, vol. 36, no. 3, pp. 543–545, 2003.

[217] Ray, B., Okamoto, Y., Kamigaito, M., Sawamoto, M., Seno, K.-i., Kanaoka, S., and Aoshima, S., "Effect of tacticity of poly(n-isopropylacrylamide) on the phase separation temperature of its aqueous solutions," *Polymer Journal*, vol. 37, no. 3, pp. 234–237, 2005.

[218] Rieger, J., Zhang, W., Stoffelbach, F., and Charleux, B., "Surfactant-free RAFT emulsion polymerization using poly(N,N-dimethylacrylamide) trithiocarbonate macromolecular chain transfer agents," *Macromolecules*, vol. 43, no. 15, pp. 6302–6310, 2010.

[219] Roberts, J. C., Adams, Y. E., Tomalia, D., Mercer-Smith, J. A., and Lavallee, D. K., "Using starburst dendrimers as linker molecules to radiolabel antibodies," *Bioconjugate Chemistry*, vol. 1, no. 5, pp. 305–308, 1990.

[220] Ru, G. and Feng, J., "Effects of end groups on phase transition and segmental mobility of poly(N-isopropylacrylamide) chains in D2O," *Journal of Polymer Science Part B: Polymer Physics*, vol. 49, pp. 749–755, 2011.

[221] Ruel-Gariépy, E., Shive, M., Bichara, A., Berrada, M., Garrec, D. L., Chenite, A., and Leroux, J.-C., "A thermosensitive chitosan-based hydrogel for the local delivery of paclitaxel," *European Journal of Pharmaceutics and Biopharmaceutics*, vol. 57, no. 1, pp. 53–63, 2004.

[222] Sadler, K. and Tam, J. P., "Peptide dendrimers: applications and synthesis," *Journal of biotechnology*, vol. 90, no. 3-4, pp. 195–229, 2002.

[223] Sanclimens, G., Crespo, L., Giralt, E., Royo, M., and Albericio, F., "Solid-phase synthesis of second-generation polyproline dendrimers," *Biopolymers (Peptide Science)*, vol. 76, pp. 283–297, 2004.

[224] Sayil, C. and Okay, O., "Macroporous poly(n-isopropylacrylamide) networks," *Polymer Bulletin*, vol. 48, no. 6, pp. 499–506, 2002.

[225] Schild, H. G., "Poly (n-isopropylacrylamide) - experiment, theory and application," *Progress in Polymer Science*, vol. 17, no. 2, pp. 163–249, 1992.

[226] Schilli, C. M., Zhang, M., Rizzardo, E., Thang, S. H., Chong, B. Y. K., Edwards, K., Karlsson, G., and Muller, A. H. E., "A new double-responsive block copolymer synthesized via RAFT polymerization: Poly(N-isopropylacrylamide)-block-poly(acrylic acid)," *Macromolecules*, vol. 37, no. 21, pp. 7861–7866, 2004.

[227] Sciannamea, V., Jérŏme, R., and Detrembleur, C., "In-situ nitroxide-mediated radical polymerization (NMP) processes: Their understanding and optimization," *Chemical Reviews*, vol. 108, no. 3, pp. 1104–1126, 2008.

[228] Segawa, Y., Higashihara, T., and Ueda, M., "Hyperbranched polymers with controlled degree of branching from 0 to 100%," *Journal of the American Chemical Society*, vol. 132, pp. 11000–11001, 2010.

[229] Sershen, S. and West, J., "Implantable, polymeric systems for modulated drug delivery," *Advanced Drug Delivery Reviews*, vol. 55, no. 3, pp. 439–439, 2003.

[230] Shanmugam, T., Raghavan, A., and Nasar, A. S., "Distribution of dendritic, terminal and linear units and relationship between degree of branching and molecular weight of AB2-type hyperbranched polymer: A 13C-NMR study," *Journal of Macromolecular Science Pure and Applied Chemistry*, vol. 43, no. 9, pp. 1387–1397, 2006.

[231] She, W., Luo, K., Zhang, C., Wang, G., Geng, Y., Li, L., He, B., and Gu, Z., "The potential of self-assembled, ph-responsive nanoparticles of mpegylated peptide dendron-doxorubicin conjugates for cancer therapy," *Biomaterials*, vol. 34, pp. 1613–1623, 2013.

[232] Shen, Z., Terao, K., Maki, Y., Dobashi, T., Ma, G., and Yamamoto, T., "Synthesis and phase behavior of aqueous poly(N-isopropylacrylamide-co-acrylamide), poly(N-isopropylacrylamide-co-N,N-dimethylacrylamide) and poly(N-isopropylacrylamide-co-2-hydroxyethyl methacrylate)," *Colloid and Polymer Science*, vol. 284, pp. 1001–1007, 2006.

[233] Shibayama, M., Morimoto, M., and Nomura, S., "Phase-separation induced mechanical transition of poly(n-isopropylacrylamide) water isochore gels," *Macromolecules*, vol. 27, no. 18, pp. 5060–5066, 1994.

[234] Shih, H. and Lin, C.-C., "Cross-linking and degradation of step-growth hydrogels formed by thiol-ene photoclick chemistry," *Biomacromolecules*, vol. 13, no. 7, pp. 2003–2012, 2012.

[235] Shoichet, M. S., "Polymer scaffolds for biomaterials applications," *Macromolecules*, vol. 43, no. 2, pp. 581–591, 2010.

[236] Siepmann, J. and Peppas, N. A., "Modeling of drug release from delivery systems based on hydroxypropyl methylcellulose (hpmc)," *Advanced Drug Delivery Reviews*, vol. 64, pp. 163–174, 2012.

[237] Silva, M. E. S. R. e., Dutra, E. R., Mano, V., and Machado, J. C., "Preparation and thermal study of polymers derived from acrylamide," *Polymer Degradation and Stability*, vol. 67, no. 3, pp. 491–495, 2000.

[238] Skrabalak, S. E., Au, L., Li, X., and Xia, Y., "Facile synthesis of ag nanocubes and au nanocages," *Nature Protocols*, vol. 2, no. 9, pp. 2182–2190, 2007.

[239] Slaughter, B. V., Khurshid, S. S., Fisher, O. Z., Khademhosseini, A., and Peppas, N. A., "Hydrogels in regenerative medicine," *Advanced Materials*, vol. 21, no. 32-33, pp. 3307–3329, 2009.

[240] Snowden, M. J., "The use of poly(n-isopropylacrylamide) lattices as novel release systems," *Journal of the Chemical Society-Chemical Communications*, no. 11, pp. 803–804, 1992.

[241] Soeriyadi, A. H., Li, G.-Z., Slavin, S., Jones, M. W., Amos, C. M., Becer, C. R., Whittaker, M. R., Haddleton, D. M., Boyer, C., and Davis, T. P., "Synthesis and modification of thermoresponsive poly(oligo(ethylene glycol) methacrylate) via catalytic chain transfer polymerization and thiol-ene michael addition," *Polymer Chemistry*, vol. 2, no. 4, pp. 815–822, 2011.

[242] Starr, A. and Edwards, M. L., "Mitral replacement - clinical experience with a ball-valve prosthesis," *Annals of Surgery*, vol. 154, no. 4, p. 726, 1961.

[243] Stern, J. M., Stanfield, J., Kabbani, W., Hsieh, J.-T., and Cadeddu, J. A., "Selective prostate cancer thermal ablation with laser activated gold nanoshells," *The Journal of Urology*, vol. 179, pp. 748–753, 2008.

[244] Su, S., Ali, M., Filipe, C. D. M., Li, Y., and Pelton, R., "Microgel-based inks for paper-supported biosensing applications," *Biomacromolecules*, vol. 9, no. 3, pp. 935–941, 2008.

[245] Sumerlin, B. S. and Vogt, A. P., "Macromolecular engineering through click chemistry and other efficient transformations," *Macromolecules*, vol. 43, pp. 1–13, 2010.

[246] Sun, L. and Du, J., "Revisiting the time for removing the unloaded drug by dialysis method based on a biocompatible and biodegradable polymer vesicle," *Polymer*, vol. 53, pp. 2068–2073, 2012.

[247] Sun, X., Zhang, G., Patel, D., Stephens, D., and Gobin, A. M., "Targeted cancer therapy by immunoconjugated gold-gold sulfide nanoparticles using protein g as a cofactor," *Annals of Biomedical Engineering*, vol. 40, no. 10, pp. 2131–2139, 2012.

[248] Sundberg, D. C. and James, D. R., "Limiting conversions in 2-phase polymer reactions," *Journal of Polymer Science Part A: Polymer Chemistry*, vol. 16, no. 2, pp. 523–529, 1978.

[249] Szwarc, M., "Living polymers," *Nature*, vol. 178, no. 4543, pp. 1168–1169, 1956.

[250] Ta, T., Convertine, A. J., Reyes, C. R., Stayton, P. S., and Porter, T. M., "Thermosensitive liposomes modified with poly(N-isopropylacrylamide-co-propylacrylic acid) copolymers for triggered release of doxorubicin," *Biomacromolecules*, vol. 11, no. 8, pp. 1915–1920, 2010.

[251] Taite, L. J., Rowland, M. L., Ruffino, K. A., Smith, B. R. E., Lawrence, M. B., and West, J. L., "Bioactive hydrogel substrates: Probing leukocyte receptor-ligand interactions in parallel plate flow chamber studies," *Annals of Biomedical Engineering*, vol. 34, no. 11, pp. 1705–1711, 2006.

[252] Takata, S., Suzuki, K., Norisuye, T., and Shibayama, M., "Dependence of shrinking kinetics of poly(n-isopropylacrylamide) gels on preparation temperature," *Polymer*, vol. 43, no. 10, pp. 3101–3107, 2002.

[253] Tam, J. P., "Synthetic peptide vaccine design: Synthesis and properties of aa high-density multiple antigenic peptide system," *Proceedings of the National Academy of Sciences of the United States of America*, vol. 85, no. 15, pp. 5409–5413, 1988.

[254] Tao, W. and Yan, L., "Thermogelling of highly branched poly(n-isopropylacrylamide)," *Journal of Applied Polymer Science*, vol. 118, no. 6, pp. 3391–3399, 2010.

[255] Techawanitchai, P., Idota, N., Uto, K., Ebara, M., and Aoyagi, T., "A smart hydrogel-based time bomb triggers drug release mediated by ph-jump reaction," *Science and Technology of Advanced Materials*, vol. 13, no. 6, 2012.

[256] Temenoff, J. S., Shin, H., Conway, D. E., Engel, P. S., and Mikos, A. G., "In vitro cytotoxicity of redox radical initiators for cross-linking of oligo(poly(ethylene glycol) fumarate) macromers," *Biomacromolecules*, vol. 4, no. 6, pp. 1605–1613, 2003.

[257] Tetko, I. V., Gasteiger, J., Todeschini, R., Mauri, A., Livingstone, D., Ertl, P., Palyulin, V. A., Radchenko, E. V., Zefirov, N. S., Makarenko, A. S., Tanchuk, V. Y., and Prokopenko, V. V., "Virtual computational chemistry laboratory - design and description," *Journal of Computer-Aided Molecular Design*, vol. 19, no. 6, pp. 453–63, 2005.

[258] Theis, A., Feldermann, A., Charton, N., Davis, T. P., Stenzel, M. H., and Barner-Kowollik, C., "Living free radical polymerization (raft) of dodecyl acrylate: Chain length dependent termination, mid-chain radicals and monomer reaction order," *Polymer*, vol. 46, no. 18, pp. 6797–6809, 2005.

[259] Thomas, D. B., Convertine, A. J., Hester, R. D., Lowe, A. B., and McCormick, C. L., "Hydrolytic susceptibility of dithioester chain transfer agents and implications in aqueous RAFT polymerizations," *Macromolecules*, vol. 37, no. 5, pp. 1735–1741, 2004.

[260] Thomas, D. B., Convertine, A. J., Myrick, L. J., Scales, C. W., Smith, A. E., Lowe, A. B., Vasilieva, Y. A., Ayres, N., and McCormick, C. L., "Kinetics and molecular weight control of polymerization of acrylamide via RAFT," *Macromolecules*, vol. 37, no. 24, pp. 8941–8950, 2004.

[261] Thompson, D. S., Markoski, L. J., and Moore, J. S., "Synthesis and characterization of hyperbranched aromatic poly(ether imide)s with varying degrees of branching," *Macromolecules*, vol. 33, pp. 6412–6415, 2000.

[262] Tomalia, D., Baker, H., Dewald, J., Hall, M., Kallos, G., Martin, S., Roeck, J., Ryder, J., and Smith, P., "Dendritic macromolecules-synthesis of starburst dendrimers," *Macromolecules*, vol. 19, no. 9, pp. 2466–2468, 1986.

[263] Tong, R., Yala, L., Fan, T. M., and Cheng, J., "The formulation of aptamer-coated paclitaxel-polylactide nanoconjugates and their targeting to cancer cells," *Biomaterials*, vol. 31, no. 11, pp. 3043–3053, 2010.

[264] Ulijn, R. V., "Enzyme-responsive materials/: a new class of smart biomaterials," *Journal of Materials Chemistry*, vol. 16, no. 23, pp. 2217–2225, 2006.

[265] Vernon, B., Kim, S. W., and Bae, Y. H., "Insulin release from islets of langerhans entrapped in a poly(n-isopropylacrylamide-co-acrylic acid) polymer gel," *Journal of Biomaterials Science-Polymer Edition*, vol. 10, no. 2, pp. 183–198, 1999.

[266] Vihola, H., Laukkanen, A., Valtola, L., Tenhu, H., and Hirvonen, J., "Cytotoxicity of thermosensitive polymers poly(N-isopropylacrylamide), poly(N-vinylcaprolactam) and amphiphilically modified poly (N-vinylcaprolactam)," *Biomaterials*, vol. 26, no. 16, pp. 3055–3064, 2005.

[267] Vo, C.-D., Rosselgong, J., Armes, S. P., and Billingham, N. C., "Raft synthesis of branched acrylic copolymers," *Macromolecules*, vol. 40, no. 20, pp. 7119–7125, 2007.

[268] Vogt, A. P., Gondi, S. R., and Sumerlin, B. S., "Hyperbranched polymers via RAFT copolymerization of an acryloyl trithiocarbonate," *Australian Journal of Chemistry*, vol. 60, pp. 396–399, 2007.

[269] Vogt, A. P. and Sumerlin, B. S., "Tuning the temperature response of branched poly(N-isopropylacrylamide) prepared by RAFT polymerization," *Macromolecules*, vol. 41, pp. 7368–7373, 2008.

[270] Voorhees, A. B., Jaretzki, A., and Blakemore, A. H., "The use of tubes constructed from vinyon-n cloth in bridging arterial defects - a preliminary report," *Annals of Surgery*, vol. 135, no. 3, pp. 332–336, 1952.

[271] Wang, A. R. and Zhu, S. P., "Modeling the reversible addition-fragmentation transfer polymerization process," *Journal of Polymer Science Part a-Polymer Chemistry*, vol. 41, no. 11, pp. 1553–1566, 2003.

[272] Wang, J.-S. and Matyjaszewski, K., "Controlled/"living" radical polymerization. halogen atom transfer radical polymerization promoted by a Cu(I)/Cu(II) redox process," *Macromolecules*, vol. 28, no. 23, pp. 7901–7910, 1995.

[273] Wang, J., Chen, L., Zhao, Y., Guo, G., and Zhang, R., "Cell adhesion and accelerated detachment on the surface of temperature-sensitive chitosan and poly(n-isopropylacrylamide) hydrogels," *Journal of Materials Science-Materials in Medicine*, vol. 20, no. 2, pp. 583–590, 2009.

[274] Wang, R., Luo, Y. W., Li, B. G., Sun, X. Y., and Zhu, S. P., "Design and control of copolymer composition distribution in living radical polymerization using semi-batch feeding policies: A model simulation," *Macromolecular Theory and Simulations*, vol. 15, no. 4, pp. 356–368, 2006.

[275] Wang, R., Luo, Y., Li, B.-G., and Zhu, S., "Modeling of branching and gelation in raft copolymerization of vinyl/divinyl systems," *Macromolecules*, vol. 42, no. 1, pp. 85–94, 2009.

[276] Wang, Z., He, J., Tao, Y., Yang, L., Jiang, H., and Yang, Y., "Controlled chain branching by RAFT-based radical polymerization," *Macromolecules*, vol. 36, no. 20, pp. 7445–7452, 2003.

[277] Weissleder, R., "A clearer vision for in vivo imaging," *Nature Biotechnology*, vol. 19, no. 4, pp. 316–317, 2001.

[278] Whittaker, M. R., Goh, Y.-K., Gemici, H., Legge, T. M., Perrier, S., and Monteiro, M. J., "Synthesis of monocyclic and linear polystyrene using the reversible coupling/cleavage of thiol/disulfide groups," *Macromolecules*, vol. 39, no. 26, pp. 9028–9034, 2006.

[279] Wiener, E. C., Brechbiel, M. W., Brothers, H., Magin, R. L., Gansow, O. A., Tomalia, D. A., and Lauterbur, P. C., "Dendrimer-based metal-chelates - a new class of magnetic-resonance-imaging contrast agents," *Magnetic Resonance in Medicine*, vol. 31, no. 1, pp. 1–8, 1994.

[280] Winnik, F. M., Ringsdorf, H., and Venzmer, J., "Methanol-water as a cononsolvent system for poly(n-isopropylacrylamide)," *Macromolecules*, vol. 23, no. 8, pp. 2415–2416, 1990.

[281] Wolinsky, J. B. and Grinstaff, M. W., "Therapeutic and diagnostic applications of dendrimers for cancer treatment," *Advanced Drug Delivery Reviews*, vol. 60, no. 9, pp. 1037–1055, 2008.

[282] Wu, C. and Zhou, S., "Volume phase transition of swollen gels: Discontinuous or continuous?," *Macromolecules*, vol. 30, pp. 574–576, 1997.

[283] Wu, H., Zhu, L., and Torchilin, V. P., "ph-sensitive poly(histidine)-peg/dspe-peg co-polymer micelles for cytosolic drug delivery," *Biomaterials*, vol. 34, no. 4, pp. 1213–1222, 2013.

[284] Wu, X. S., Hoffman, A. S., and Yager, P., "Synthesis and characterization of thermally reversible macroporous poly(n-isopropylacrylamide) hydrogels," *Journal of Polymer Science Part a-Polymer Chemistry*, vol. 30, no. 10, pp. 2121–2129, 1992.

[285] Wu, Z., Liang, H., and Lu, J., "Synthesis of poly(n-isopropylacrylamide)-poly(ethylene glycol) miktoarm star copolymers via raft polymerization and aldehyde-aminooxy click reaction and their thermoinduced micellization," *Macromolecules*, vol. 43, no. 13, pp. 5699–5705, 2010.

[286] Xia, Y., Burke, N. A. D., and Stver, H. D. H., "End group effect on the thermal response of narrow-disperse poly(n-isopropylacrylamide) prepared by atom transfer radical polymerization," *Macromolecules*, vol. 39, no. 6, pp. 2275–2283, 2006.

[287] Xiao, L., Isner, A. B., Hilt, J. Z., and Bhattacharyya, D., "Temperature responsive hydrogel with reactive nanoparticles," *Journal of Applied Polymer Science*, vol. 128, no. 3, pp. 1804–1814, 2013.

[288] Xu, F. J., Li, J., Yuan, S. J., Zhang, Z. X., Kang, E. T., and Neoh, K. G., "Thermo-responsive porous membranes of controllable porous morphology from triblock copolymers of polycaprolactone and poly(n-isopropylacrylamide) prepared by atom transfer radical polymerization," *Biomacromolecules*, vol. 9, no. 1, pp. 331–339, 2008.

[289] Xu, X.-D., Zhang, X.-Z., Yang, J., Cheng, S.-X., Zhuo, R.-X., and Huang, Y.-Q., "Strategy to introduce a pendent micellar structure into

poly(n-isopropylacrylamide) hydrogels," *Langmuir*, vol. 23, no. 8, pp. 4231–4236, 2007.

[290] Xue, W., Champ, S., Huglin, M. B., and Jones, T. G. J., "Rapid swelling and deswelling in cryogels of crosslinked poly(n-isopropylacrylamide-co-acrylic acid)," *European Polymer Journal*, vol. 40, no. 3, pp. 467–476, 2004.

[291] Xue, W., Hamley, I. W., and Huglin, M. B., "Rapid swelling and deswelling of thermoreversible hydrophobically modified poly(n-isopropylacrylamide) hydrogels prepared by freezing polymerisation," *Polymer*, vol. 43, no. 19, pp. 5181–5186, 2002.

[292] Yamada, K., Nakano, T., and Okamoto, Y., "Stereospecific free radical polymerization of vinyl esters using fluoroalcohols as solvents," *Macromolecules*, vol. 31, pp. 7598–7605, 1998.

[293] Yamazaki, Y., Matsunaga, T., Syohji, K., Arakawa, T., and Sato, T., "Effect of anionic/siloxy groups on the release of ofloxacin from soft contact lenses," *Journal of Applied Polymer Science*, vol. 127, no. 6, pp. 5022–5027, 2013.

[294] Yan, J.-J., Hong, C.-Y., and You, Y.-Z., "An easy method to convert the topologies of macromolecules after polymerization," *Macromolecules*, vol. 44, no. 6, pp. 1247–1251, 2011.

[295] Yang, H. and Kao, W. Y. J., "Dendrimers for pharmaceutical and biomedical applications," *Journal of Biomaterials Science-Polymer Edition*, vol. 17, no. 1-2, pp. 3–19, 2006.

[296] Yang, H., Zhang, Q., Lin, B., Fu, G., Zhang, X., and Guo, L., "Thermosensitive electrospun fibers prepared by a sequential thiol-ene click chemistry

approach," *Journal of Polymer Science Part A: Polymer Chemistry*, vol. 50, no. 20, pp. 4182–4190, 2012.

[297] Yang, H. and Kao, W. J., "Dendrimers for pharmaceutical and biomedical applications," *Journal of Biomaterial Science Polymer Edition*, vol. 17, no. 1-2, pp. 3–19, 2005.

[298] Yang, X., Grailer, J. J., Rowland, I. J., Javadi, A., Hurley, S. A., Matson, V. Z., Steeber, D. A., and Gong, S., "Multifunctional stable and ph-responsive polymer vesicles formed by heterofunctional triblock copolymer for targeted anticancer drug delivery and ultrasensitive mr imaging," *ACS Nano*, vol. 4, no. 11, pp. 6805–6817, 2010.

[299] Yavuz, M. S., Cheng, Y. Y., Chen, J. Y., Cobley, C. M., Zhang, Q., Rycenga, M., Xie, J. W., Kim, C., Song, K. H., Schwartz, A. G., Wang, L. H. V., and Xia, Y. N., "Gold nanocages covered by smart polymers for controlled release with near-infrared light," *Nature Materials*, vol. 8, no. 12, pp. 935–939, 2009.

[300] Yin, X., Hoffman, A. S., and Stayton, P. S., "Poly(N-isopropylacrylamide-co-propylacrylic acid) copolymers that respond sharply to temperature and pH," *Biomacromolecules*, vol. 7, no. 5, pp. 1381–1385, 2006.

[301] Yoo, M. K., Sung, Y. K., Lee, Y. M., and Cho, C. S., "Effect of polyelectrolyte on the lower critical solution temperature of poly(N-isopropyl acrylamide) in the poly(NIPAAm-co-acrylic acid) hydrogel," *Polymer*, vol. 41, pp. 5713–5719, 2000.

[302] Yoshida, M., Langer, R., Lendlein, A., and Lahann, J., "From advanced biomedical coatings to multi-functionalized biomaterials," *Polymer Reviews*, vol. 46, no. 4, pp. 347–375, 2006.

[303] Yoshida, R., Sakai, K., Okano, T., and Sakurai, Y., "Drug release profiles in the shrinking process of thermoresponsive poly(n-isopropylacrylamide-co-alkyl methacrylate) gels," *Industrial and Engineering Chemistry Research*, vol. 31, no. 10, pp. 2339–2345, 1992.

[304] Yoshikawa, C., Goto, A., Tsujii, Y., Fukuda, T., Yamamoto, K., and Kishida, A., "Fabrication of high-density polymer brush on polymer substrate by surface-initiated living radical polymerization," *Macromolecules*, vol. 38, no. 11, pp. 4604–4610, 2005.

[305] Yu, Y.-Y., Chang, S.-S., Lee, C.-L., and Wang, C. C., "Gold nanorods: Electrochemical synthesis and optical properties," *Journal of Physical Chemistry B*, vol. 101, no. 34, pp. 6661–6664, 1997.

[306] Yun, J., Lee, D. H., Im, J. S., and Kim, H. I., "Improvement in transdermal drug delivery performance by graphite oxide/temperature-responsive hydrogel composites with micro heater," *Materials Science and Engineering C-Materials for Biological Applications*, vol. 32, no. 6, pp. 1564–1570, 2012.

[307] Zambito, Y., Pedreschi, E., and Di Colo, G., "Is dialysis a reliable method for studying drug release from nanoparticulate systems?-a case study," *International Journal of Pharmaceutics*, vol. 434, no. 1-2, pp. 28–34, 2012.

[308] Zargar, A., Chang, K., Taite, L. J., and Schork, F. J., "Mathematical modeling of hyperbranched water-soluble polymers with applications in drug delivery," *Macromolecular Reaction Engineering*, vol. 5, no. 9-10, pp. 373–384, 2011.

[309] Zargar, A. and Schork, F. J., "Copolymer sequence distributions in controlled radical polymerization," *Macromolecular Reaction Engineering*, vol. 3, no. 2-3, pp. 118–130, 2009.

[310] Zargar, A. and Schork, F. J., "Design of copolymer molecular architecture via design of continuous reactor systems for controlled radical polymerization," *Industrial & Engineering Chemistry Research*, vol. 48, no. 9, pp. 4245–4253, 2009.

[311] Zhang, X. Z., Xu, X. D., Cheng, S. X., and Zhuo, R. X., "Strategies to improve the response rate of thermosensitive pnipaam hydrogels," *Soft Matter*, vol. 4, no. 3, pp. 385–391, 2008.

[312] Zhang, Y., Furyk, S., Bergbreiter, D. E., and Cremer, P. S., "Specific ion effects on the water solubility of macromolecules: PNIPAM and the Hofmeister series," *Journal of the American Chemical Society*, vol. 127, no. 41, pp. 14505–14510, 2005.

[313] Zhou, H. S., Honma, I., Komiyama, H., and Haus, J. W., "Controlled synthesis and quantum-size effect in gold-coated nanoparticles," *Physical Review B*, vol. 50, no. 16, pp. 12052–12056, 1994.

[314] Zhu, J., "Double optical limiting in gold nanoshell: tuning from visible to infrared region by shell thickness," *Applied Optics*, vol. 47, no. 31, pp. 5848–5852, 2008.

[315] Zhuo, R. X. and Li, W., "Preparation and characterization of macroporous poly(n-isopropylacrylamide) hydrogels for the controlled release of proteins," *Journal of Polymer Science Part a-Polymer Chemistry*, vol. 41, no. 1, pp. 152–159, 2003.